OPTIMAL PROCESS PARAMETERS FOR DIRECT METAL LASER SINTERING OF TI64 FOR MEDICAL IMPLANT PRODUCTION

JOHAN ELS

Dissertation submitted in fulfilment of the requirements for the Degree

MAGISTER TECHNOLOGIAE:

ENGINEERING: MECHANICAL

in the

Department of Mechanical and Mechatronics Engineering

Faculty of Engineering and Information Technology

at the

Central University of Technology, Free State

Study Leader: Prof M Truscott, PhD Microbiology

Co-supervisor: Mr GJ Booysen, M.Tech Eng. Mech

Co-supervisor: Dr JG van der Walt, D.Tech Eng. Mech

BLOEMFONTEIN

JANUARY 2016

DECLARATION WITH REGARD TO INDEPENDENT WORK

I, JOHAN ELS, identity number [redacted] and student number [redacted], do hereby declare that this dissertation submitted to the Central University of Technology, Free State for the Degree MAGISTER TECHNOLOGIAE: ENGINEERING: MECHANICAL, is my own independent work; and complies with the Code of Academic Integrity, as well as other relevant policies, procedures, rules and regulations of the Central University of Technology, Free State; and has not been submitted before to any institution by myself or any other person in fulfilment (or partial fulfilment) of the requirements for the attainment of any qualification.

_____ _____

SIGNATURE OF STUDENT **DATE**

ABSTRACT

Direct Metal Laser Sintering (DMLS) is a layer-by-layer Additive Manufacturing (AM) process that creates physical metal parts from three-dimensional (3D) Computer Aided Design (CAD) data. For DMLS to be generally accepted by industry as a manufacturing technology, high mechanical integrity of final components needs to be demonstrated. Properties of manufactured components are directly affected by the quality of each individual laser sintered track of each consecutive layer. The purpose of this work is to study the geometrical characteristics of single tracks produced through DMLS and determine the optimal process parameters for three of the most influential process parameters in order to process Titanium-6Aluminium-4Vanadium(Ti-6Al-4V) powder namely: appropriate laser power, scanning speed and powder layer thickness. State of the art metal powder-based technology, the commercialisation process and current DMLS systems are presented. Properties and applications of titanium and its alloy in aerospace, marine and energy industry, consumer market and biomedical applications are described. Powder material characteristics were defined by scanning electron microscopy and the use of an optical granulomorphometer. The DMLS experiments were conducted on an EOSINT M270 machine. Geometrical characteristics of single tracks, their shape and stability varied significantly when process parameters changed. To estimate to what extent laser power and scanning speed have an influence on Ti-6Al-4V material fusion, several experiments were conducted on a Ti-6Al-4V substrate without powder. For 150-170 W laser power and 600-2000 mm/s scanning speed, different regimes of laser track were found: “keyhole” mode, “conductive” mode and “humping” mode. The empirical data were compared to a melt pool width and depth prediction simulation program in order to verify its predictive capability. This model is useful for estimating geometrical characteristics of single tracks in “conductive mode”. Single tracks of Ti-6Al-4V powder from TLS Technik GmbH were produced at 15, 30 and 45 µm powder layer thicknesses. More stable tracks were obtained at 15-30 µm layer thickness, 150-170 W laser power and scanning speeds between 1000 and 1200 mm/s where powder deposition imperfections, roughness of the substrate and even some variation in laser scanning speed did not result in large differences in geometry of the tracks. An analysis of each single track’s shape, width and height of tracks, melting depth into the substrate and track melted surface area permitted the estimation of some of the optimal process parameters.

Keywords: Additive Manufacturing, Direct Metal Laser Sintering, Titanium alloy

To my wife, Jeni, my parents Johan and Lienkie and my mother-in-law Elsa

ACKNOWLEDGEMENTS

I wish to express my sincerest gratitude to the following people and institutions for their various contributions:

My supervisors: Prof. Michèle Truscott, Mr. Gerrie Booysen and Dr. Kobus van der Walt for all their patience, encouragement and support.

A special word of appreciation to Dr. Igor Yadroitsev and Dr. Ina Yadroitsava for all their guidance and collaboration, willingness to help with the experimental analysis and suggestions during this study.

The staff members of the Centre for Rapid Prototyping and Manufacturing (CRPM) at the Central University of Technology, Free State, for their encouragement and support.

My parents, Johan and Lienkie, for all their prayers, love and support.

My mother-in-law, Elsa, for all her understanding and support.

Most importantly, my wife Jeni, for all her unconditional love, encouragement, support and understanding throughout this study.

.

"Rejoice in hope; be patient in tribulation; be constant in prayer." – Romans 12:12

PUBLICATIONS TO DATE

1. Booysen G.J., Truscott M., Els J., de Beer D.J.2011.Development of patient-specific implants using Direct Metal Laser Sintering in Titanium, **5th International Conference on Advanced Research in Virtual and Physical Prototyping (VRAP 2011)**, 28 September – 1 October, Leiria, Portugal.
2. Els J., Truscott M., Booysen G.J., Van der Walt J.G. 2012. Preliminary findings on an investigation into the three most important process parameters that influence Laser Sintering of Ti64 and validation of a melt pool simulation model, **13th Annual International Rapid Product Development Association of South Africa Conference**, 31 October – 2 November, KwaMaritane Bush Lodge, South Africa.
3. Els J., Truscott M., Booysen G.J., Van der Walt J.G. 2013. Preliminary findings on an investigation into the three most important process parameters that influence laser sintering of Ti64 and validation of a melt pool simulation model, **Interim: Interdisciplinary Journal** 2013 Vol 12 No 3, pp 195-209, ISSN: 1684-498X
4. Els J., Truscott M., Booysen G.J., Van der Walt J.G. 2013. Establishing the optimal process parameters for the laser sintering of Ti64 for layer thicknesses of 15 µm and 30 µm and validation of a melt pool simulation model, **14th Annual International Rapid Product Development Association of South Africa Conference**, 29 October – 1 November, SANParks Golden Gate Hotel, South Africa. ISBN 9787-0-620-58681-8
5. Els J., Truscott M., Van der Walt J.G., Booysen G.J. 2014. Establishing the optimal process parameters for the laser sintering of Ti64 for layer thicknesses of 15 µm and 30 µm and validation of a melt pool simulation model, **Advanced Materials Research** 2014 Vol 1019, pp 254-258, ISSN: 1662-8985
6. Yadroitsava I., Els J., Booysen G.J., Yadroitsev I. 2014.Peculiarities of single track formation from ti6al4v alloy at different laser power densities by selective laser melting **15th Annual International Rapid Product Development Association of South Africa Conference**, 6 – 7 November, STIAS Conference Centre, Stellenbosch, South Africa.
7. Yadroitsava I., Els J., Booysen G.J., Yadroitsev I. 2015. Peculiarities of single track formation from ti6al4v alloy at different laser power densities by selective laser melting. (Accepted forpublication in South African Journal of Industrial Engineering)

TABLE OF CONTENTS

ABSTRACT ..... **III**

ACKNOWLEDGEMENTS ..... **V**

PUBLICATIONS TO DATE ..... **VI**

LIST OF FIGURES ..... **XII**

LIST OF TABLES ..... **XIX**

ACRONYMS ..... **XXI**

CHAPTER 1 ..... **22**

INTRODUCTION AND BACKGROUND OF THE STUDY **22**

1.1 Introduction **22**

1.2 Problem statement **24**

1.3 Hypothesis **24**

1.4 Aim of study **24**

1.5 Importance of study **24**

1.6 Methodology **25**

1.7 Scope of study **25**

1.8 Structure of dissertation **25**

CHAPTER 2 ..... **28**

STATE OF THE TECHNOLOGY **28**

2.1 Introduction **28**

2.2 Historical Perspective **30**

2.2.1 Early patents 30

2.2.2 Commercialisation 32

2.3 Laser Beam Melting 34

2.3.1 DMLS – Electro Optical Systems GmbH, Germany 34

2.3.1.1 EOSINT M270 35

2.3.1.2 EOSINT M280 35

2.3.2 LaserCUSING®– Concept Laser GmbH, Germany 37

2.3.2.1 Concept Laser M1 and M2 CUSING 37

2.3.2.2 Concept Laser M3 Linear 37

2.3.2.3 Concept Laser Mlab CUSING R 38

2.3.3 Selective Laser Melting – SLM Solutions GmbH, Germany 39

2.3.3.1 Laser Beam Melting System SLM®125^{HL} 39

2.3.3.2 Laser Beam Melting System SLM®250^{HL} 39

2.3.3.3 Laser Beam Melting System SLM®280^{HL} 40

2.3.3.4 Laser Beam Melting System SLM®500^{HL} 40

2.3.4 Selective Laser Melting – Phenix Systems, France 42

2.3.5 Selective Laser Melting–ReaLizer GmbH, Germany 43

2.3.5.1 ReaLizer SLM™50 43

2.3.5.2 ReaLizer SLM™100 43

2.3.5.3 ReaLizer SLM™250 44

2.3.6 Selective Laser Melting – Renishaw plc, United Kingdom 45

2.3.7 Selective Laser Melting – 3D Systems Corporation 46

2.4 Electron Beam Melting (EBM) 48

2.4.1 ARCAM AB®, Sweden 48

2.4.1.1 ARCAM A1 48

2.4.1.2 ARCAM A2 48

2.5 Metal Laser Sintering Hybrid Milling Machine 50

2.5.1 Matsuura, Japan 50

2.5.1.1 Matsuura LUMEX Avance-25 50

2.6 Conclusions 51

CHAPTER 3 52

TITANIUM AND ITS APPLICATIONS 52

3.1 Introduction 52

3.2 History of titanium 52

3.3 Properties and applications of titanium and titanium alloys 52

3.3.1 Aerospace 53

3.3.2 Marine 54

3.3.3 Consumer products 54

3.3.4 Energy industry 55

3.3.5 Biomedical applications 56

3.4 Processing of titanium through AM 57

3.4.1 Challenges associated with processing metal powder through DMLS 57

3.4.1.1 Process parameters 57

3.4.1.2 Material properties 58

3.4.2 Consolidation of Ti-6Al-4V powder through DMLS 60

3.5 Summary 65

CHAPTER 4 66

MATERIALS AND METHODOLOGY 66

4.1 Introduction 66

4.2 Powder characterisation 66

4.3 Powder chemical composition 67

4.4 Single track formation 68

4.4.1 Experimental study and numerical modelling of laser–substrate interaction .. 68

4.4.2 Experimental design of tracks produced in powder 68

4.5 Summary 71

CHAPTER 5 72

RESULTS AND DISCUSSION 72

5.1 Background 72

5.2 Powder characterisation 72

5.2.1 Particle size 72

5.2.2 Particle shape 73

5.3 Chemical composition analysis of powder 78

5.4 Single tracks produced without powder 80

5.5 Evaluation of melt pool temperature distribution simulation program 83

5.6 Results of single tracks in powder experiments 87

5.7 Discussion 96

CHAPTER 6 105

CONCLUSIONS AND FUTURE DEVELOPMENTS 105

6.1 Conclusions 105

6.1.1 State of the technology 105

6.1.2 Titanium and its applications 105

6.1.3 Results and discussion 106

6.2 Future experimental work 111

REFERENCES **113**

APPENDIX 1 ..... **120**

LIST OF FIGURES

Page

Figure 1.1: AM applications for different branches of industry [1]..... 22

Figure 1.2: Schematic representation of dissertation structure..... 27

Figure 2.1a: Classification of AM technologies [12]..... 29

Figure 2.1b: Classification of Metal AM(MAM) technologies..... 29

Figure 2.2: Patent of Ciraud [13,14]..... 30

Figure 2.3: Patent of Housholder [13,15]..... 30

Figure 2.4: The development process of metal powder bed processes[5,13]... 31

Figure 2.5: Schematic representation of the DMLS process [23]..... 35

Figure 2.6: EOSINT M270 [26]..... 36

Figure 2.7: EOSINT M280 [27]..... 36

Figure 2.8: M1 CUSING [29]..... 37

Figure 2.9: M2 CUSING [29]..... 37

Figure 2.10: M3 Linear [30]..... 39

Figure 2.11: MlabCUSING R [28]..... 39

Figure 2.12: SLM® 125^{HL}[37]..... 40

Figure 2.13: SLM® 250^{HL}[38]..... 40

Figure 2.14: SLM® 280^{HL}[39]..... 41

Figure 2.15: SLM® 500HL[40]..... 41

Figure 2.16: Phenix PXS[42]..... 42

Figure 2.17: Phenix PXM [43].....42

Figure 2.18: Phenix PXL [44].....42

Figure 2.19: ReaLizerSLM™ 50 [48]..... 44

Figure 2.20: ReaLizer SLM™ 100 [48]..... 44

Figure 2.21: ReaLizer SLM™ 250 [48]..... 44

Figure 2.22: Renishaw AM 125 [50]..... 46

Figure 2.23: Renishaw AM 250 [51].....46

Figure 2.24: 3D Systems sPro™ 125 [53].....47

Figure 2.25: 3D Systems sPro™ 250 [54]..... 47

Figure 2.26: ARCAM A1 [57]..... 49

Figure 2.27: ARCAM A2 [58]..... 49

Figure 2.28: Matsuura LUMEX Avance-25 [60].....51

Figure 3.1: Boeing 777 main landing gear titanium forging applications (all labelled parts are Ti-10V-2Fe-3Al) [65]..... 53

Figure 3.2: Example of one of the first titanium drivers introduced by TaylorMade® in 1997 [71].....55

Figure 3.3: First tennis balls in the world utilising titanium introduced by Wilson [70]..... 55

Figure 3.4: Titanium alloy taper stress joints in offshore floating platform riser systems [72]…… 56

Figure 3.5: The first ever titanium alloy taper stress joint which was successfully employed in the Placid Oil Canyon production riser system in the Gulf of Mexico [72]…….…….. 56

Figure 3.6: Front view of a total knee replacement titanium implant with a high density polyethylene wearing surface [77]…….……..57

Figure 3.7: Side view of a total knee replacement titanium implant showing its placement on the femur and tibia [77]…….…… 57

Figure 3.8: Material-based input parameters in AM [79]…….……58

Figure 3.9a: SEM photograph of TLS powder at ×500 magnification…….59

Figure 3.9b: SEM photograph of TLS powder at ×3000 magnification……..…….59

Figure 3.10: Premier layer height-view (a), 3D image (b), and profile of the layer from stainless steel grade 316L (c) [5]…..……..……60

Figure 3.11: Top view of a laser sintered track made from stainless steel grade 316L (sub 25 μm) powder on stainless steel substrate. Laser power is 50 W, scanning speed is 100 mm/s, thickness of the deposited powder layer is 40 μm [5]…..…… 62

Figure 3.12: Regimes (modes) of 304 steel welding [88]. Power density ($\frac{P}{\pi D^2/4}$) for 2.5-4 kW and spot size 450 μm is 1.57 - 2.52 mW/cm^2…….. 63

Figure 3.13: Appearance of keyhole and melt pool with increased scanning speed [89]…….…… 64

Figure 3.14: Cross-section of tracks on steel 304L. P=50 W for different scanning speeds V=60, 120 and 280 mm/s. Power density ($\frac{P}{\pi D^2/_4}$) is 1.3 mW/cm^2 [5]…… 64

Figure 4.1a: Optical granulomorphometer ALPAGA 500 NANO …….... 67

Figure 4.1b: Vacuum dispersion device VDD270…..…….. 67

Figure 4.2: Tescan Vega 3 Easy Probe Scanning Electron Microscope……..… 68

Figure 4.3: 6 mm Titanium plate fixed to building platform with laser sintered tracks……..…….. 69

Figure 4.4: Schematic representation of experiment with titanium powder……. 70

Figure 5.1: Granulometric study based on sieving diameter…….. 72

Figure 5.2a: Morphology study based on Legendre ellipse ……..73

Figure 5.2b: Morphology study based on circle of the same area of particle…....73

Figure 5.3: Morphology study based on roundness……...……75

Figure 5.4: Morphology study based on concavity index…….…….. 75

Figure 5.5: Equivalent diameter distributions by number (I) and by volume (II) of powder…….... 75

Figure 5.6: Bivariate scatterplots: equivalent diameter*versus*sieve diameter (a), concavity (b), elongation (c),shape factor (d), satellity (e) and roundness (f) ……..…….. 77

Figure 5.7: Micrograph indicating the two zones that were analysed……..78

Figure 5.8: A typical EDS spectrum and chemical analysis of selected zones…79

Figure 5.9a: Top view and cross-sectional view of single tracks formed on a substrate without powder with laser power 150 W and 170 W and 600 mm/s scanning speed[4]…… 80

Figure 5.9b: Top view and cross-sectional view of single tracks formed on a substrate without powder with laser power 150 W and 170 W and 1200 mm/s scanning speed……..…… 81

Figure 5.9c: Top view and cross-sectional view of single tracks formed on a substrate without powder with laser power 150 W and 170 W and 2000 mm/s scanning speed…… 82

Figure 5.10: Track width,w1 (a); track height, h1 and re-melt depth, h2 (b), track surface area S1 and re-melt surface area S2 measurement (c)……..…… 84

Figure 5.11a: Track width of the experimental data compared to the data obtained from the numerical simulation program……85

Figure 5.11b: Re-melt depth of the experimental data compared to the data obtained from the numerical simulation program……..…. 86

Figure 5.11c: Calculated temperature profiles for the semi-infinite Ti-6Al-4V plate: XY plane (i); XZ plane and YZ planes (ii); 3D-plot (iii) for scanningspeed 1000 mm/s and laser power 170 W……..…….. 87

Figure 5.12: Single tracks produced with 150 W laser power, powder layer thickness of 30 µm and scanning speeds of 1600 mm/s (a), 1800 mm/s (b) and 2000 mm/s (c) ……..…..88

Figure 5.13a-d: Measured track widths for powder thickness of 15, 30 and 45 µm……..…97

Figure 5.13e-f: Illustration of a stable track (e), versus an unstable track (f)……97

Figure 5.14a-d:Measured track heights for powder thickness of 15, 30 and 45 µm…….…… 98

Figure 5.15a-d:Measured re-melt depth for powder thickness of 15, 30 and 45 µm……....99

Figure 5.16a-d:Total re-melt height (h1+h2) for powder thickness of 15, 30 and 45 µm……...100

Figure 5.17a-d:Measurement of the track melt area (S1) for powder thickness of 15, 30 and 45 µm…….……...101

Figure 5.18: The mechanism of interaction of laser radiation with a powder medium [5]…….102

Figure 5.19a-d:Substrate re-melt area (S2) for powder thickness of 15, 30 and 45 µm……....103

Figure 5.20a-d:Total re-melt area S=S1+S2 for powder thickness of 15, 30 and 45 µm……104

Figure 6.1: Comparison of measured track widths (w1) in µm for powder thickness of 15, 30 and 45 µm…...……107

Figure 6.2: Top view (a) and cross-section (b) of optimal single track produced at 15 µm layer thickness, 170 W laser power and scanning speed of 1200 mm/s……..….108

Figure 6.3: Top view (a) and cross-section (b) of optimal single track producedat 30 µm layer thickness, 170 W laser power and scanning speed of 1200 mm/s…….…..108

Figure 6.4: Proposed optimal parameter set for high surface quality components: 15 µm powder layer thickness, 1000 mm/s scanning speed and 150 W laser power ……..…….110

Figure 6.5: Proposed optimal parameter set for thin-walled components: 30 µm powder layer thickness, 1400 mm/s scanning speed and 170 W laser power ……..……..…….110

Figure 6.6: Top view of tracks synthesised from 904L stainless steel powder on substrate at different hatch distances: (a), (b), (c) – one, three, and five tracks at 60 µm hatch distance [94]……..……..112

Figure 6.7: Cross-sectional view of tracks produced on top of each other in 904L stainless steel powder with the following parameters: Scanning speed is 100 mm/s; thickness of each powder layer is 50 µm; laser power is 50 W [5]…….....112

LIST OF TABLES

Page

Table 2.1: Technical Data of the EOSINT M270 and M280 [23,25]..... 36

Table 2.2: Technical Data of the Concept Laser range of machines [28]..... 38

Table 2.3: Technical Data of the SLM® range of systems [33-36]..... 41

Table 2.4: Technical Data of the Phenix PXS, PXM and PXL systems [41].....43

Table 2.5: Technical Data of the three ReaLizer metal AM systems [45-47]... 45

Table 2.6: Technical Data of the Renishaw AM125 and AM 250 systems [49]..... 46

Table 2.7: Technical Data of the sPro™ 125 and sPro™ 250 from 3D Systems [52]..... 47

Table 2.8: Technical Data of the ARCAM A1 and A2 systems [55,56].....49

Table 2.9: Technical Data of the Matsuura LUMEX Avance-25 machine [59].. 50

Table 5.1: Elongation of particles of different elliptical shape..... 73

Table 5.2: Shape factor of particles of different form.....74

Table 5.3: Granulomorphometrical characteristics[3] of Ti-6Al-4V powder..... 76

Table 5.4: Measured track widths (w1) in µm for powder thickness of 15, 30 and 45µm..... 89

Table 5.5: Measured track heights (h1) in µm for powder thickness of 15, 30and 45µm..... 90

Table 5.6: Measured track re-melt depth (h2) in µm for powder thickness of 15, 30and 45µm……..…..……..……..… 91

Table 5.7: Total re-melt height (h1+h2) in µm for powder thickness of 15, 30 and 45µm…….…. 92

Table 5.8: Measurement of the track surface area (S1) in µm² for powder thickness of 15, 30 and 45µm…….…….. 93

Table 5.9: Substrate re-melt area (S2) in µm² for powder thickness of 15, 30 and 45µm……...……..…. 94

Table 5.10: Total re-melt area (S1 + S2) in µm² for powder thickness of 15, 30 and 45µm……..…….……..…. 95

ACRONYMS

3D	Three Dimensional
3D P	Three Dimensional Printing
.stl	Standard Triangulated Language
AM	Additive Manufacturing
ASTM	American Society for Testing and Materials
CAD	Computer Aided Design
CAGR	Compound Annual Growth Rate
CRPM	Centre for Rapid Prototyping and Manufacturing
CSIR	Council for Scientific and Industrial Research
CUT	Central University of Technology, Free State
DIPI	Laboratory of Diagnostics and Engineering of Industrial Processes
DMLS	Direct Metal Laser Sintering
DTM	Desk Top Manufacturing
EBM	Electron Beam Melting
EDS	Energy Dispersive X-Ray Spectroscopy
ENISE	National Engineering School of Saint-Etienne
EOS	Electro Optical Systems (GmbH)
ERD	Electrolux Rapid Development
FDM	Fused Deposition Modelling
LENS	Laser Engineered Net Shaping
LOM	Layered Object Manufacturing
MAM	Metal Additive Manufacturing
NLC	National Laser Centre
PGLSS	Part Generation by Layerwise Selective Sintering
SEM	Scanning Electron Microscopy
SLA	Stereolithography
SLM	Selective Laser Melting
SLS	Selective Laser Sintering
Ti-6Al-4V	Titanium-6Aluminium-4Vanadium alloy
USA	United States of America
UT	University of Texas

CHAPTER 1
INTRODUCTION AND BACKGROUND OF THE STUDY

1.1 Introduction

Additive Manufacturing (AM) technology is a process in which objects are produced directly from three-dimensional (3D) Computer Aided Design (CAD) data by sequential deposition of material and/or energy in contrast to “classical or conventional” technologies, where substrate material is removed from a blank piece of material to create a functional part. Direct Metal Laser Sintering (DMLS) is an AM process where parts are manufactured by scanning of a laser beam, layer-by-layer, onto metal powder to create a solid object. AM technology is most commonly used for modelling, prototyping, tooling and short-run production applications in various industries (Figure 1.1). As AM technology grew in popularity and became more widely adopted by the role players in the manufacturing industry, the need to produce components that could be employed as a final working part was identified.

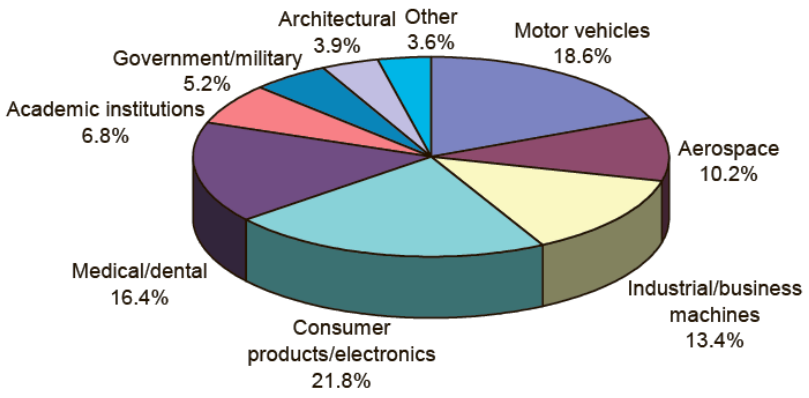

Figure 1.1: AM applications for different branches of industry [1]

AM is a potentially growing market in every manufacturing sector with a global AM market of $1,843.2 million in 2012 and is expected to grow at a Compound Annual Growth Rate (CAGR) of 13.5% to reach $3,471.9 million by 2017 [2]. The latest development has been the production of metal parts via AM processes that can be applied with confidence in the aerospace and medical industries. One of the leaders in AM applications is the

automotive industry which uses AM production for end-products inmotor vehicle engines and spare parts as well as other internal and external parts [2].

With regards to DMLS technology, the ability to manufacture complex metal parts without tools offers the opportunity to create new products that help boost product performance (e.g. tool inserts with cooling channels or highly efficient injection nozzles) [3]. Another benefit is the creation of objects with desired shape, internal structure and engineered composition, including special surface properties, within a single fabrication step.

Selective Laser Melting (SLM) technology, of which DMLS forms part, is able to manufacture parts with the desired microstructure as well as macrostructure [4]. The properties of the parts produced by DMLS depend strongly on the nature of the material, characteristics of each single track and each single layer, as well as the strength of the connections between the layers[5].

AM on the whole, and DMLS technology as part of the AM market, are developing rapidly; new powder materials are constantly introduced and elaboration of the algorithm for the determination of optimal process parameters is an actual and vital task.

The global orthopaedic implant market is estimated to grow to a staggering 41.8 billion U.S. dollars by 2016, of which 54.8% will be joint reconstruction at 22.9 billion U.S. dollars [6,7,8]. Companies have been successful in attaining the CE mark for prosthetic implants for sale in Europe created by the Electro Optical Systems' (EOS) DMLS process and ARCAM's Electron Beam Melting (EBM) process. One of these, an acetabular cup system offered by Italian orthopaedic company Lima Orthopaedics, has been used clinically in more than 15,000 patients over a period of three years between 2007 and 2010 [9]. To gain a competitive edge in today's highly competitive markets, a medical device company needs to produce high quality products repeatedly, in a short time frame and at a competitive price. For such a company to reach its economic potential, effective and efficient systems have to be implemented. This should encourage continuous improvements in quality and increased customer satisfaction.

1.2 Problem statement

Reproducibility of results, high quality and reliability of customised titanium medical implants produced through DMLS must be guaranteed.

1.3 Hypothesis

In order to achieve the aforementioned, part quality has to start with a detailed analysis of single laser track formation at different process parameters. The high quality of 3D objects produced by DMLS can be improved through precise monitoring of the parameters that influence the DMLS process. In order to fully understand the DMLS process, it is necessary to thoroughly investigate the parameters that affect the DMLS process.

1.4 Aim of study

Based on the problem statement and hypothetical resolutions mentioned above, the major objectives of this study are:

- to identify the main variations between the currently available metal powder-bed AM systems that make use of a melting binding process, including a historical perspective to understand how this technology came to be from where it began, up to the state of the technology in 2014;
- to establish the granulomorpholocial and chemical compositional characteristics of the powder material;
- to study geometrical characteristics of single tracks produced through DMLS and determining optimal process parameters for Ti-6Al-4V powder: appropriate laser power, scanning speed and powder layer thickness to produce continuous tracks with regular shape;
- to compare the empirical data with results from a simulation program in order to verify its predictive capability;

1.5 Importance of study

Premature failure of a medical implant will be catastrophic and it is thus of utmost importance to produce Ti-6Al-4V implants of a high, repeatable quality and standard.

1.6 Methodology

The methodology of this study includes an investigation of granulomorphometric characteristics of employed powder, peculiarities of single track formation during DMLS, and their geometrical characteristics depending on process parameters.

1.7 Scope of study

This research study is concerned with establishing the optimal process parameters to manufacture fully-dense custom medical implants by melting Ti-6Al-4V powder by means of DMLS. The end result that this research aims to achieve is the production of fully-dense, high quality medical implants. In order to achieve this, one has to ensure that all avenues of the DMLS process are duly investigated which will be a very lengthy study. Following the initial literature review, it soon became evident that a magnitude of parameters play a role in the DMLS process and it would be impossible to consider all influencing factors for this study. Therefore, three parameters, namely laser power, scanning speed and powder layer thickness, which the operator has control over will be considered for this particular study,.

1.8 Structure of dissertation

The layout of the dissertation is as follows:

- Chapter 1 presents an introduction and background to the work. In this chapter, the problem statement, hypothesis, the study objectives and its importance are explained.
- Chapter 2 presents an account of the literature survey performed to identify the main variations between the currently available metal AM systems, including a historical perspective to understand how this technology came to be from where it began, up to the state of the technology in 2014.
- Prior to committing to the experimental phase, Chapter 3 considers the history of titanium material and its applications.
- Chapter 4 deals with the methods used for analysing the specific powder utilised for this study as well as the methodology followed for the numerical modelling of the meltpool width prediction as well as the experimental design of the single track formation in powder.
- Chapter 5 gives an account of the characterisation and chemical composition results obtained from powder analysis as well as the simulated meltpool width prediction and

experimental results obtained with the EOS (GmbH) DMLS process at the Centre for Rapid Prototyping and Manufacturing (CRPM) at the Central University of Technology, Free State (CUT) in Bloemfontein, South Africa

- Chapter 6 concludes with an overall conclusion and recommendations for future work.

A schematic representation of the structure of this dissertation is shown in Figure 1.2 on page 27.

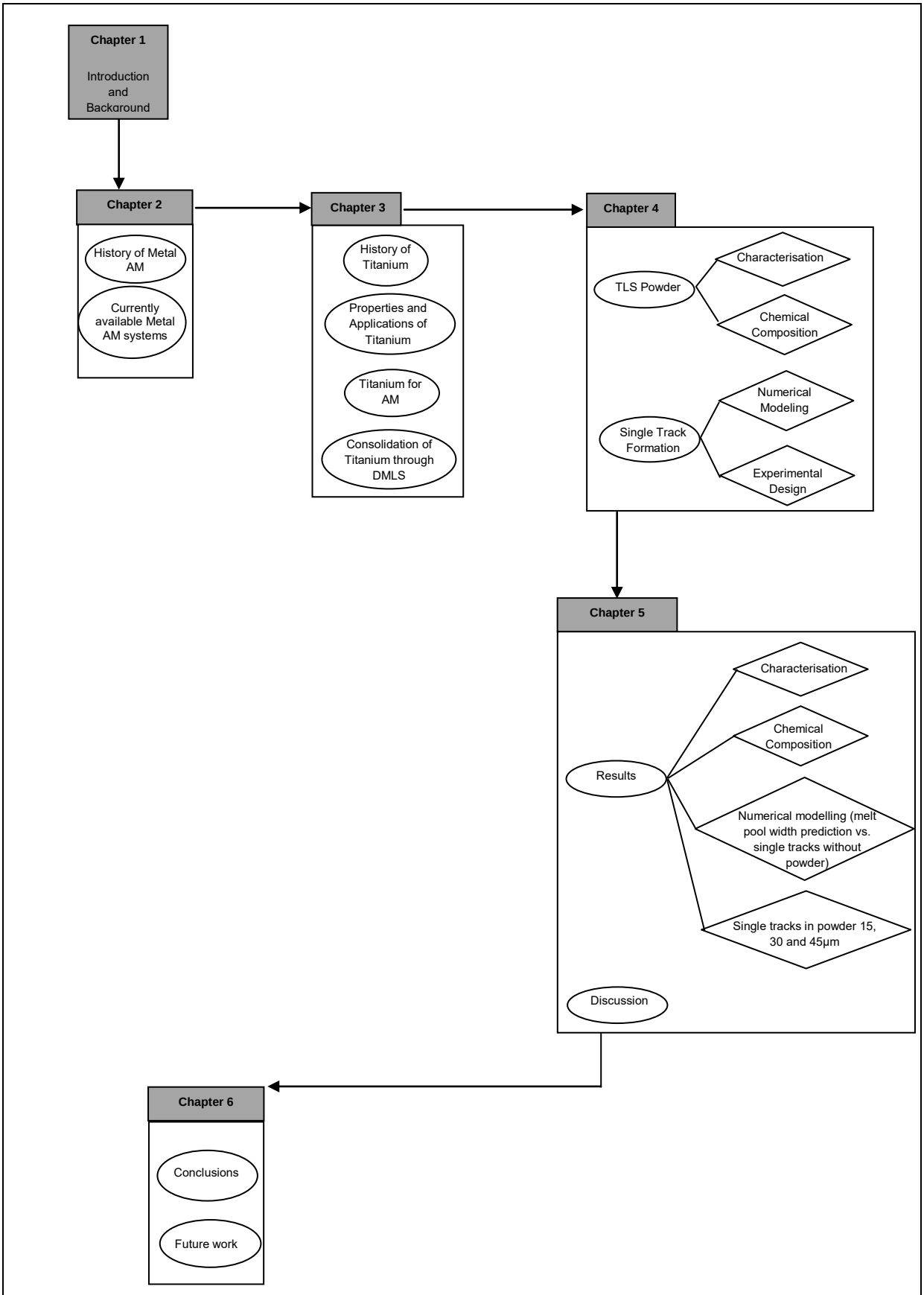

Figure 1.2: Schematic representation of dissertation structure

CHAPTER 2
STATE OF THE TECHNOLOGY

2.1 Introduction

Additive Manufacturing (AM) is described by the American Society for Testing and Materials (ASTM) International, as a process of joining materials to make objects from 3D model data, usually layer-upon-layer, as opposed to subtractive manufacturing methodologies, such as traditional machining. Synonyms include *additive fabrication*, *additive processes*, *additive techniques*, *additive layer manufacturing*, *layer manufacturing* and *freeform fabrication* [1]. Murr et al. [10] recognised in 2012 that AM is changing the manufacturing industry as we know it, calling AM the “renaissance in manufacturing”. Parts produced during the earlier stages of AM were mainly utilised as prototypes for form and fitment verification. As the technology grew in popularity and became more widely adopted by the role players in the manufacturing industry, the need to produce components that could be employed as a final working part were identified. From this point forward, many machine manufacturers developed AM systems that no longer merely produce prototypes but rather produce components that can bestructurally compared to components that have been conventionally manufactured via processes such as machining or injection moulding.

The latest development has been the production of metal parts via AM processes that can be applied with confidence in the aerospace, automotive and medical industries[11]. AM can be classified in many different ways. The most generally accepted method is to classify the different processes according to the binding of the raw material of which there are three, namely liquid-, solid-, and powder-based processes (Figure 2.1a) [12]. Metal powder-based AM processes making use of melting to bind the raw material can be classified in the major categories namely: Laser Beam Melting (different machine manufacturers refer to Laser Beam Melting as DMLS, LaserCusing®, SLM), Electron Beam Melting (EBM) and Metal Laser Sintering Hybrid Milling (Figure 2.1b). These processes all have the same objective but each makes use of a different approach.

This chapter identifies the main variations between the currently available metal powder bed AM systems that make use of a melting binding process, including a historical perspective to understand how this technology came to be,the developments that followed and the state of the technology in 2014.

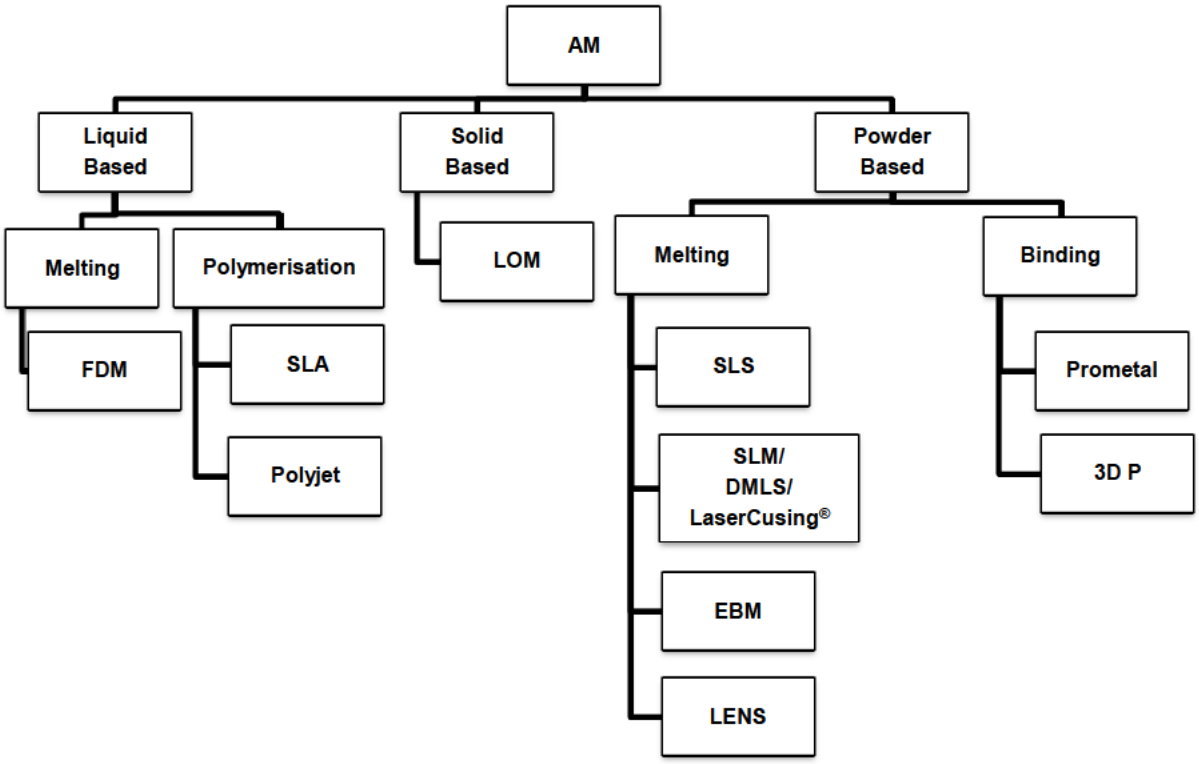

Figure 2.1a: Classification of AM technologies [12]

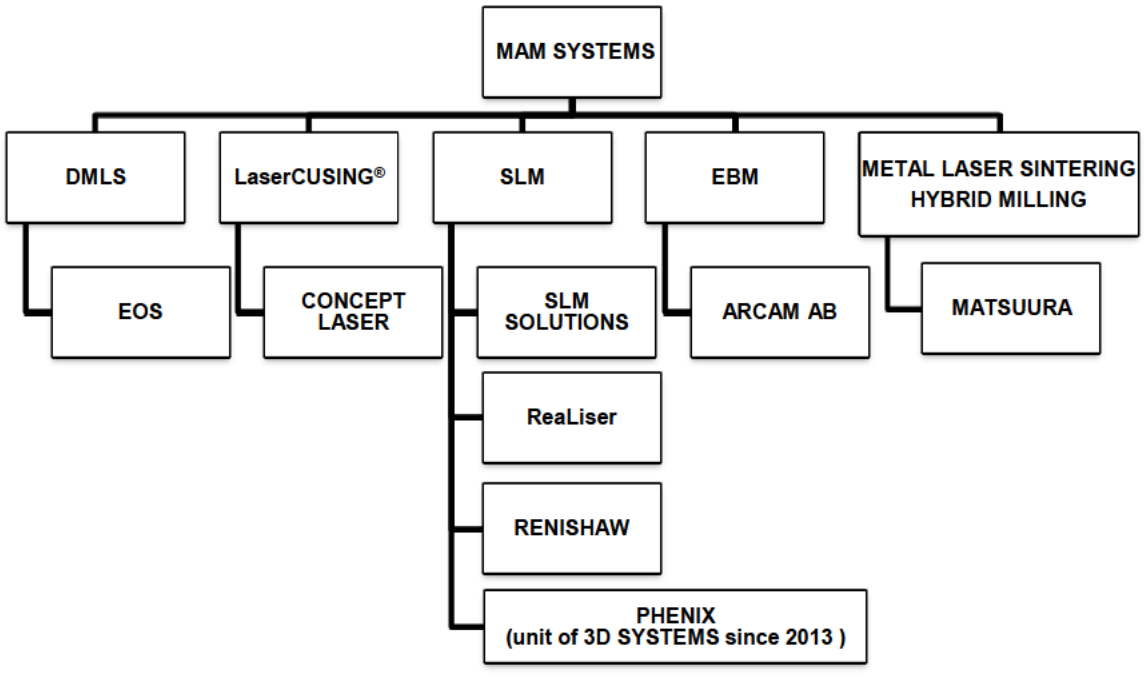

Figure 2.1b: Classification of Metal AM (MAM) technologies

2.2 Historical Perspective

2.2.1 Early patents

The idea to create metal parts by fusing layers of powder material was born as early as the 1970's when the Frenchman, Pierre Ciraud, filed a patent application (Figure 2.2) describing a method to produce any geometry by applying metal powder to a substrate and melting it by means of a beam of energy. The aim of his invention was "…the manufacture of parts which can have extremely complex shapes, without the need for casting moulds". This idea relates strongly to the basic idea of today's AM technology. In 1977 another inventor, Ross Housholder, filed a patent application which bears a close resemblance to current laser AM systems (Figure 2.3). In Housholders words, "…fusible particles are employed to form each layer which is then selectively fused by a laser beam to fuse an area in each layer which defines that portion of the article in the layers". Housholder's invention was not commercialised at the time, probably due to the high cost of lasers and remained unknown until it was discovered by Desk Top Manufacturing (DTM) Corporation (currently owned by 3D Systems since 2001) during their own patent filings. DTM licensed the patent and used it for many years [5,13]. Figure 2.4 summarises the development process of metal powder bed processes.

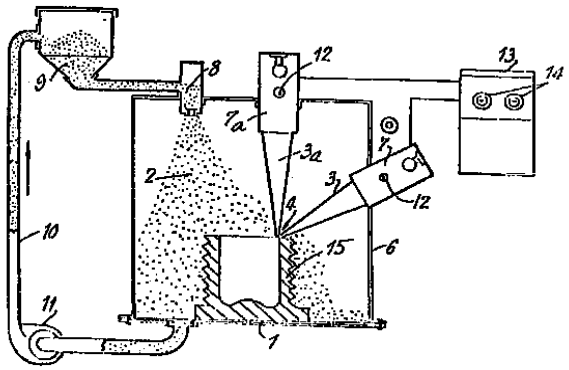

Figure 2.2: Patent of Ciraud [13,14]

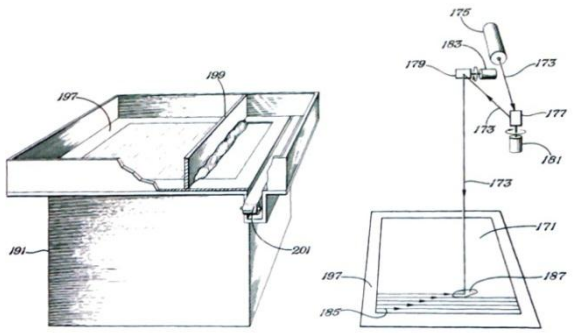

Figure 2.3: Patent of Housholder [13,15]

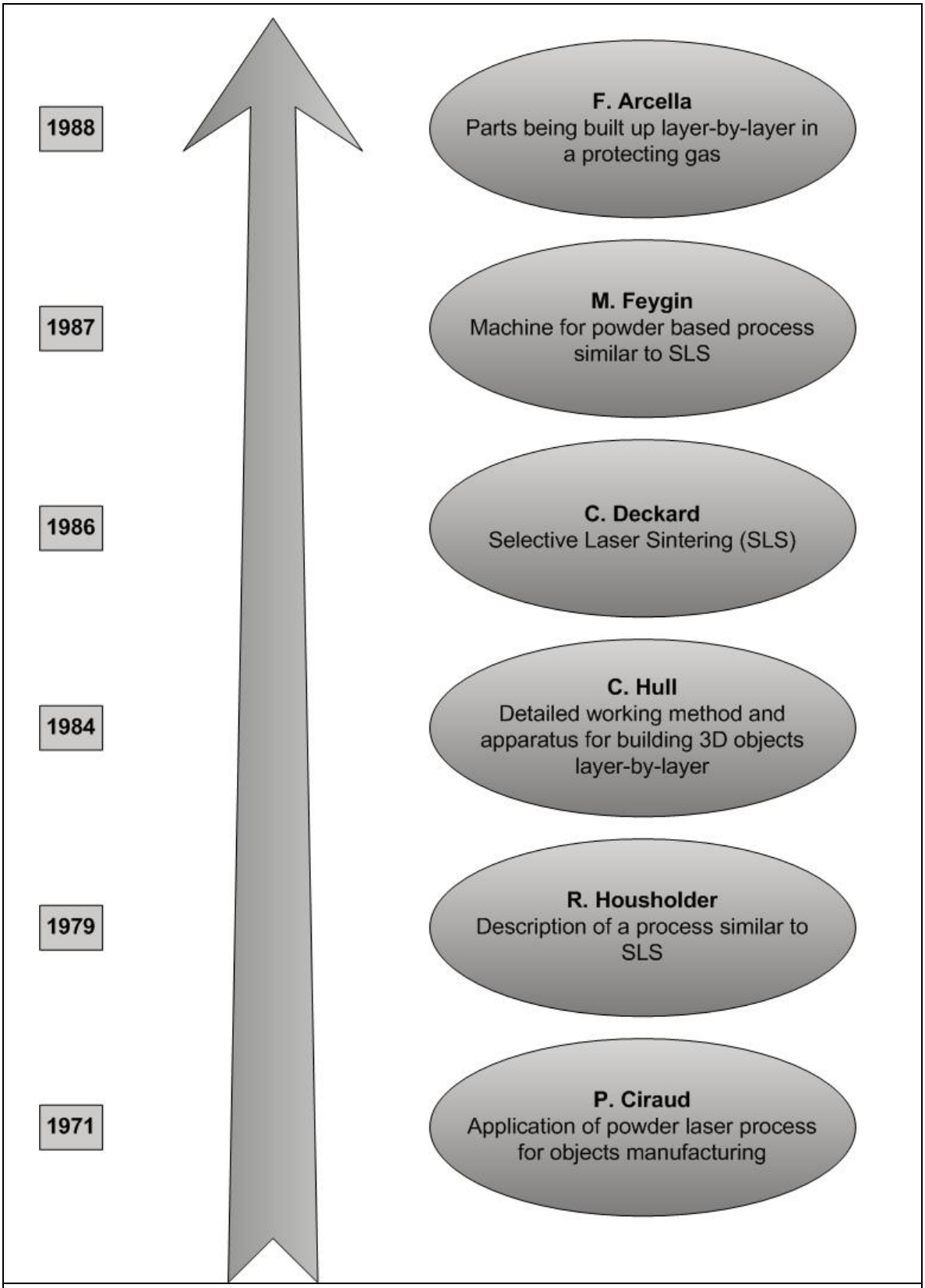

Figure 2.4: The development process of metal powder bed processes [5,13]

2.2.2 Commercialisation

The first steps toward commercialisation of AM were seen during mid-1980. Chuck Hull founded the company 3D Systems to commercialise the technology he described in his patent US 4,575,330 filed during August 1984. The technology Hull developed made use of a vat of liquid resin. He soon realised that the concept was not limited to liquids and gave it the generic name “stereolithography” and filed broad patent claims covering any “material capable of altering its physical state”. Many of the fundamentals still forming part of today’s AM technologies were patented by Hull and his colleagues, such as data preparation via triangulated models (.stl file), slicing and exposure strategies such as alternating hatch direction. Electro Optical Systems (EOS GmbH) of Munich, Germany acquired the exclusive rights to the entire laser sintering patent portfolio of 3D Systems in 1997. Carl Deckard, a master’s student at the University of Texas (UT), investigated a similar process to that of Hull during 1986 but made use of powder materials. Deckard first called this process Part Generation by Layerwise Selective Sintering (PGLSS) and later changed it to Selective Laser Sintering (SLS)[13].

Deckard’s patent application described a “computer aided laser apparatus which sequentially sinters a plurality of powder layers to build the desired part in a layer-by-layer fashion”. This technology was licensed from UT to a company that was set up to commercialise it as DTM.

In April 1987, an independent inventor, Michael Feygin, patented a similar idea to that of Deckard and established Helisys, a company to commercialise his ideas. His inventions included a powder-based process described as follows: “The new technique is based upon powder metallurgy and also uses a scanning laser. A layer (0.05mm to 0.5 mm) of powdered metal is spread on a base and partially bonded by running a heated roller over the powder at a controlled pressure. The layer is then scanned by the laser in the pattern of the desired cross-sectional slice. This completes the sintering of the metal” [13]. At Westinghouse Electric Corp. a similar development, headed by Frank Arcella, also resulted in a patent being filed in 1988. This technology could “cast shapes without using either a mold or die … shapes are cast in a fluidized bed using a laser or electron gun … Examples of suitable metals include stellite, stainless steel, aluminium and titanium. The preferred metal is titanium. If the powder is a metal, a CO_2 laser is preferred”. The parts were built up in an inert atmosphere [13].

The first commercial laser sintering system, shipped in December 1992, was the Sinterstation 2000 from DTM, the result of the research and development by Deckard, Beaman and colleagues at UT as well as the commercialisation efforts of DTM. DTM chose to take an indirect approach by laser sintering a polymer-coated metal powder in the Sinterstation to form a so-called “green” part, followed by a furnace process to remove the polymer, bond the metal matrix and infiltrate it with a secondary metal to remove the porosity [13]. The second laser sintering system, the EOSINT P350, was launched by EOS GmbH in 1994.

The first commercial DMLS system was the result of a combination of EOS’ plastic laser sintering technology and a powder metallurgy development from Electrolux Rapid Development (ERD) of Rusko, Finland. Nyrhilä invented a novel powder in 1989 for pressureless sintering with a low shrinkage. In 1994, a patent licence and cooperation was agreed between EOS and ERD and the first commercial system, named the EOSINT M250, which made use of a modified version of Nyrhilä’s bronze-nickel-based powder, was installed in 1995. This enabled the direct production of large complex metal parts with high accuracy and good surface finish, a feat not yet accomplished by any other direct metal process by that time. After the introduction of the EOSINT M250, DMLS rapidly became a commercial success. Over the years, the EOSINT M250 underwent some improvements such as increased laser power and improved atmosphere control and in 2004, a completely new system utilising a solid-state fibre laser, the EOSINT M270, saw the light. During this time, EOS entered into an additional licence agreement with 3D Systems whereby EOS acquired the rights to all the relevant patents of DTM and UT [13].

In the early 2000s, Fockele and Schwarze developed a system called “ReaLizer” and named the process “Selective Laser Melting” (SLM). Concept Laser introduced a machine called the M3 Linear during 2001 and named the process “LaserCusing®”. Phenix Systems is a manufacturer of an SLM machine that can print fully dense metal and ceramic parts. 3D Systems however closed its acquisition of Phenix Systems in July 2013. The company paid $15.1 million for 81% of the share capital[16].ARCAM AB® developed a similar process using an electron beam instead of a laser beam. All of the above mentioned machines make use of Housholder’s principle whereby a thin layer of powder is applied onto a platform, exposed by a scanning laser or electron beam which fuses the powder together in the shape of a cross-section of the part, followed by the application of another powder layer and the process repeated until each layer is fused to the previous one. This adoption of DMLS shows that the technology is maturing as an accepted manufacturing process with a high market potential [1,13].

Current metal powder bed AM system technologies can be divided into three main categories according to the way the metal powder is bonded together namely Laser Beam Melting, Electron Beam Melting and Metal Laser Sintering Hybrid Milling.

2.3 Laser Beam Melting

The most widely employed, is laser beam melting, commercially known as DMLS or SLM technology DMLS, LaserCusing® or SLM™ makes use of a laser beam to fully melt the powder particles to form a 3D part. Manufacturers making use of this technology include EOS, Concept Laser, SLM™ Solutions, 3D Systems Corporation (Phenix Systems), ReaLizer and Renishaw.

2.3.1 DMLS – ElectroOptical Systems GmbH, Germany

At the onset of AM in the 1990's, the general purpose of the technology was to make prototypes with the sole aim of reducing product development time and decreasing the period between design and testing. Nowadays, highly complex and functional metal components are being manufactured via AM [17]. DMLS technology, as a typical AM technique, enables the production of three-dimensional (3D) parts directly from metal powder in a short period of time [18]. The DMLS process creates parts in a layer-by-layer fashion by selectively melting thin layers of loose metal powder with a scanning laser beam (figures 2.5 and 2.6). Each scanned layer represents a cross-section of the object's mathematically sliced CAD model.The DMLS process starts off with scanning the first cross-section of the model into the powder that was laid down on the building platform. The powder is melted together as well as melted onto the substrate. Adequate bonding between the first layer of powder and the building platform is extremely important. After the scanning of a cross-section, the building platform is lowered by one layer thickness according to the slice thickness on the CAD model followed by a new layer of powder scraped across the powder bed on top of the building platform by the recoating arm. The process is repeated until the 3D part is completed [19,20,21]. This process allows the production of parts with high accuracy, detail resolution, and good surface quality. Materials available for this process include cobalt-chrome (Co-Cr), stainless steel, titanium alloys, bronze, maraging steel, aluminium (Al) and Inconel.

Challenges for DMLS are: i) manufacturing multi-material objects with engineered lattice structures instead of the bulk material targeting multi-functional performance; ii) using

materials with different particle size distributions; and iii) application of multi-scan strategies by several laser beams [5,22].

The current industrial requirement is to produce parts with a micron-scale resolution and a relief height ranging from hundreds of micrometres up to several centimetres.

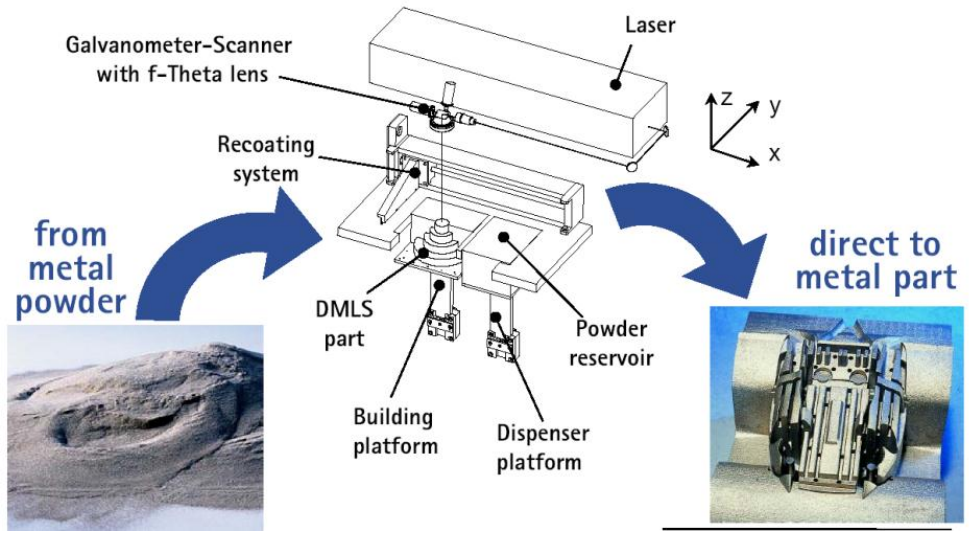

Figure 2.5: Schematic representation of the DMLS process [23]

2.3.1.1 EOSINT M270

The EOSINT M270 (Figure 2.6) is a state of the art DMLSsystem. Fine focusing optics enables excellent detail resolution and part quality. The gas-tight process chamber offers an efficient use of a protective atmosphere which enables a wide range of materials to be processed [23,24].

2.3.1.2 EOSINT M280

The EOSINT M280 (Figure 2.7) is a vast improvement on its predecessor, the M270. The most significant features that set it apart from the M270 is the laminar gas flow across the building platform compared to the turbulent gas flow of the M270. This change not only

improves part quality, but also has a dramatic effect on part quality repeatability. Increased productivity is achieved by reducing cleaning time with the new process chamber that is more ergonomic and easier to clean. A summary of more technical features of the machine can be found in Table 2.1 [25].

Figure 2.6: EOSINT M270 [26]

Figure 2.7: EOSINT M280 [27]

Table 2.1: Technical Data of the EOSINT M270 and M280 [23,25].

	EOSINT M270	EOSINT M280
Building volume (mm – x,y,z)	250 x 250 x 215	250 x 250 x 325
Build rate (mm³/s)	2 – 4	2 – 8
Layer thickness (µm)	20 – 100	20 – 80
Energy source (W)	200(Yb-fibre laser)	200 or 400 (Yb-fibre laser)
Scanning speed (mm/s)	Up to 7000	Up to 7000
Available materials	Bronze, Maraging Steel, Stainless Steel, Co-Cr, Ti,Al	Bronze, Maraging Steel, Stainless Steel, Co-Cr, Ti,Inconel, Al

2.3.2 LaserCUSING®–ConceptLaser GmbH, Germany

2.3.2.1 Concept LaserM1 and M2 CUSING

M1 and M2 CUSING machines produce components with high densities and very good mechanical properties. Automatic powder exchange and good accessibility to the machine is made possible by a mobile powder handling system which also avoids direct contact with the metal powder. Innovative exposure strategies allow higher construction rates and improved component quality. The M2 CUSING is similar to the M1 (Figures 2.8 and 2.9) with the additional feature of being able to process reactive materials such as aluminium and titanium alloys [28].

Figure 2.8: M1 CUSING [29]

Figure 2.9: M2 CUSING [29]

2.3.2.2 Concept LaserM3 Linear

The M3 Linear (Figure 2.10) is a modular concept with two insert modules. One machine is made up of three laser technologies namely LaserCUSING®, 3D laser material erosion and laser marking. Large volume mould inserts can be manufactured in build envelopes of 250 x 250 x 250mm³ up to 300 x 350 x 300 mm³ (x,y,z). A unique system of linear direct drives and mirrors control beam deflection normally associated with fixed optical lenses which leads to elliptical laser beam cross-sections when there is a large deflection over a large building area. This enables high accuracy over a large building envelope. Solid, large volume components with minimal internal stresses can be manufactured with the M3 Linear's patented exposure strategy. More technical features can be found in Table 2.2 [28].

2.3.2.3 Concept LaserMlabCUSINGR

The MlabCUSING R (Figure 2.11) is the fourth and most recently added machine to the Concept Laser line up of machines. The MlabCUSING R can produce parts in titanium as well as cobalt-chromium, stainless steel and precious metals such as silver and gold. It has a pull-out drawer system that holds the building platform, powder dispensing- and collector modules. The small 50 W laser spot size diameter of less than 25 µm and layer thickness of 15 µm enables the manufacturing of fine structures and excellent surface quality, making this system ideal for the production of complex parts such as jewellery. The small footprint of only 705 mm wide and 240V single phase powered machine makes it ideal for any environment [28].

Table 2.2: Technical Data of the Concept Laser range of machines [28].

	M1 CUSING	M2 CUSING	M3 Linear	MlabCUSING R
Building volume (mm³ – x,y,z)	250 x 250 x 250	250 x 250 x 280	Up to 300 x 350 x 300	90 x 90 x 80 70 x 70 x 80 or 50 x 50 x 80
Build rate (cm³/h)	2 – 10	2 – 20	2 – 20	1 – 5
Layer thickness (µm)	20 – 80	20 – 50	20 – 80	15 – 50
Energy source (W)	200 (fibre laser)	200 (fibre laser)	100 (diode-pumped solid state laser)	50 / 100
Scanning speed (mm/s)	Up to 7000	Up to 7000	Up to 7000	Up to 7000
Available materials	Stainless Steel, Hot-work steel, Inconel	Stainless Steel, Hot-work steel, Ti,Inconel, Al	Stainless Steel, Hot-work steel	Stainless Steel, Co-Cr,Ti, gold, silver

	
Figure 2.10: M3 Linear [30]	Figure 2.11: MlabCUSING R [28]

2.3.3 Selective Laser Melting –SLMSolutions GmbH, Germany

During 2011, MTT Technologies Group separated its German and United Kingdom branches. The German branch formed a privately owned company; SLM Solutions GmbH and theUnited Kingdom branch formed the company Renishaw plc. MTT Technologies Group was a spin-off company from MCP-HEK Tooling GmbH that took over commercialisation of the SLM technology from Fockele and Schwarze [31,32].

2.3.3.1 Laser Beam Melting System SLM® 125HL

Small series production is made possible with this highly economical system. It is also well-suited for a research environment. The patented bi-directional powder loader movement makes the SLM® 125HL (Figure 2.12) the fastest system in its class. The system offers a safe-filter system and highly effective inert gas consumption made possible by internal recirculation of the protective gas at laminar flow [33].

2.3.3.2 Laser Beam Melting System SLM® 250HL

The modular design of the SLM® 250HL (Figure 2.13) is divided into various sectors that can be individually serviced, replaced or extended, making it ideal for a manufacturing environment. The building platform can be heated to 200°C and has a maximum Z-direction travel of 350 mm. The SLM® 250HL also makes use of the patented bi-directional loader movement that recoats powder in two directions and of the safe-filter system [34].

2.3.3.3 Laser Beam Melting System SLM® 280^{HL}

The SLM System 280^{HL} (Figure 2.14) makes use of a unique double beam technology together with the optics with the highest quality lenses that not only improves the laser beam profile but also the quality of the components manufactured in this system. The SLM® 280^{HL} provides a building chamber with a size of 280 x 280 x 350 mm³. The SLM® 280^{HL} is equipped with a 400 W fibre laser and newly added 1 KW fibre laser. The SLM® 280^{HL} also makes use of the patented bi-directional loader movement and safe-filter system similar to that of the SLM® 125^{HL} and SLM® 250^{HL} [35].

2.3.3.4 Laser Beam Melting System SLM® 500^{HL}

The SLM System 500^{HL} (Figure 2.15) provides a large building platform with a size of 500 x 280 x 325 mm³ together with double beam technology. Both fibre lasers (400 W or 1000 W option) work on the powder bed simultaneously. The SLM® 500^{HL} makes use of a shell-core-building strategy with two different beam profiles that can be used separately but also simultaneously during the process which in turn will improve productivity. Due to the increased volumes and weights, the movement of powder to the machine is realised by an automated continuous conveying system. This eliminates the manual handling of bottles and containers to fill the system [36]. A summary of technical data for each of the four models in the SLM® range can be found in Table 2.3.

Figure 2.12: SLM® 125^{HL} [37]

Figure 2.13: SLM® 250^{HL} [38]

Figure 2.14: SLM® 280HL [39]

Figure 2.15: SLM® 500HL [40]

Table 2.3: Technical Data of the SLM® range of systems [33-36].

	SLM® 125HL	SLM® 250HL	SLM® 280HL	SLM® 500HL
Building volume (mm³)	125 x 125 x 75 (125)	248 x 248 x 250 (350)	280 x 280 x 350	500 x 280 x 325
Build rate (cm³/h)	15	20	35	70
Layer thickness (µm)	20 – 75	20 – 75 (100)	20 – 150	20 – 200
Energy source (W)	100/200 (Fiber Laser)	400/1000 (Fiber Laser)	400/1000 (Fiber Laser)	X2 400/1000, (max 2800) (Fiber Laser)
Scanning speed (mm/s)	20 000	20 000	15 000	15 000
Available materials	Ti, Al, Co-Cr Stainless Steel, Tool Steel, Super Alloys	Ti, Al, Co-Cr Stainless Steel, Tool Steel, Super Alloys	Ti, Al, Co-Cr Stainless Steel, Tool Steel, Super Alloys	Ti, Al, Co-Cr Stainless Steel, Tool Steel, Super Alloys

2.3.4 Selective Laser Melting–PhenixSystems, France

Phenix Systems, with its patented technology, is positioned as a specialist in the field of AM providing them with a competitive advantage. Phenix Systems is the only manufacturer that offers the possibility to process both metallic and ceramic powders. Attention to ergonomics is visible across the complete PX-Range of systems. Each of the three models (PXS, PXM and PXL) (Figures 2.16-2.18) was developed witha specific technico-economic environment in mind. Safe powder handling constitutes one of the major advances benefiting users. Technical data of the Phenix range can be found in Table 2.4 [41].

Figure 2.16: Phenix PXS [42]

Figure 2.17: Phenix PXM [43]

Figure 2.18: Phenix PXL [44]

Table 2.4: Technical Data of the Phenix PXS, PXM and PXL systems [41].

	PXS	PXM	PXL
Building volume (mm^3)	100 x 100 x 80	140 x 140 x 100	250 x 250 x 300
Build rate (cm^3/h)	n/a	n/a	n/a
Layer thickness(µm)	Adjustable (10 – 30)	Adjustable (10 – 30)	Adjustable (10 – 30)
Energy source (W)	50 (fibre laser)	300 (fibre laser)	500 (fibre laser)
Scanning speed (mm/s)	3000	n/a	n/a
Available materials	Non-ferrous alloys, Stainless Steel, Tool Steel,Super Alloys, Ceramics	Non-ferrous alloys, StainlessSteel,Tool Steel,Super Alloys, Ceramics	Non-ferrous alloys, Stainless Steel,Tool Steel,Super Alloys, Ceramics

2.3.5 Selective Laser Melting–ReaLizerGmbH, Germany

2.3.5.1 ReaLizer SLM™ 50

The ReaLizer SLM™ 50 (Figure 2.19) is a desktop metal AM machine. This system has been designed for the manufacturing of small components with a diameter of up to 70 mm and a height of up to 40 mm. Being the developers of SLM, ReaLizer launched the first world-wide SLM™ machine for metal AM components in 1999 [45].

2.3.5.2 ReaLizer SLM™ 100

The ReaLizer SLM™ 100 (Figure 2.20) is ideal for smaller components where high precision and surface quality is required. The system has a building platform of 125 x 125 x 100 mm^3z-height possibility. This construction area enables the system to focus the laser beam diameter to 20 µm that can produce delicate structures and thin walls down to 60 µm. The

ReaLizer SLM™ 100 with its compact design is well-suited for use in laboratories and small environments [46].

2.3.5.3 ReaLizer SLM™ 250

The ReaLizer SLM™ 250 (Figure 2.21) has a construction space measuring 250 x 250 x 300 mm³ that makes it ideal for laboratories as well as the industrial production of components. A high-capacity 600 W laser can be fitted to this system if a high-quantity component output is the main focus for the employment of this machine. ReaLizer also offers an automated sieving machine with a powder removal system, which recycles the powder from the construction area. An optional exchangeable lens system is available that enables a higher focus (20 µm) to produce delicate structures with exceptional high surface quality [47]. More technical details can be found in Table 2.5 below [45-47].

Figure 2.19: ReaLizer SLM™ 50 [48]

Figure 2.20: ReaLizer SLM™ 100 [48]

Figure 2.21: ReaLizer SLM™ 250 [48]

Table 2.5: Technical Data of the three ReaLizermetal AM systems [45-47].

	SLM™ 50	SLM™100	SLM™ 250
Building volume (mm^3)	70x70x40	125x125x100	250x250x300
Build rate (cm^3/h)	n/a	n/a	n/a
Layer thickness (µm)	20 – 50	20 – 100	20 – 100
Energy source (W)	20 – 120 (fibre laser)	100 / 200(fibre laser)	200 / 400 / 600 (fibre laser)
Scanning speed	n/a	Up to 2000	Up to 2000
Available materials	Co-Cr, Stainless Steel, Au, Ag, Ti - alloys	Tool Steel, Stainless Steel, Inconel, Al, Au, Ti, Co-Cr, Ceramic materials (under development)	Tool Steel, Stainless Steel,Al, Ti, Inconel, Au, Co-Cr

2.3.6 Selective Laser Melting – Renishawplc, United Kingdom

Renishawplc, formerly known as the United Kingdom branch of MTT Technologies Group, purchased the line of machines from MTT in 2011 [31,32].

Renishaw'ssystems (AM125 and AM250) are capable of producing fully dense metal parts making use of a high-powered fibre laser (figures 2.22 and 2.23). Components are manufactured from a wide range of fine metal powders that are melted in a controlled atmosphere, in layer thicknesses ranging from 20 to 100 microns. These systems are widely employed for the manufacture of customised medical implants, efficient heat exchangers, lightweight aerospace- and motor-sport components, and injection moulding inserts with conformal cooling channels. Safe processing of reactive materials such as titanium and aluminium is a standard feature on all Renishaw laser melting systems. Machine users also benefit from minimal waste product as over 98% of the unmelted material is re-usable after refinement with the Renishaw powder conditioning system. Technical data of the Renishaw's laser melting AM systems can be found in Table 2.6 [49].

Table 2.6: Technical Data of the Renishaw AM125 and AM250 systems [49].

	AM125	AM250
Building volume (mm³)	120x120x125	245x245x300
Build rate(cm³/h)	5 – 20	5 – 20
Layer thickness(µm)	20 – 100	20 – 100
Energy source (W)	100 / 200 (fibre laser)	200 / 400 (fibre laser)
Scanning speed (mm/s)	Up to 2000	Up to 2000
Available materials	Stainless Steel, Tool Steel, Co-Cr, Inconel, Ti, Al	Stainless Steel, Tool Steel, Co-Cr, Inconel, Ti, Al

Figure 2.22: Renishaw AM 125 [50]

Figure 2.23: Renishaw AM 250 [51]

2.3.7 Selective Laser Melting – 3DSystems Corporation

3D Systems has been selling the Renishaw line of machines in the United States under their own brand since 2008 known as the sPro™ 125 and sPro™ 250 (figures 2.24 and 2.25). These machines provide the company's main technology for manufacturing metal components [31,32,52]. Technical specifications can be found in Table 2.7.

Table 2.7: Technical Data of the sPro™ 125 and sPro™ 250 from 3D Systems [52].

	sPro™ 125	sPro™ 250
Building volume (mm³)	125x125x125	250x250x320
Build rate(cm³/h)	5 – 20	5 – 20
Layer thickness(µm)	20 – 100	20 – 100
Energy source(W)	100 or 200 (fibrelaser)	200 or 400 (fibrelaser)
Scanning speed (mm/s)	Up to 1000	Up to 1000
Available materials	Stainless Steel, Tool Steel, Co-Cr, Inconel, Ti, Al	Stainless Steel, Tool Steel, Co-Cr, Inconel, Ti, Al

Figure 2.24: 3D Systems sPro™ 125[53]

Figure 2.25: 3D Systems sPro™ 250[54]

2.4 Electron BeamMelting (EBM)

The second technology category is EBM. EBM employs a powerful electron beam as energy source to melt the powder material to create a physical part. The only manufacturer to make use of this patented technology is ARCAM AB® [13].

2.4.1 ARCAM AB®, Sweden

2.4.1.1 ARCAM A1

The ARCAM A1 (Figure 2.26) is an AM machine specifically designed for cost effective production of both standard and custom medical implants. The A1 has easy powder handling that ensures a fast cycle time. A high cooling rate of the completed job results in a shorter turnaround time to start the next job. An insulated powder bed also increases the build rate. ARCAM's patented MultiBeam™ technology allows the improvement of the surface quality.

The EBM technology enables high productivity by making use of high energy which in turn provides a high melting capacity. Medical implants are manufactured at increased temperatures and in a vacuum environment resulting in stress relieved implants with material properties comparable to the wrought material [55].

2.4.1.2 ARCAM A2

The ARCAM A2 (Figure 2.27) is the ultimate solution for AM in the digital age. It is developed for cost-effective production of demanding applications such as structural aerospace components, meeting the highest material standards [56]. The large build volume of the A2 enables the manufacturing of large components. The A2 has a simple and easy to use operator interface and also includes Logstudio™, a tool for process validation and quality control. MultiBeam™ technology ensures high productivity and surface quality. Another special feature of the A2 is the two interchangeable build tanks delivered with each machine giving a choice between "wide" and "tall" depending on the build at hand.A summary of all technical details of the A1 and A2 can be found in Table 2.8.

Table 2.8: Technical Data of the ARCAM A1 and A2 systems [55,56].

	A1	A2
Building volume (mm³)	200 x 200 x 180	250 x250 x 400 (tall) 350 x 350 x 250 (wide)
Build rate (cm³/h)	55 to 80	55 to 80
Layer thickness(µm)	50	50 to 200
Energy source (W)	50 – 3000 (electron beam)	50 – 3500 (electron beam)
Scanning speed(mm/s)	Up to 8000 000	Up to 8000 000
Available materials	Titanium alloys	Titanium alloys

Figure 2.26: ARCAM A1 [57]

Figure 2.27: ARCAM A2 [58]

2.5 Metal Laser Sintering Hybrid Milling Machine

The third technology category identified is a patented hybrid technology usinglaser sintering as well as high-speed milling. The Matsuura Company patented this unique technology and in 2003 production and distribution of metal laser sintering hybrid-milling machines began [59].

2.5.1 Matsuura, Japan

2.5.1.1 Matsuura LUMEX Avance-25

A decade of research and development by Matsuura, Japan, resulted in a unique one-step solution to AM, namely the LUMEX Avance-25 metal laser sintering/high speed milling hybrid machine (Figure 2.28). More technical specifications are summarised in Table 2.9 [59].

Table 2.9: Technical Data of the Matsuura LUMEX Avance-25 machine [59].

	LUMEX Avance-25
Building volume (mm³)	260x260x100
Build rate	n/a
Layer thickness(µm)	50
Energy source (W)	400 (fibre laser)
Spindle speed (rpm)	45 000
Scanning speed (mm/s)	n/a
Available materials	Tialloys, Stainless Steel

Figure 2.28: Matsuura LUMEX Avance-25 [60]

2.6 Conclusions

When considering all of the above mentioned MAM systems, one can clearly see that the diversity of the systems available caters for industry-specific requirements. Some will produce parts with outstanding surface quality; others specifically produce parts with a rough surface in order to fulfil a niche market such as bone ingrowth into an implant also known as osseo-integration. Some systems make use of innovative concepts in order to increase productivity whereas others focus on high precision to create specialised structures.

At the stage when this research project started, only two different MAM systems were available in South Africa, namely a Concept Laser M2 at the University of Stellenbosch and an EOS M270 available at the Central University of Technology (CUT), Free State located in Bloemfontein. It was decided to focus this study on the closest available MAM system, which was the EOS M270. CUT focuses on the manufacturing of medical implants by means of DMLS, and in particular making use of titanium. The next chapter will investigate titanium andexplain why it is a material of choice across the manufacturing arena when it comes to specialised applications.

CHAPTER 3
TITANIUM AND ITS APPLICATIONS

3.1 Introduction

There is increasingly more interest in processing titanium on metal powder bed systems as described in Chapter 2. The reason that titanium has grown in popularity amongst the manufacturing industry in recent years is mainly due to its unique metallurgical properties such as high strength, low density, corrosion resistance, high operating temperatures and bio-compatibility [61]. For the purpose of this chapter, the history of titanium will be reviewed as well as typical applications of the metal. Furthermore, this chapter will give an overview of titanium in the AM environment, focussing firstly on the typical problems associated with the process, secondly explaining how the powder particles are characterised and lastly looking at the granulomorphometric analysis of the powder particles. The final portion of this chapter is dedicated to previous work done that was found in literature relating to the processing of titanium by means of the DMLS process.

3.2 History of titanium

William Gregor, an amateur mineralogist, initially discovered titanium in dark magnetic iron sand called “ilmenite” in 1791. The metal was given the name “titanium” with reference to the titans of Greek mythology, symbols of enormous power and strength. Titanium was not used often during this time mainly due to the difficulty of extraction from the ore. The commercialisation of the Kroll process in 1950 made the recovery of the metal from the ore easier. Titanium is the ninth most abundant element in the earth’s crust and is the fourth most abundant metallic element. Titanium is number 22 on the Periodic Table of Elements, has an atomic weight of 47.9, and is represented by the symbol “Ti”. The element itself is found in the forms of rutile (a natural oxide, TiO_2) and ilmenite (a mixed oxide with iron, $FeTiO_3$). Today the rutile is generally mined in Australia and South Africa [61,62,63].

3.3 Properties and applications of titanium and titaniumalloys

Titanium’s structural efficiency and corrosion resistance makes it the metal of choice for many diverse applications including aerospace, industrial, chemical processing, marine, medical, sporting, and consumer goods. Titanium’s structural qualities are a direct result of

its high strength and low density. Titanium alloys are tailored specifically by altering the alloy chemistry in order to obtain optimal properties to meet the need for specific end-use applications. The higher melting temperature of titanium makes it the material of choice over aluminium in structural applications where temperatures exceed 130°C to 150°C [61]. Due to the bio-compatibility of titanium and its alloys, the metal is used extensively in the human body [64].

3.3.1 Aerospace

Some of the principal justifications for making use of titanium in the aerospace market include: weight reduction, operating temperature, space limitations and corrosion resistance. Due to titanium's high strength-to-weight ratio, weight saving becomes an obvious application. The lower density of titanium compared to steel permits weight savings despite titanium having higher strength. Titanium can also replace aluminium when the operating temperatures exceed 130°C which is the normal operating temperature of aluminium. These conditions exist for instance in the wing anti-icing systems of airframe structures. Perfect examples of making use of titanium where space is limited can be found on the landing gear beams of the Boeing 747, 757 and 777 (Figure 3.1).

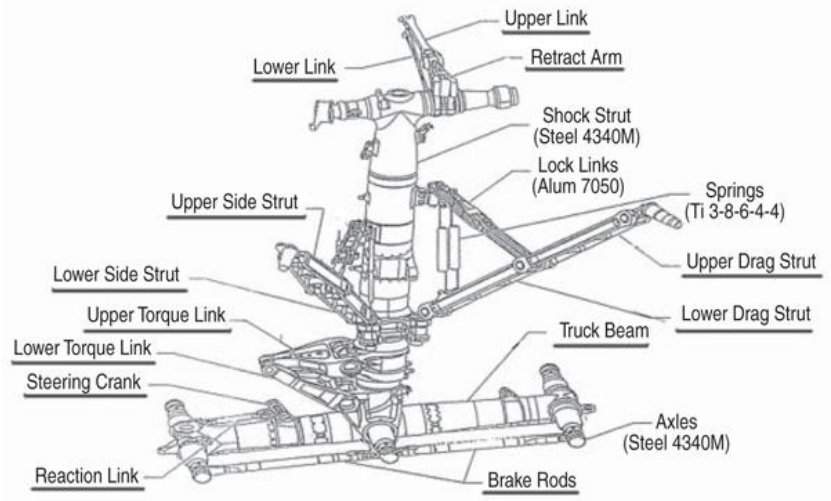

Figure 3.1: Boeing 777 main landing gear titanium forging applications (all labelled parts are Ti-10V-2Fe-3Al) [65]

The Boeing 747 landing gear beam is one of the largest titanium forgings produced. The ideal material for this application would have been an aluminium alloy, mainly because the cost would be lower. However, in order to carry the required loads, the aluminium component would not fit within the wing where it retracts. The corrosion resistance of

titanium is as such that corrosion resistant coatings or paint are not required making it the ideal material for the high corrosion environment of the floor support structure beneath the galleys and lavatories, providing high structural durability [66].

3.3.2 Marine

The high corrosion resistance of the titanium makes it an ideal choice for marine applications with specific reference to engineering structures for the extraction of hydrocarbons in offshore areas. Under the aforementioned conditions, the material needs to have a wide range of performance and strength characteristics under static, cyclic and dynamic loading. Another requirement for marine applications is cold resistance within a temperature range of up to minus 50°C. Titanium is readily used for the manufacturing of deep water risers and piping, pumps and filters of sea water systems, heat exchanging equipment, hull structures of deep-water equipment and high pressure vessels [67].

3.3.3 Consumer products

Consumer market-related applications did not develop at the expected rate when titanium was first industrialised. In the early 1980's, the Ford Motor Company in the United States of America (USA) seriously started to investigate titanium; evaluating the material for possible applications in suspension springs, valves and valve springs. Unfortunately, titanium was not adopted for large volume production models and was limited to optional components on high-performance models and concept cars. Titanium was used to a lesser extent in sporting equipment such as skis, tennis rackets and golfing equipment. The most recent major application was in the development of titanium driver golf club heads [68]. The first titanium golf club head was made in 1990 at a high cost. Cost reductions and expansion of the market helped with a widespread adoption of this application. Driver clubs that have large volumes can be manufactured from titanium due to its high specific strength. The inertia moment of the club head increases as the volume of the head increases which in turn provides a wide "sweet spot" and stable directionality. The decrease in weight of the club head also enabled the use of a longer shaft that also increases the swing speed to optimise carry distance with a high trajectory (Figure 3.2) [69]. An interesting application in the sporting goods market was the announcement by the company Wilson of their Titanium Tennis Ball (Figure 3.3). This tennis ball is made from an advanced rubber compound, featuring a titanate powder coupling agent to bond all the materials in the tennis ball core into a cohesive unit. This is said to improve durability, consistency and performance of the ball [70].

	
Figure 3.2: Example of one of the first titanium drivers introduced byTaylorMade® in 1997 [71]	Figure 3.3: First tennis balls in the world utilising titanium introduced byWilson [70]

3.3.4 Energy industry

Energy extraction from the earth's crust via hydrocarbon and hot geothermal brine production necessitates containment and handling of severely corrosive fluids and demands high-performance well components to operate in these adverse environments. General trends in the energy industry under current development include increasing well depths, increasing reservoir fluid temperatures and pressures as well as higher brine acidity and chlorine levels. The above mentioned extreme well environments pose great material, technological and economic challenges to the energy industry. These challenges have been met through the improvement and qualification of cost and performance optimised titanium alloys designed to fully resist these harsh natural environments. Successful utilisation of these improved products can be found in geothermal brine well production, offshore riser taper stress joints and deep water offshore drilling. Recent applications include dynamic offshore risers and flexible drill pipes for special drilling applications (figures 3.4 and 3.5) [72].

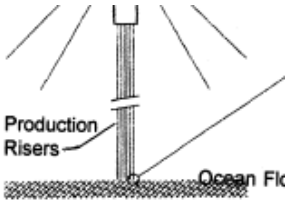	
Figure 3.4: Titanium alloy taper stress joints in offshore floating platform riser systems [72]	Figure 3.5: The first ever titanium alloy taper stress joint which was successfully employed in the Placid Oil Canyon productionriser system in the Gulf of Mexico [72]

3.3.5 Biomedical applications

The evaluation of titanium as a surgical implant material soon followed its commercial introduction around 65 years ago. Titanium's excellent bio-compatibility was established by Bothe et al. [73] and Leventhal [74] during the 1940's and 1950's. Commercial pure titanium offered higher corrosion resistance and bio-compatibility compared to stainless steel but its comparatively lower strength and wear properties limited its use to pacemaker cases, heart valve cages and reconstruction devices. The introduction of Grade 5 Titanium or Titanium-6Aluminium-4Vanadium (Ti-6Al-4V) in the late 1970's opened up the possibility for total joint replacements due to its high strength, low elastic modulus, corrosion resistance and bio-compatibility. Current applications include hip and knee prostheses, trauma/fixation devices such as screws, wires, nails and plates, instruments and dental implants (figures 3.6 and 3.7) [75]. Parts built from this alloy can be machined, spark-eroded, welded, micro-shot-peened, polished, and coated if required. The bio-compatibility of Ti-6Al-4V makes it ideal for medical applications [76].

Figure 3.6: Front view of a total knee replacement titanium implant with a high density polyethylene wearing surface [77]

Figure 3.7: Side view of a total knee replacement titanium implant showing its placement on the femur and tibia [77]

3.4 Processingof titaniumthrough AM

AM of titanium components, especially in the form of Ti-6Al-4V alloy, has seen major advances during the past ten years. Complex net-shaped metal components are now directly manufactured layer-upon-layer from titanium powder. This manufacturing technique cuts down on extensive machining and material costs can be reduced due to the fact that AM produces a lot less waste compared to conventional subtractive manufacturing techniques [78].

3.4.1 Challengesassociated with processing metal powder through DMLS

3.4.1.1 Process parameters

To process a metal material such as Ti-6Al-4V by means of DMLS is a complicated process, and several parameters take effect on the DMLS process [5,19,79,80,81]. Processing parameters such as laser power, scan speed, scan line spacing (hatching), thickness of layer, scanning strategy, working atmosphere and powder bed temperature have an effect on material properties of objects manufactured by DMLS. Chemical composition, thermal-, optical-, metallurgical-, mechanical- and rheological characteristics of material also play a significant role in DMLS (Figure 3.8) [5]. Process parameters can be defined as variables

that influence and control the laser sintering process and determine the amount of energy delivered to the surface.

Recent advances have improved DMLS significantly; however, many defects still hinder the successful manufacturing of commercially acceptable metal components with adequate microstructure and material properties. The aforementioned defects are mainly caused by the poor understanding of the complex non-equilibrium nature of the DMLS process. Typical defects associated with DMLS include porosity, distortion and delamination [18]. Some of the more modern AM machines try to address these shortcomings by ensuring a cleaner processing area, higher bed temperatures and optical monitoring systems.

3.4.1.2 Material properties

Material properties include chemical constitutions and the purity of the material (oxygen, carbon and nitrogen content), the method of alloying (elemental or pre-alloy) and lastly the particle characteristics (size, distribution and shape) (Figure 3.8).

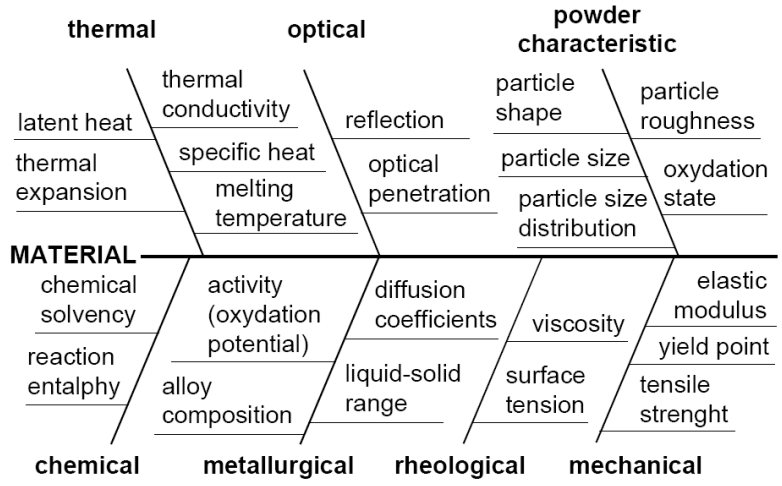

Figure 3.8: Material-based input parameters in AM [79]

The characteristics of the powder material that is used are of special concern for AM. Powder size distribution and morphology of powder particles have an effect on the powder layer deposition and fusion process as a whole. Irregularities in powder layer and anisotropic orientation of powder particles can provoke non-uniform shrinkage and formation of the pores in the final part, which is undesirable in AM. Finer particles provide a larger surface area to absorb more laser energy, thereby increasing the particle temperature and the sintering kinetics [82,83]. The large quantity of small particles results in a greater specific

surface area which increases the friction between particles and subsequently decreases the apparent density and increases agglomeration. Agglomeration in turn can cause amplification of the reflectivity of the powder bed thereby reducing the amount of energy absorption and densification kinetics [84]. Certainly, humidity plays an important role in powder deposition. Therefore, the powder is heated up to +80°C for the duration of 12 hours, and then cooled in the chamber.

Powder morphology refers to the shape of the individual powder particles. A small sample of Ti-6Al-4V powder (sub 45µm from TLS GmbH) was analysed by means of scanning electron microscopy[1] (SEM) which was carried out with a Tescan Vega 3 at 20 kV accelerating voltage and 15–20 mm working distance. In the SEM photographs it is clearly seen that the most of the Ti-6Al-4V powder particles have a high sphericity (figures 3.9a and 3.9b).

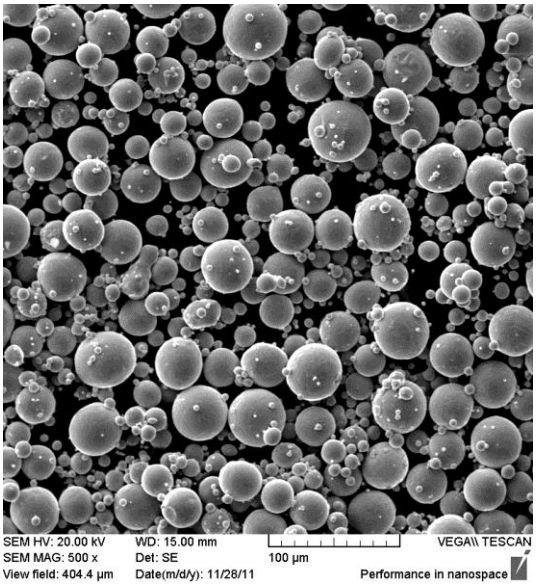

Figure 3.9a: SEM photograph of TLS powder at×500 magnification

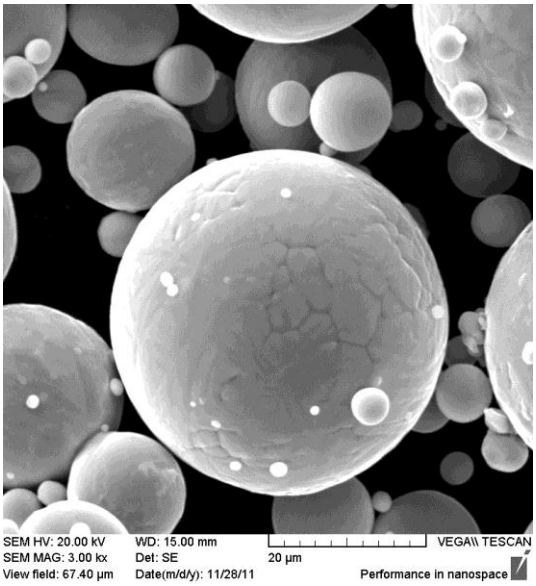

Figure 3.9b: SEM photograph of TLS powder at×3000 magnification

[1]SEM analysis was carried out at the National Engineering School of Saint-Etienne's (ENISE) Laboratory of Diagnostics and Engineering of Industrial Processes (DIPI) in France.

3.4.2 Consolidation of Ti-6Al-4V powderthrough DMLS

Since AM is a layer-by-layer manufacturing technique, the quality of the deposited layer is of prime importance for the DMLS process. The layers must be deposited at a constant thickness; thicker regions, insufficiently attached to the previous sintered layer, can provoke pore formation. Yadroitsev [5] showed that for the first layer of stainless steel 316L (sub 25 µm) powder deposited on a stainless steel substrate by the Phenix System deposition module (roller), an arithmetic mean of 40 ± 3.91 µm for total height of roughness profile (R_t) was achieved (Figure 3.10).

Since the thickness of a deposited layer determines how much powder will be involved in the melting process by a single laser scan, irregularities in the deposited layer can have an effect on the geometrical characteristics and shape of single tracks and therefore could result in imperfections such as porosity, inaccuracy and a rough surface finish in 3D objects.

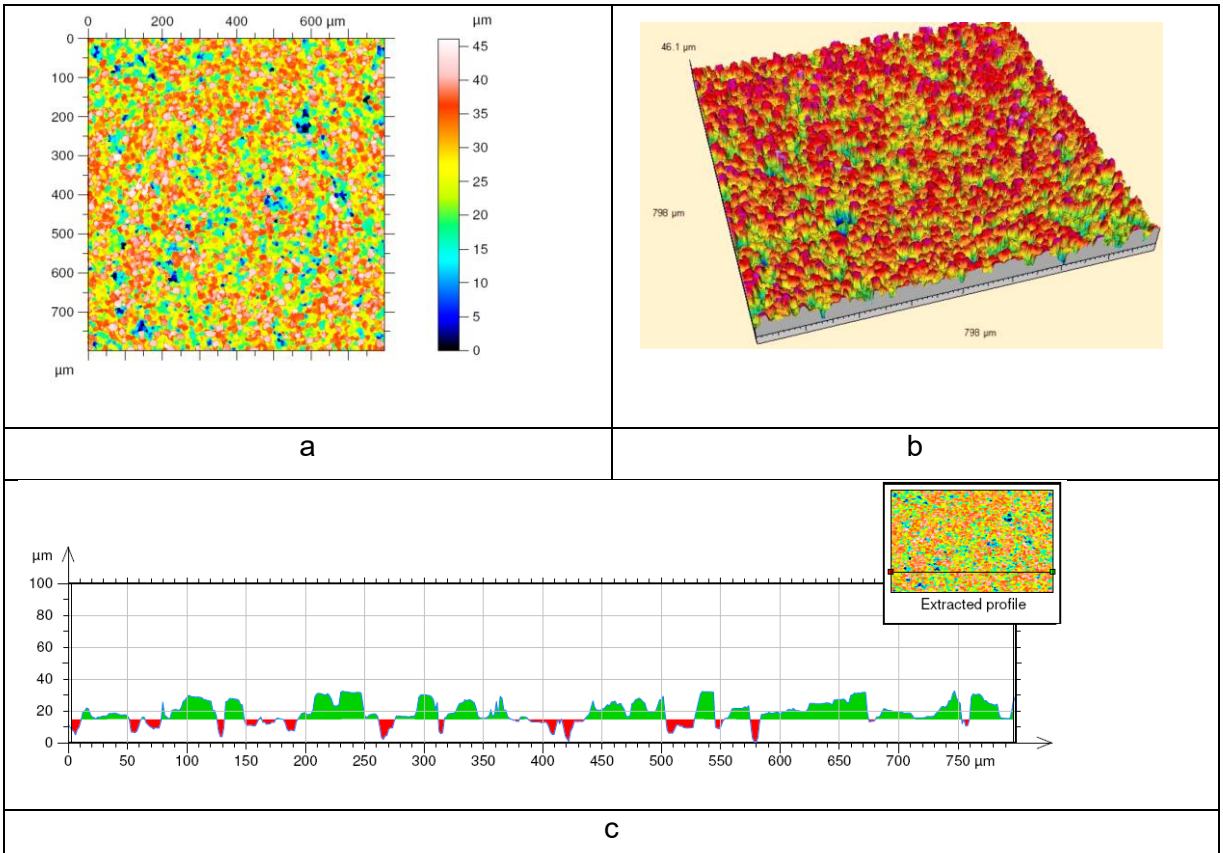

Figure3.10: Premier layer height-view (a), 3D image(b), and profile of the layer from stainless steel grade 316L (c) [5]

During DMLS, a laser beam scans over the thin powder layer preplaced on the substrate and it melts powder and substrate material. Under the effect of surface tension, the melt pool takes the shape of a circular or segmental cylinder. Melt hydrodynamics plays an important role in shape pool features. Fragmentation of the melted tracks is a well-known drawback of DMLS, referred to as the “balling” effect [85]. Balling occurs when the melted powder does not bind to the building platform or previous sintered layer thereby forming small spheres or balls due to surface tension. This balling effect has a great influence on the thermodynamic and kinetic characteristics during melting. DMLS is carried out track-by-track and this balling effect causes the formation of uneven and discontinuous tracks. It can contribute to the uneven deposition of a new powder layer that in turn can cause poor inter-layer bonding between the consecutive layers [19].

The tracks’ stability depends on the laser power, scanning speed, powder layer thickness, substrate material, physical properties and granulomorphometry of the powder used. Each cross-section (layer) of the part is sequentially filled with elongated tracks of melted powder. Figure 3.11 shows photographs of a single track made from metal powder formed on a stainless steel substrate. A light halo around the sintered track indicates the effect of denudation of the substrate owing to the fact that not only the powder in the laser irradiation zone is involved in the process of single track formation, but also the powder from the adjacent areas [5].

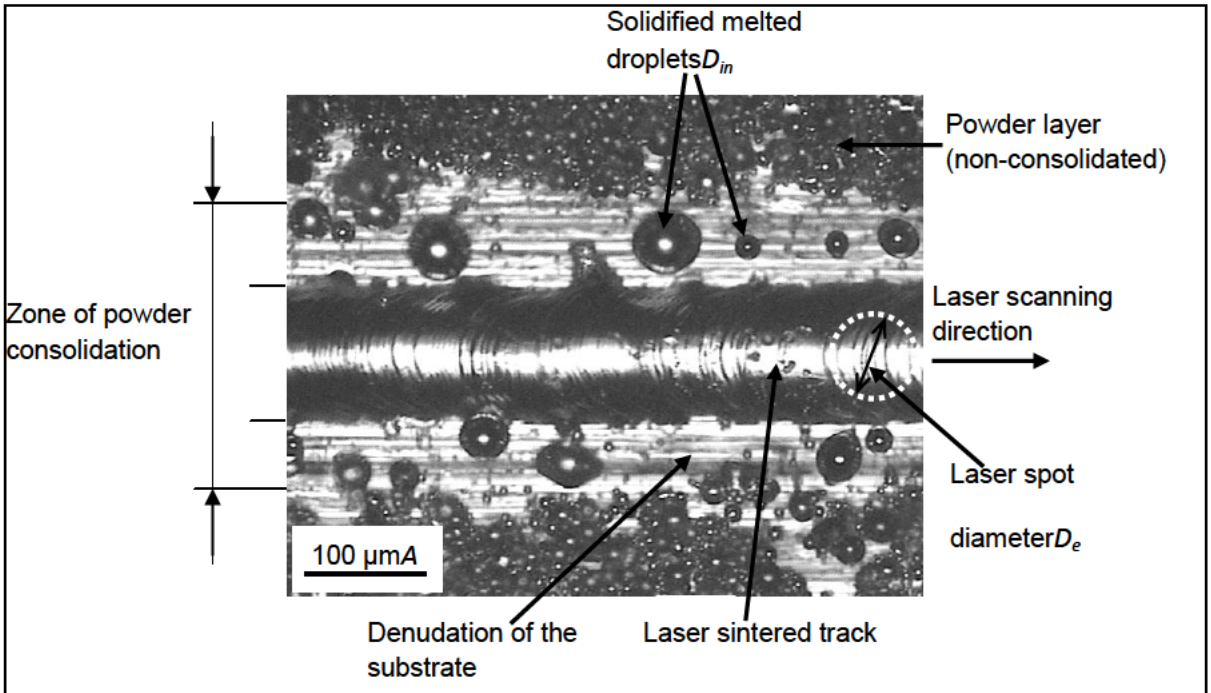

Figure 3.11: Top view of a laser sintered track made from stainless steel grade 316L (sub 25 µm) powder on stainless steel substrate. Laser power is 50 W, scanning speed is 100 mm/s, thickness of the deposited powder layer is 40 µm [5]

According to Rońda and Siwek [86], laser welding can take place via two routes, namely, the conduction- or keyhole modes, depending on the energy density of the laser beam. During low power density, energy transport follows the conduction mode. At a higher power density (related to the slow scanning speeds), the energy transport follows the keyhole mode and causes material to evaporate from the laser interaction region that leads to the creation of a deep and narrow “keyhole”.

The hydrodynamics of the melt pool is complicated with different regimes of keyhole and melt pool occurring (figures 3.12 and 3.13). Rippling or humping is determined by the formation of a capillary wave on the free surface. Under surface tension, the pressure differences created at a curve interface support deformation of the interface.

Wei [87]indicated the following mechanisms of instability of the melt pool:

- Kelvin-Helmholtz instability due to difference in velocities between gas and liquid;
- Rayleigh-Taylor instability due to density differences, when a heavier liquid overlies a lighter liquid;
- Rayleigh capillary instability due to capillary pressure difference;
- Morphological instability due to solute super saturation;
- Thermocapillary instability produced by surface tension gradient;
- Evaporation instability provoked by evaporation pressure difference;
- Hydraulic jump occurring when the pressure gradient becomes increasingly adverse as the flow proceeds downstream;
- Laser interaction: polarisations;
- Gravitational-electromagnetic instability;
- Interactions between gravitational and electromagnetic forces.

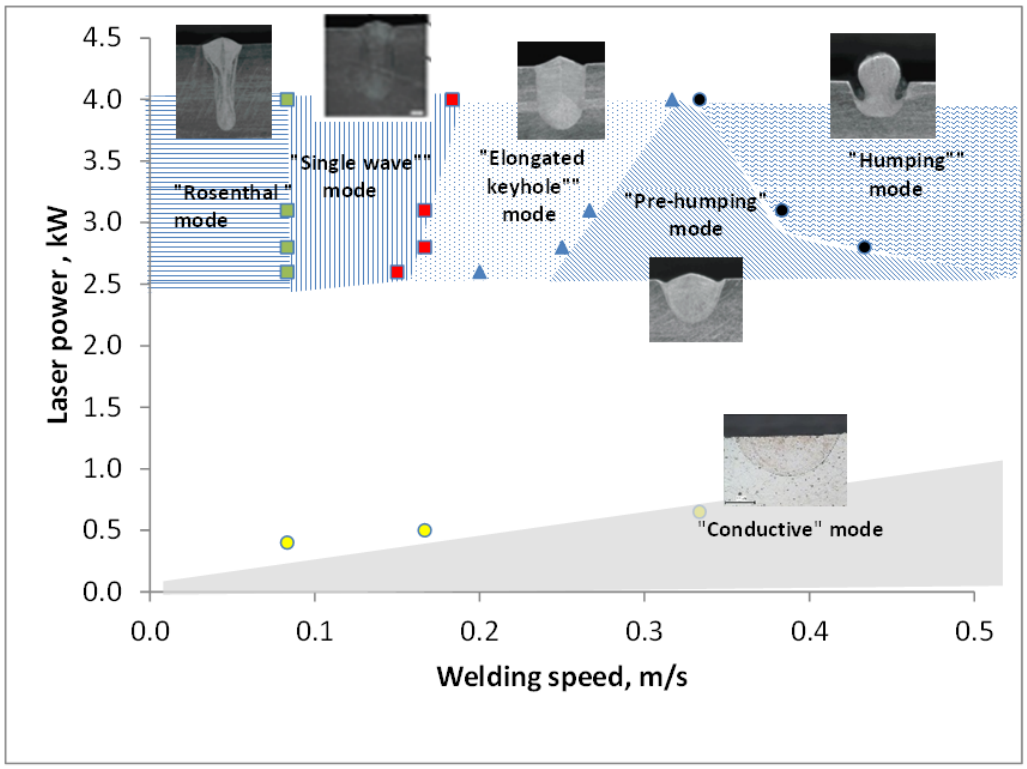

Figure 3.12: Regimes (modes) of 304 steel welding [88]. Power density ($\frac{P}{\pi D^2/4}$) for 2.5 - 4 kW and spot size 450 μm is 1.57-2.52 mW/cm^2

It was shown that by increasing the scanning speed, the geometrical size of the melt pool was changed: the length of melt pool became longer and shallower. Capillary waves on the surface occurred. High laser power caused higher temperature and fair-sized melt pool [5]. Higher temperature provoked a decrease in viscosity; therefore hydrodynamics of the melt pool became more expressed for higher laser power. For 50 W laser power with 70 µm spot diameter, humping effects and keyhole modes were not found [5] (Figure 3.14). Yadroitsev et al [5] developed a melt pool simulation programme to predict the size, shape and temperature of the melt pool. This programme will be discussed in the next chapter.

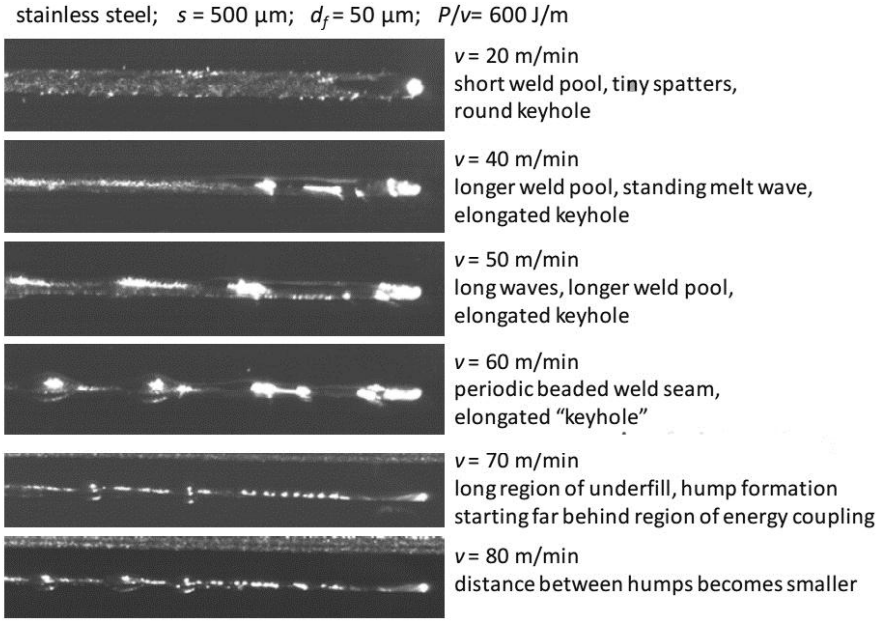

Figure 3.13: Appearance of keyhole and melt pool with increased scanning speed [89]

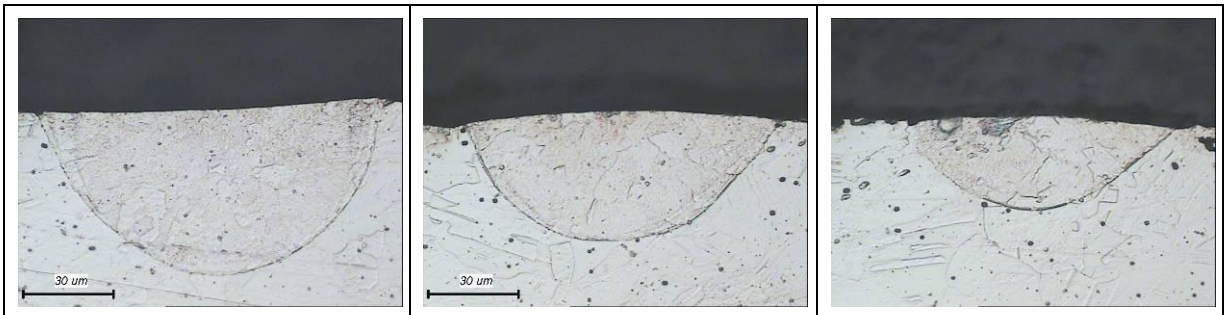

60mm/s	120mm/s	280mm/s

Figure 3.14: Cross-section of tracks on steel 304L. P=50 W for different scanning speeds V=60, 120 and 280 mm/s. Power density ($\frac{P}{\pi D^2/4}$) is 1.3 mW/cm^2[5]

3.5 Summary

Titanium currently plays an ever increasingly important role in the aerospace-, energy-, consumer products- and biomedical industries, just to name a few. Many of these applications pose great challenges to the material and manufacturing technology areas due to high demands from extreme environments and operating conditions as well as structural integrity. However, to remain a prominent role player in the aforementioned industries, future efforts must be directed to lower the titanium cost structure. More widespread adoption of titanium and its alloys in expanding markets such as AM will play an important role in realising this goal.Promising emerging technology to lower current acquisition and processing costs will ensure future widespread use.

The material properties of titanium, specifically in Ti-6Al-4V alloy, combined with the design freedom that AM provides, enables very unique applications for this material. Processing Ti-6Al-4V by means of AM brings with it its own set of challenges, not only process-related but related to material characteristics as well. It is clearly evident from literature on the processing of metal powder by DMLS that there is vast scope for future research aimed at fully understanding this highly complex process.

CHAPTER 4
MATERIALS AND METHODOLOGY

4.1 Introduction

As already mentioned in Chapter 3 there are many parameters that influence the DMLS process but for this study laser power, scanning speed and powder layer thickness will be considered. These three parameters were identified as the parameters the operator has the most control over. The purpose of this chapter is to study the geometrical characteristics of single laser sintered tracks, and to determine optimal process parameters for Ti-6Al-4V powder.

The following research methodology was followed:

- Characterisation of Ti-6Al-4V powder utilised for this study through granulomorphic and chemical analysis
- Formation of single tracks on a substrate without powder at different laser energies and scanning speeds. The empirical data was then compared to a melt pool width and re-melt depth prediction simulation program in order to verify its predictive capability.
- Formation of single tracks at different laser powers and scanning speeds in powder of different layer thicknesses.

4.2 Powder characterisation

In order for Ti-6Al-4V to be successfully processed by means of AM, the material needs to possess certain characteristics. For the purpose of this research, a sample of Ti-6Al-4V powder currently utilised for DMLS at the Centre for Rapid Prototyping and Manufacturing (CRPM) at the Central University of Technology (CUT), Free State located in Bloemfontein, South Africa, was examined.

To define quantitative characteristics of the employed Ti-6Al-4V powder, an optical granulomorphometer ALPAGA 500 NANO (a real time optical sieving system) and the CALLISTO image analysis software, products of OCCHIO s.a., were used. This equipmentprovides characterisation of any kind of powder or granular material, even transparent or friable ones, ranging from 0.5 µm, up to several millimetres. The system combines an integrated vacuum dispersion device VDD270, monochromatic collimated

back-light, telecentric lens for unrivalled image quality, wide depth of focus, integrated computer and electronics and advanced software for size and morphometric analysis (figures4.1a and 4.2b).

Figure 4.1a: Optical granulomorphometer ALPAGA 500 NANO

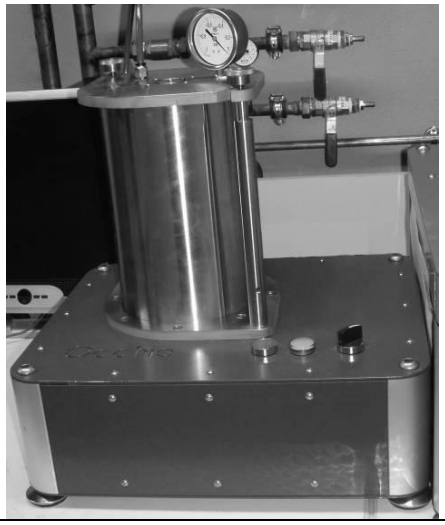

Figure 4.1b: Vacuum dispersion device VDD270

4.3 Powder chemicalcomposition

Ti-6Al-4V supplied from TLS Technik GmbH is a pre-alloyed gas-atomised powder with the nominal chemical composition (wt.%): Ti – balance, Al – 5.84, V – 4.21, C – 0.004, Fe – 0.042, O – 0.086, N – 0.005, H – 0.002.

SEM[2] was carried out with a Tescan Vega 3 Easy Probe Scanning Electron Microscope at 20 kV accelerating voltage and 15-20 mm working distance (Figure 4.2). Energy Dispersive X-Ray Spectroscopy (EDS) was done on a Bruker EDS detector and the energy spectra were calibrated to the Cobalt (Co) standard.

[2]SEM analysis was carried out at the National Engineering School of Saint-Etienne's (ENISE) Laboratory of Diagnostics and Engineering of Industrial Processes (DIPI) in France.

Figure 4.2: Tescan Vega 3 Easy Probe Scanning Electron Microscope

4.4 Single track formation

4.4.1 Experimental study and numerical modelling of laser–substrate interaction

The influence of the power input and scanning speed on melt pool geometry was studied by producing tracks without any powder present on a Ti-6Al-4V substrate by a laser beam (spot size d=100 μm) with the power of 150 W and 170 W at different scanning speeds ranging from 600 mm/s to 2000 mm/s with 200 mm/s increments. The results of these tracks produced without any powder were compared to a MatLab® simulation program that uses the same experimental inputs in order to predict the width and re-melt depth of the laser meltpool.

4.4.2 Experimental design of tracks produced in powder

To study the combined effect of these parameters on the formation of single tracks in the DMLS process, an experiment was carried out on Ti-6Al-4Vin an EOSINT M270 machine from EOS GmbH. The M270 machine is equipped with a 200 W fibre-optic laser with an effective spot size of 100 μm.

Single tracks made from Ti-6Al-4V powder were produced that were 20 mm in length and spaced 5 mm apart at two different laser powers: 150 W and 170 W respectively and for

each of the scanning speeds that varied from 600 mm/s to 2000 mm/s with 200 mm/s intervals. Instead of sintering the tracks onto the building platform, as would be done for producing parts, it was sintered onto a 6 mm Grade 5 titanium plate that was screw-mounted onto the building platform. This was done to aid the visual inspection of the tracks under a microscope considering that it would be easier to cut the 6 mm plate into smaller sections rather than to try and inspect the building platform that is 22 mm thick.

The Ti-6Al-4V powder was deposited across the surface of the plate (which was aligned within tolerance) with a layer thickness that varied from 0 µm on the left side to 60 µm on the right side of the plate (figures 4.3 and 4.4). Measurements were taken by making cross-sectional cuts on the 6 mm plate at 15 µm, 30 µm and 45 µm powder thickness positions (red dotted line on figure 4.4). The top view of the laser sintered tracks will be considered in order to identify uniform tracks with constant width and a continuity. The cross-sections will be examined in order to identify tracks with adequate material deposition as well as penetration depth into the substrate. All tracks were produced in the powder on the plate in an argon atmosphere with an oxygen content of <0.13%.

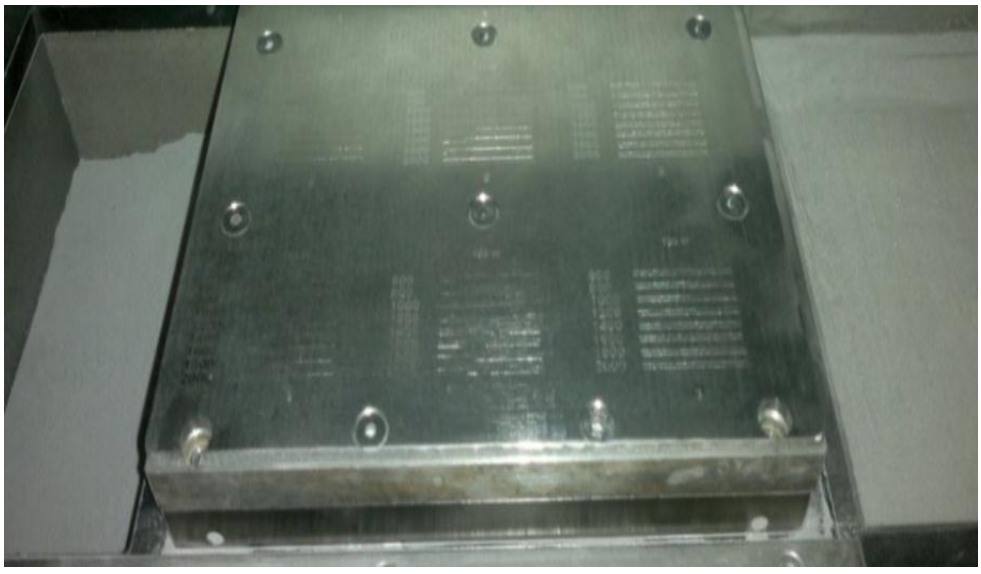

Figure 4.3: 6 mm Titanium plate fixed to building platform with sintered tracks

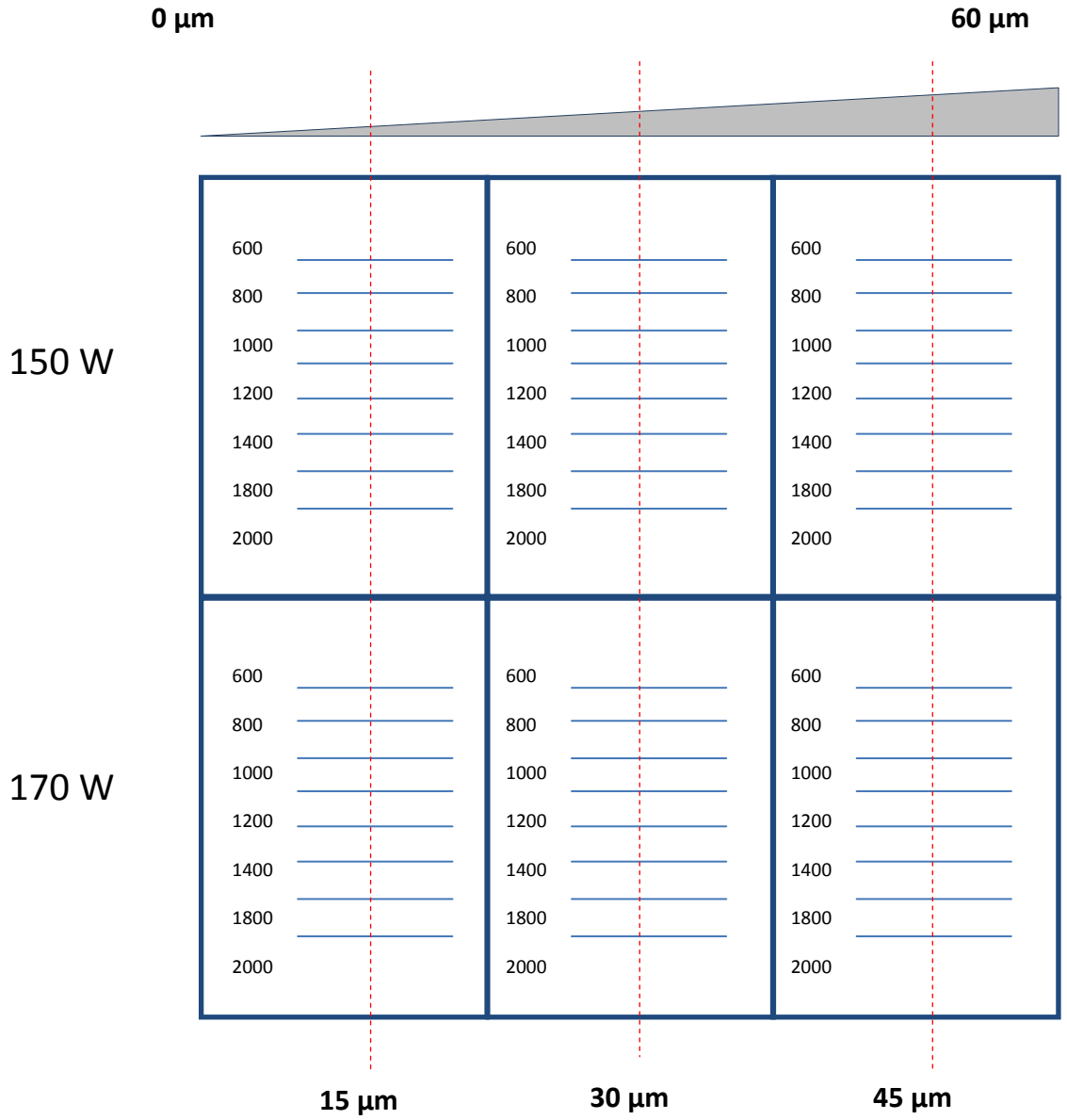

Figure 4.4: Schematic representation of experiment with titanium powder with scanning speeds ranging from 600-2000 mm/s

4.5 Summary

Powder size distribution and morphology of Ti-6Al-4V powdersupplied from TLS Technik GmbH were analysed. This specific powder is employed in the experimental study on the fabrication of single tracks.

Measured track width and re-melt depth from tracks produced without powder on a titanium substrate will be compared to a meltpool width and re-melt depth prediction simulation program in order to test its predictive capability.

Single tracks produced in 15 µm, 30µm and 45µm powder will be analysed in order to establish how laser powder and scanning speed will affect single track formation at these specified powder layer thicknesses in order to identify an optimal set of process parameters that could potentially be used as starting point to manufacture fully dense 3D objects.

CHAPTER 5
RESULTS AND DISCUSSION

5.1 Background

Previous studies have shown that laser melting/sintering is a complicated process influenced by more than 130 parameters. In addition to these processing parameters, the characteristics of the powder material are of special concern [5].

In order to comprehend the results obtained in the first section of the chapter it is necessary to clarify what is meant by powder characterisation.

5.2 Powder characterisation

Geometric properties such as particle size, particle shape, elongation, specific surface area, microporosity all play an important role in the production of sintered materials [5].

5.2.1 Particle size

For particle size, the exact measurement of a sieving diameter D_{in} needs to be performed by computing the maximum inscribed disk within a particle (Figure 5.1).

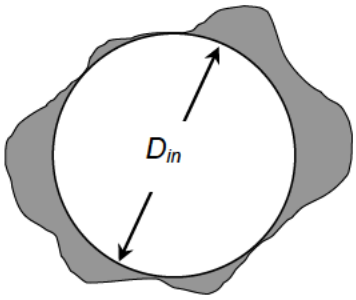

Figure 5.1: Granulometricstudy based on sieving diameter

5.2.2 Particleshape

Different shape factors, such as ellipticity parameters or elongation have to be calculated, for the characterisation of particle shape [90]. To characterise elongation, aspect E_I is used

$$E_I = 1\text{-}D_b/D_a \qquad (5.1)$$

whereD_a and D_b are the axes of the Legendre ellipse (figure 5.2a and 5.2b).

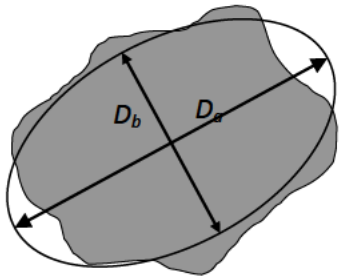

Figure 5.2a: Morphology study based on Legendre ellipse

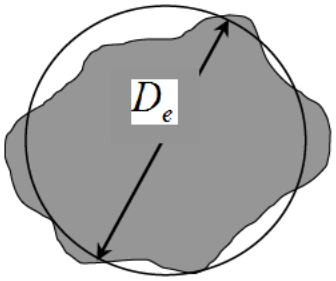

Figure 5.2b: Morphology based on circle of same projected area of particle

According to Yadroitsev [5] “The Legendre ellipse is an ellipse with the centre in the object’s centroid and with the same geometrical moments up to the second order as the original object area. Elongation grows for the ellipses with an increase in the ratio of the major and secondary axes”. Evolution of the elongation index is presented in Table. 5.1.

Table 5.1: Elongation of particles of different elliptical shape.

Ratio between ellipse height: ellipse width (D_b/D_a)	1:1	1:2	1:3	1:4	1:5	1:10
E_I (%)	0	50	67	75	80	90

Equivalent circle diameter is calculated by

$$D_e = \sqrt{\frac{4A}{\pi}} \text{ [5]} \qquad (5.2)$$

where *A* is projected area of the object. Another well-known characteristic of a particle is the shape factor (circularity index) – ratio (illustrated in Table 5.2) between the perimeter *P* and area *A* expressed as

$$SF = \frac{4\pi A}{P^2} \tag{5.3}$$

Table 5.2: Shape factor of particles of different form.

Configuration					
SF (%)	100	94.8	90.7	78.6	60.5

The Roundness index

$$W_i = \frac{\sum_{i=1}^{N} D_i}{ND_{in}} \tag{5.4}$$

where *Di* – *i*^{h} is the diameter of curvature along the particle profile which is smaller than the radius of the largest inscribed circle, *N* is the total number of radii of curvature smaller than the inscribed circle, and D_{in} is the sieving diameter (diameter of the largest inscribed circle) (Figure 5.3).

The convex envelope of a shape is defined as the shortest possible contour circumscribing a shape and displaying no concavity. Such a measurement is not only convenient to characterise a concavity index but also efficient to filter out convex particles from each other. For practical purposes, the explicit concavity parameter is better than calculating only the particle's area (Figure 5.4) [90].

The Concavity parameter is calculated by:

$$I_c = \frac{A_c - A}{A_c} \tag{5.5}$$

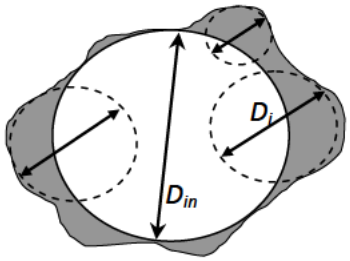

Figure 5.3: Morphology study based on roundness

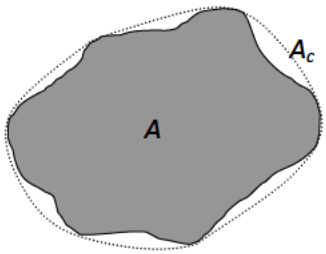

Figure 5.4: Morphology study based on concavity index

Results of the powder characterisation analysis show that equivalent diameters of particles (weighted by volume) were d_{10} = 14.4 µm, d_{50} = 34.0 µm, and d_{90} = 46.5 µm (Figure 5.5). The total number of particles analysed was 10737 (Table 5.3). A Bivariate scatterplot for sieve and equivalent diameters indicated a straight line and had a linear dependence because most of the particles were spherical (Figure 5.6a). The concavity index and internal elongation were higher for finer particles because they agglomerated (figures 5.6b and 5.6c). Agglomerates from fine particles had an irregular form so their circularity indexes, or shape factors were less than 60% (Figure 5.6d). Some larger particles had satellites (Figure 5.6e).

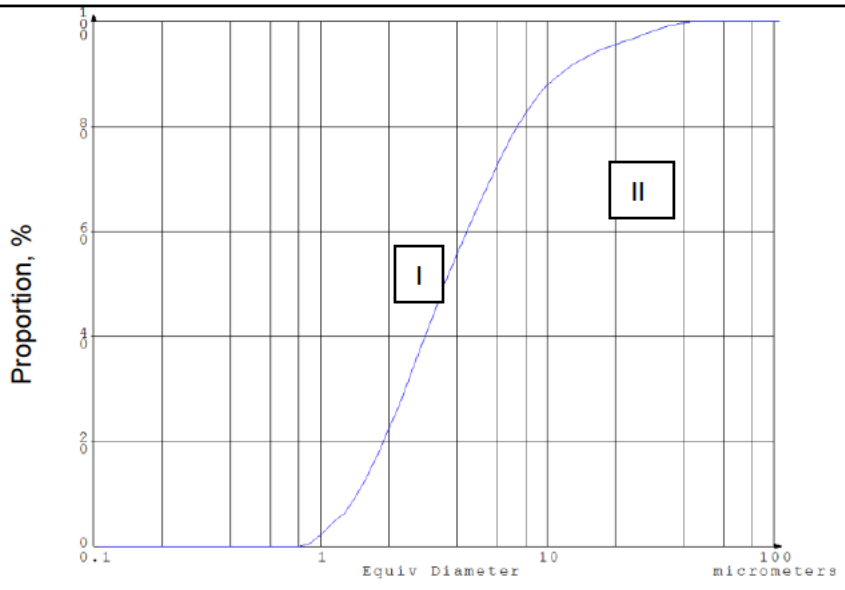

Figure5.5: Equivalent diameter distributions by number (I) and by volume (II) of powder

Table 5.3: Granulomorphometrical characteristics[3] of Ti-6Al-4V powder.

	Min	10%	25%	Median	75%	90%	Max
Sieving diameter, µm	0.5	12.6	22.8	29.8	36.8	41.5	47.5
Equivalent diameter, µm	0.9	14.4	25.9	34.0	41.2	46.5	49.3
Concavity, %	0	2.2	2.6	3.9	6.5	8.7	43.8
Elongation, %	0	3.1	5.5	11.7	25	38.3	78.9
Shape factor,%	23.3	80.3	89	98.5	99	100	100
Roundness, %	13.4	44.2	57.7	73.1	89.4	96.2	100
Satellites, %	0	0.2	0.2	0.4	1.9	4.4	20

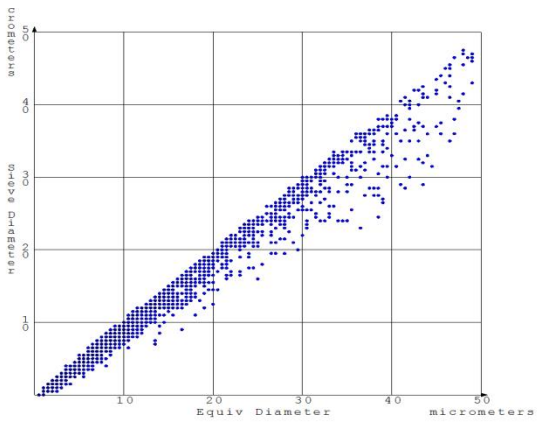

a

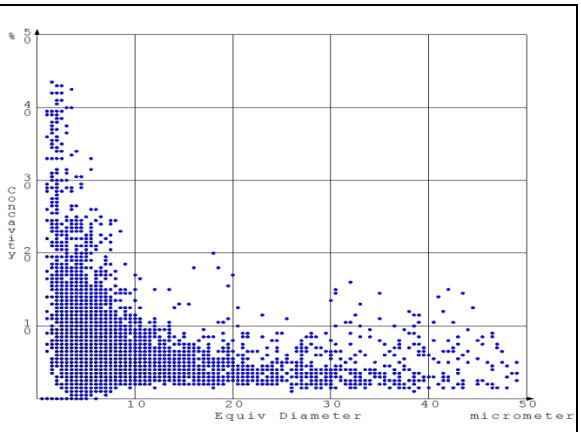

b

[3]Weighted by volume

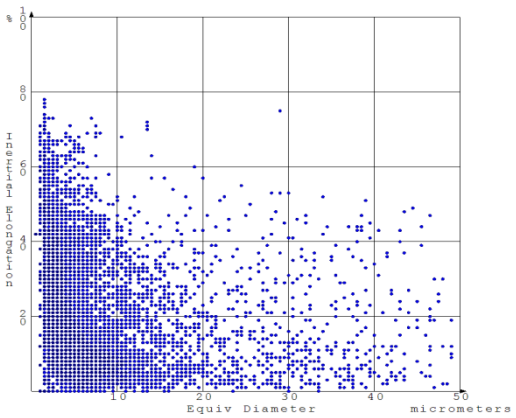

c

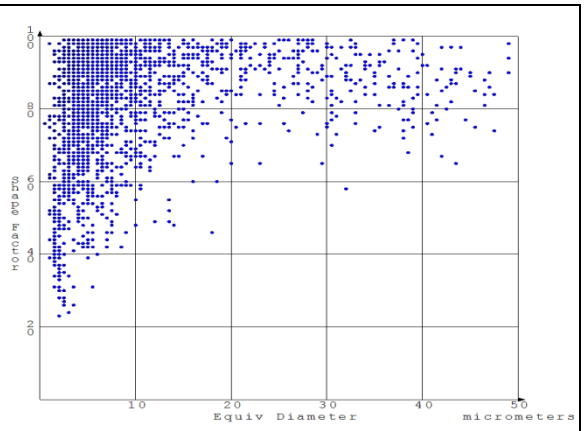

d

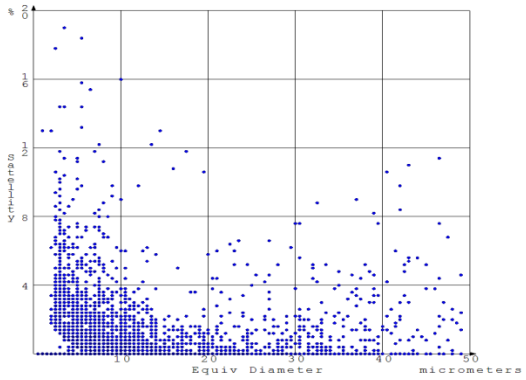

e

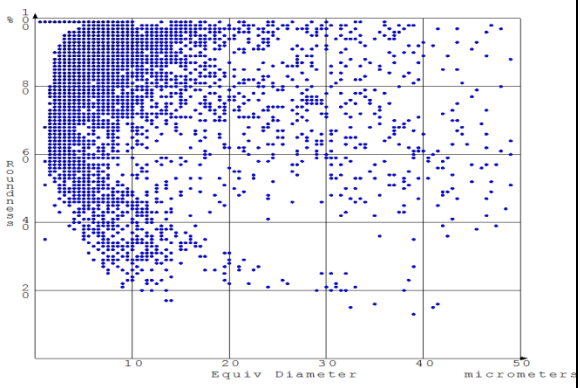

f

Figure 5.6: Bivariate scatterplots: equivalent diameter *versus* sieve diameter (a), concavity (b), elongation (c), shape factor (d), satellity (e) and roundness (f)

5.3 Chemical composition analysis of powder

Powder particles were tested for the presence of oxygenin EDS spectra (Figure 5.7). There were no detected peaks of oxygen (K-alpha 0.525 keV). Inaccuracy in the Vanadium content may be attributed tothe Vanadium concentration being below 5 wt% [91]. VKα line of V is too low and overlapped with Kβ line of Ti (Figure 5.8).

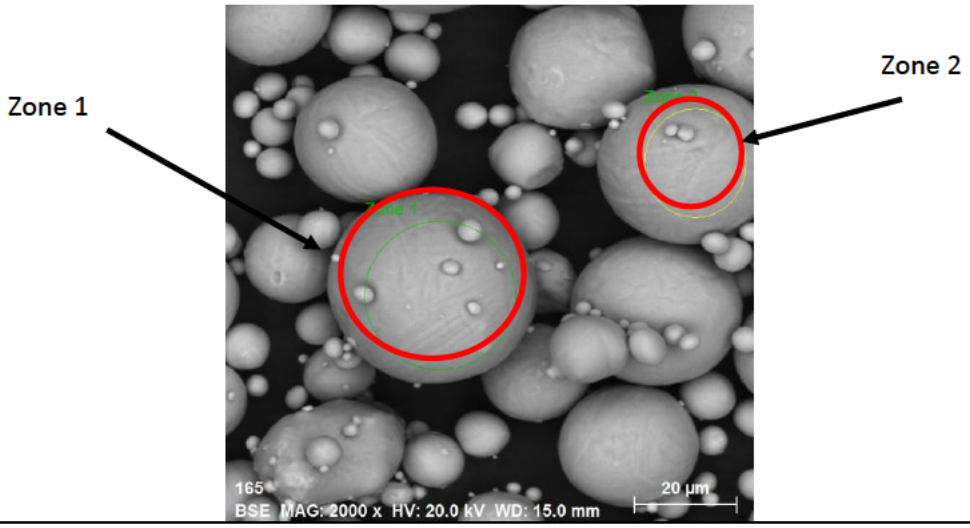

Figure 5.7: Micrograph indicating the two zones that were analysed

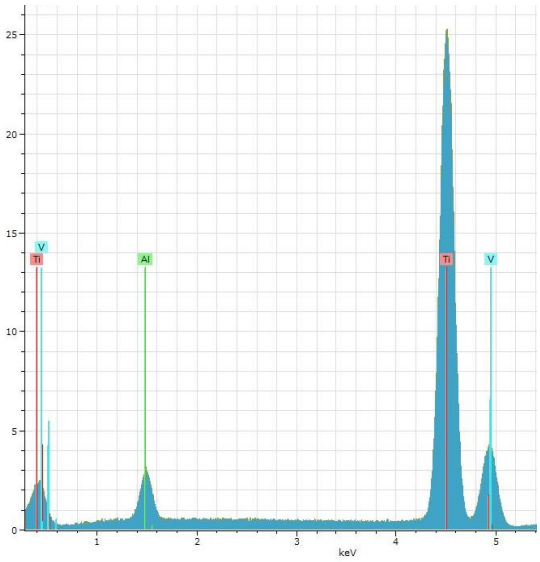

Zone 1

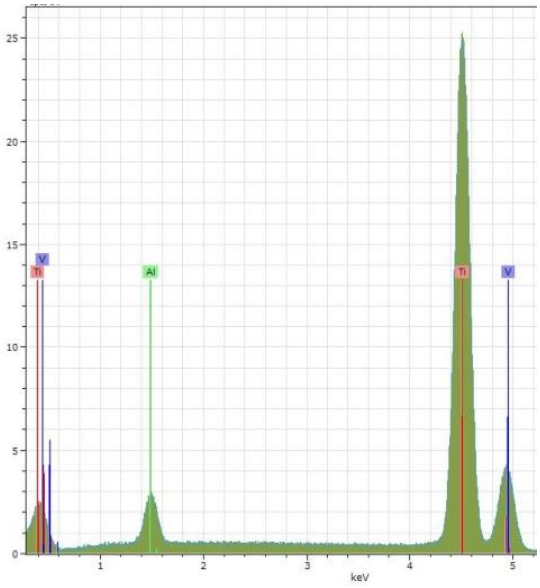

Zone 2

Element	Series	Zone 1 norm. C [wt.%]	Zone 2 norm. C [wt.%]
Ti	K-series	91.56±3.1	91.94±3.2
Al	K-series	5.73±0.3	5.49±0.3
V	K-series	2.7±1.7	2.58±1.7
	Total:	100	100

Figure 5.8: A typical EDS spectra and chemical analysis of selected zones

5.4 Single tracksproducedwithoutpowder

When considering the re-melt depth, the “keyhole” phenomenon was clearly visible for low scanning speeds at both 150 W and 170 W laser powers (Figure 5.9a). After visual inspection of the tracks, a definite “humping” of the tracks at higher scanning speeds was visible (Figures 5.9b and 5.9c). Fabbro [88] defines “humping” as “the occurrence of a prominent weld seam with negative strong undercuts, composed of solidified large swellings of quite ellipsoidal shape, separated by smaller valleys”. During investigation some of these undercuts measured up to 20 µm deep.

	150 W	170 W
600 mm/s Top View	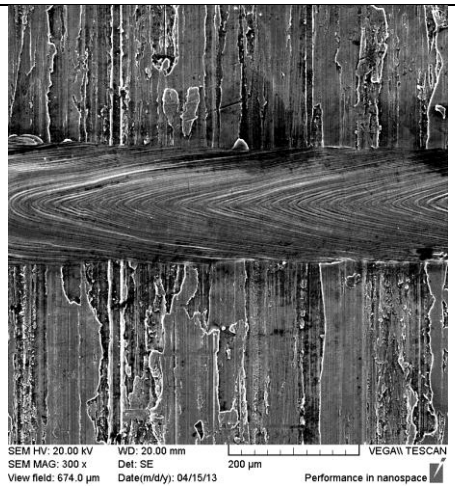	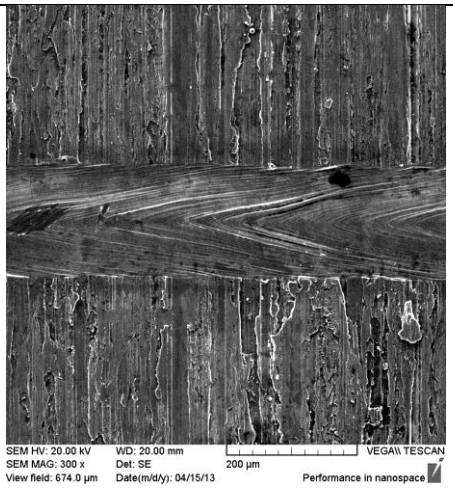
Cross-section	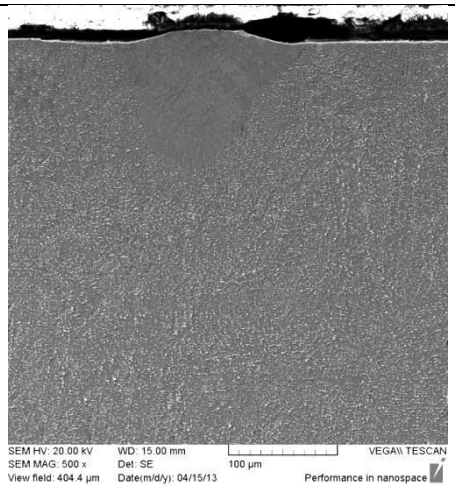	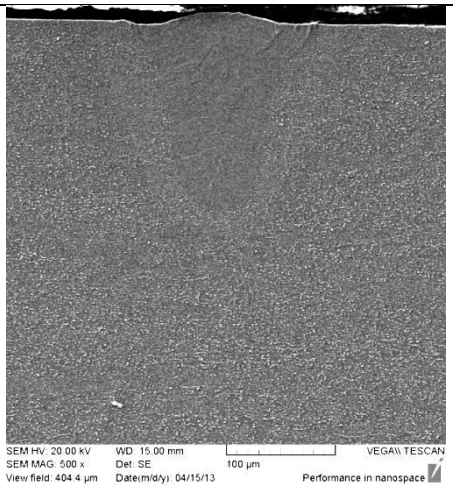

Figure 5.9a: Top view and cross-sectional view of single tracks formed on a substrate without powder with laser power 150 W and 170 W and 600 mm/s scanning speed[4]

[4]For SEM and optical microscope investigations cross-sections of the samples were etched in Kroll’s reagent with a composition of 100 ml distilled water, 3 ml HF and 3 ml HNO_3.

	150 W	170 W
1200 mm/s Top View	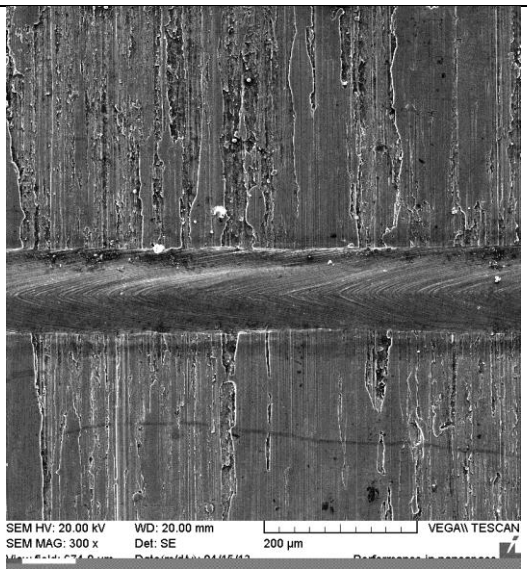	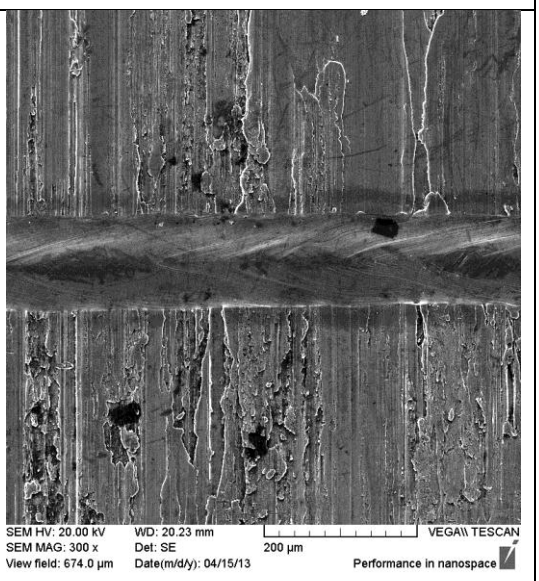
Cross-section	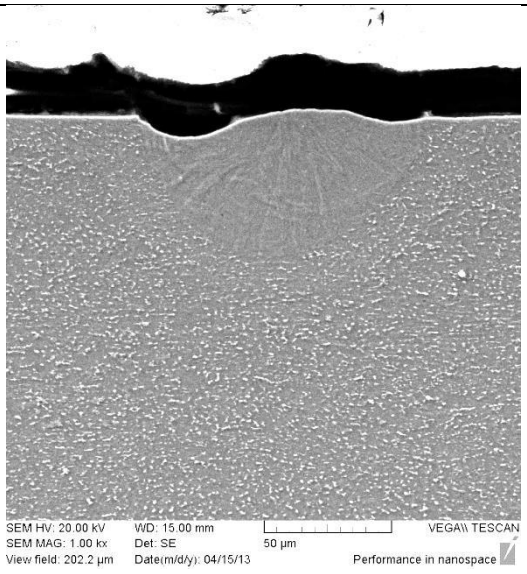	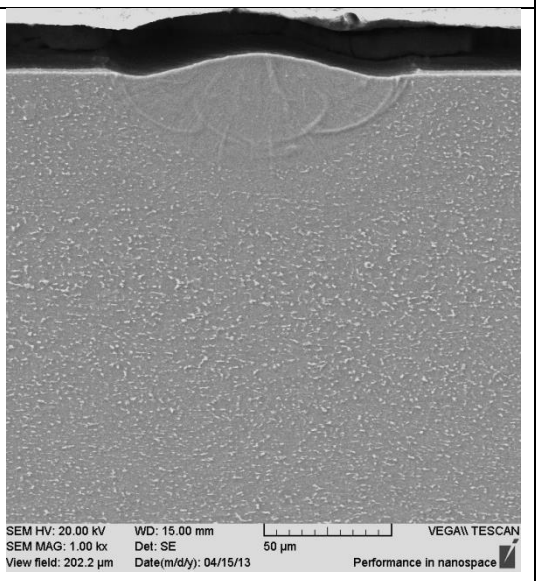

Figure 5.9b: Top view and cross-sectional view of single tracks formed on a substrate without powder with laser power 150 W and 170 W and 1200 mm/s scanning speed

	150 W	170 W
2000 mm/s Top View	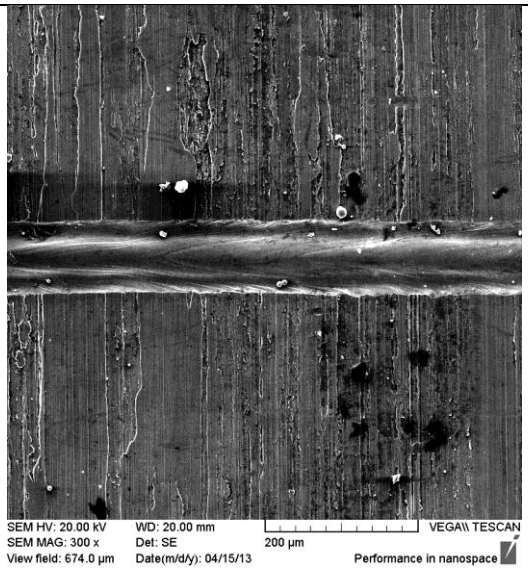	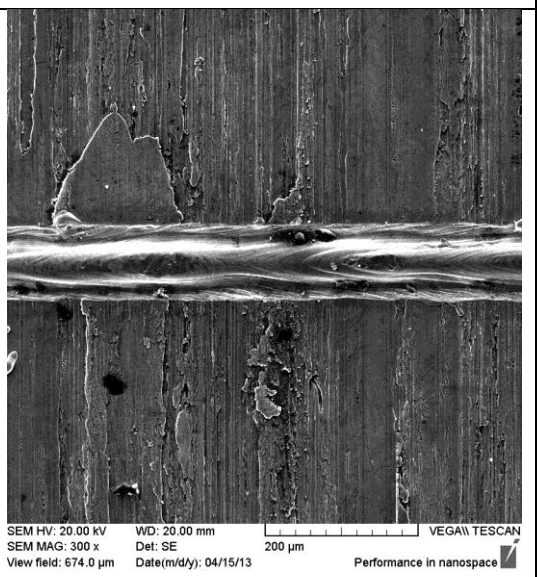
Cross-section	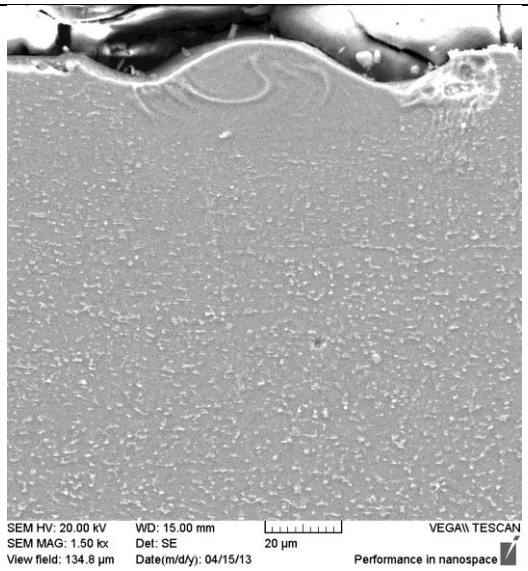	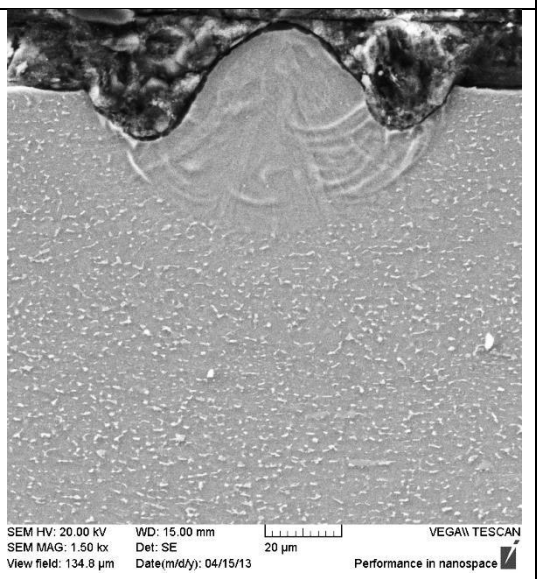

Figure 5.9c: Top view and cross-sectional view of single tracks formed on a substrate without powder with laser power 150 W and 170 W and 2000 mm/s scanning speed

5.5 Evaluation ofmelt pool temperature distribution simulation program

The empirical data of the tracks without any powder were compared to melt pool width prediction of a MATLAB (matrix laboratory) melt pool temperature distribution simulation program [5,92] in order to test its predictive capability. In this program, thermal distribution on a semi-infinite plate and continuous Gaussian heat source, with power *P* moving along *OX* axis and for adiabatic conditions, was calculated according to the moving heat source theory of Carslaw and Jaeger, Rosenthal as well as Rykalin[93].

The following variables are typical values used as inputs into the simulation model for Ti-6Al-4V heating:

- Laser duration: 10 sec
- Effective spot size diameter:D= 100 μm
- Absorption coefficient: 0.3
- Melting temperature: 1933 Kelvin
- Thermal diffusivity of Ti-6Al-4V:2.86 x 10^{-6} m^2/s

The thermal diffusivity

$$a = \frac{k}{(Cp)\rho}, \tag{5.6}$$

where thermal conductivity k = 6.7 W/m K, heat capacity Cp =526 J/kg K, density ρ = 4430 kg/m^3.

Figure 5.10 indicates how the cross-section of each sintered track was microscopically analysed. Please see Appendix 1 for the complete set of micrographs depicting the laser sintered tracks and cross-sections produced without powder as well as at 15 μm, 30 μm and 45 μm powder thicknesses.

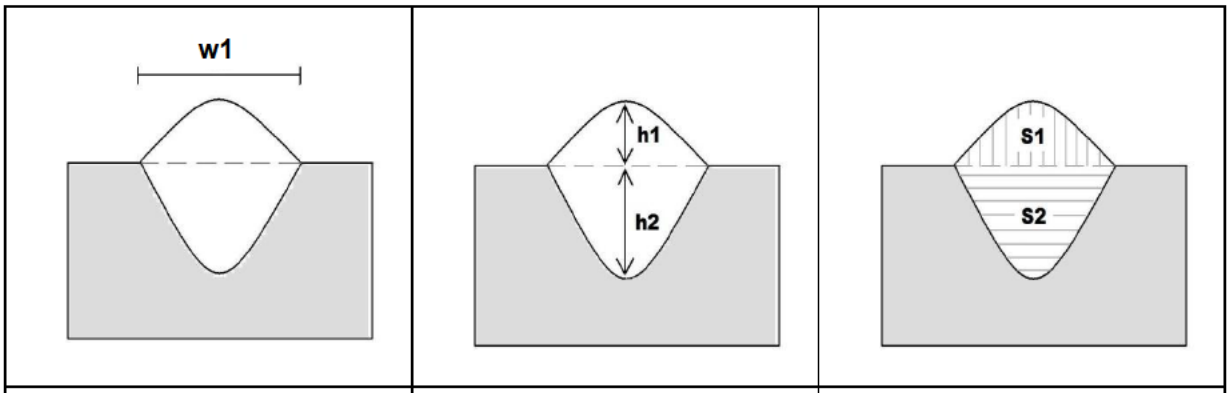

a	b	c

Figure 5.10: Track width,w1 (a); track height, h1 and re-melt depth, h2 (b), track surface area S1 and re-melt surface area S2 measurement (c)

The results of the numerical simulation are shown in Figures 5.11a and 5.11b. The numerical simulation estimated that the width of the track and re-melt depth is decreased with the increase in input power and increased scanning speed of the laser beam (Figure 5.11a). With high scanning speeds.the melt pool became longer and shallower [5]. At scanning speeds ranging from 200 to 1000 mm/s this model was not in agreement with the experimental data because, for 150 - 170 W power input, 100 µm spot size and slow scanning speeds, high temperatures are achieved and convective heat transfer plays a significant role in the temperature profile, the melt pool shape and size and the current numerical model does not account for heat transfer by convection [5]. During the conduction mode, this model is useful for estimating geometrical characteristics of single tracks.

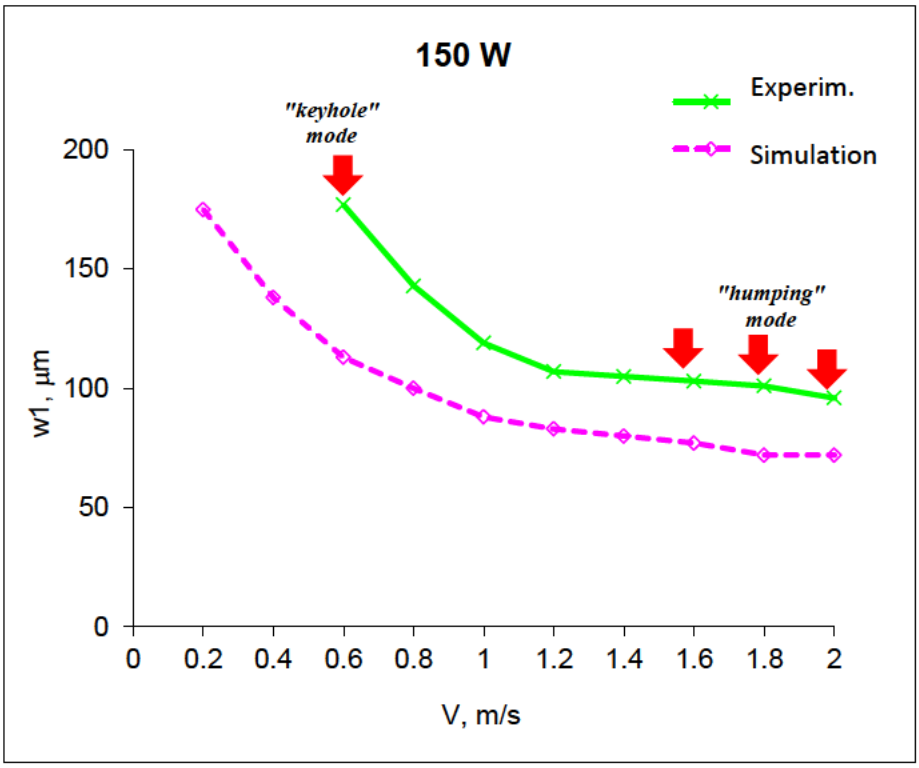

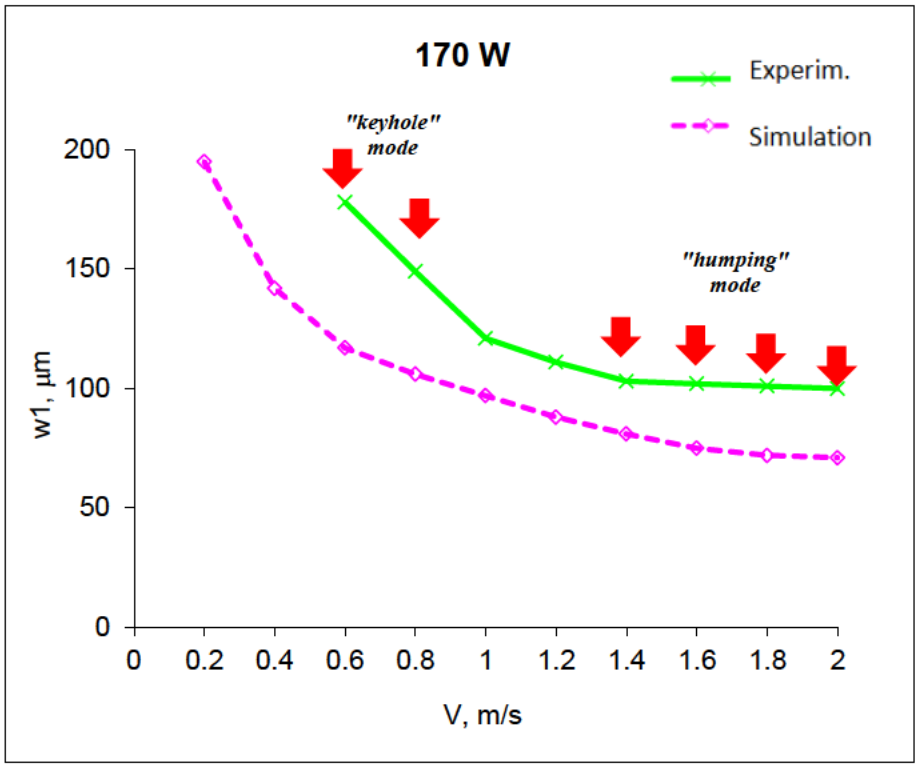

Figure 5.11a: Track width of the experimental data compared to the data obtained from the numerical simulation program

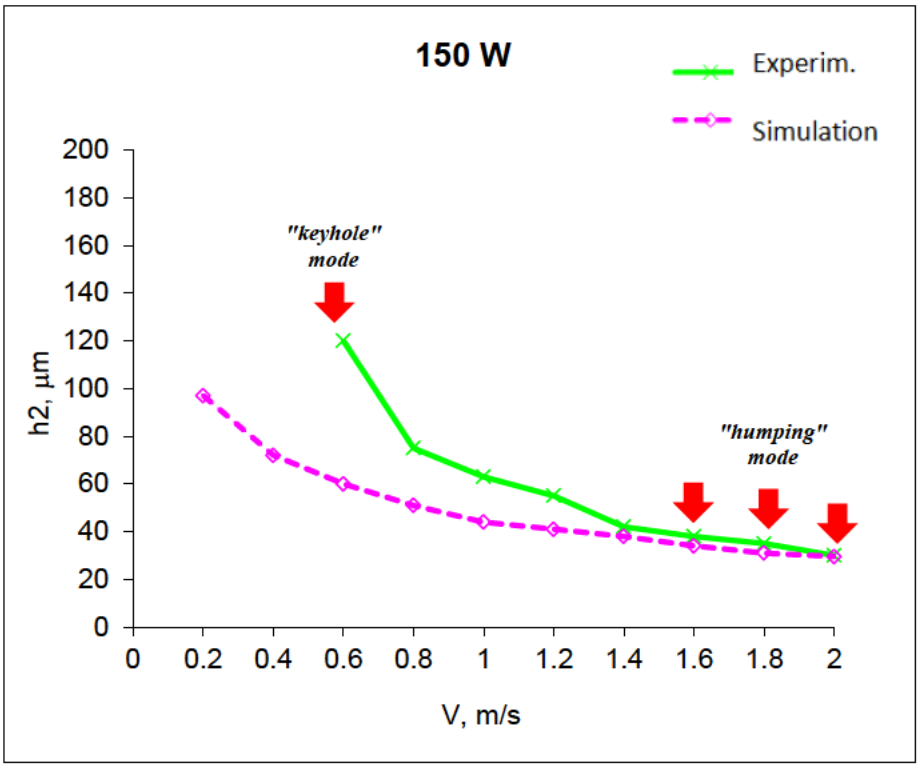

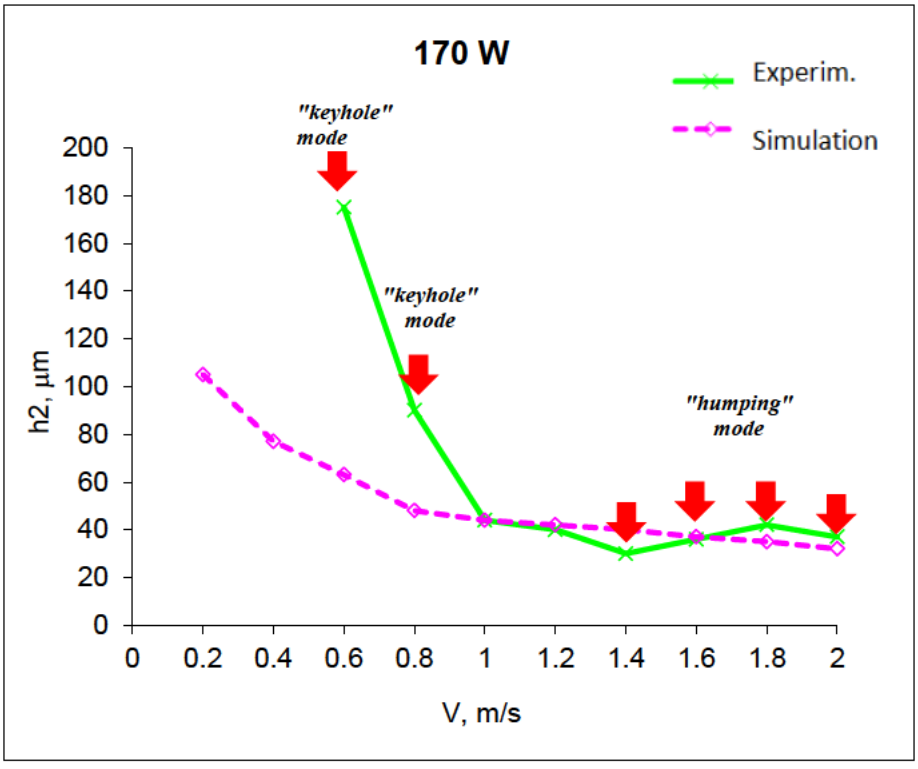

Figure 5.11b: Re-melt depth of the experimental data compared to the data obtained from the numerical simulation program

Figure 5.11c represents a typical result from the simulation software program that indicates the temperature profile for a specific set of parameters that were entered.

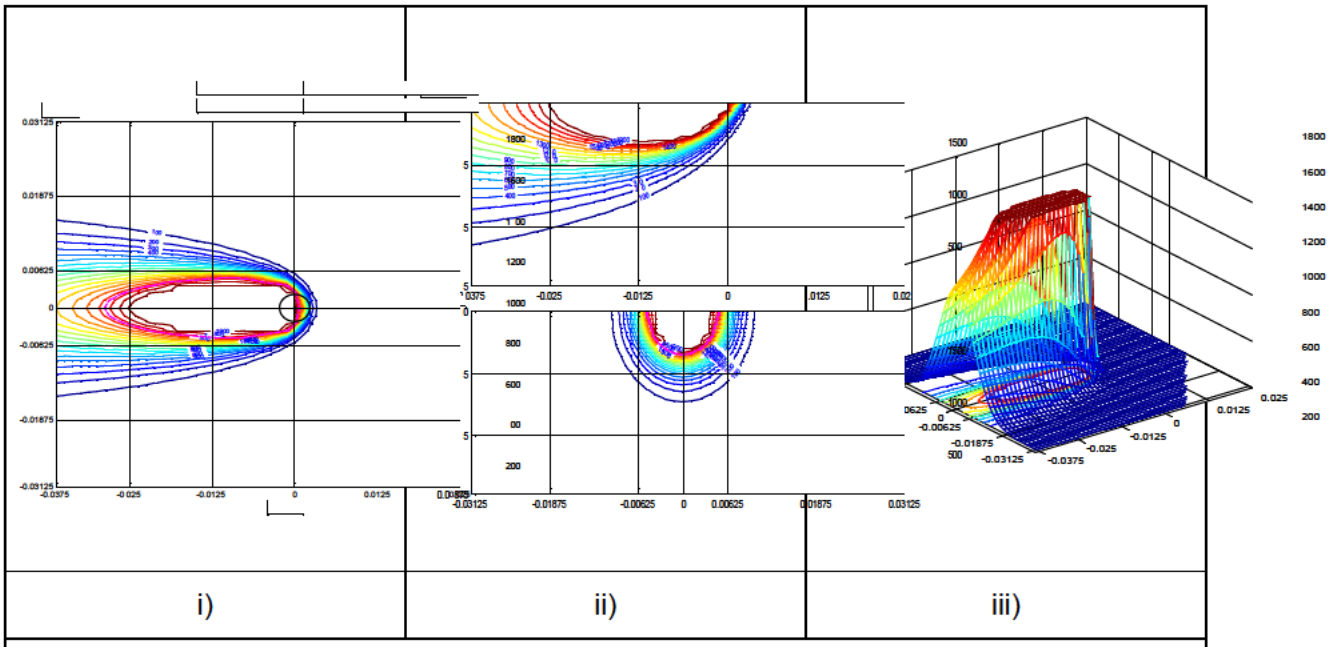

Figure 5.11c: Calculated temperature profiles for the semi-infinite Ti-6Al-4V plate: XY plane i); XZ plane and YZ planes ii); 3D-plot iii) for scanning speed 1000 mm/s and laser power 170 W

5.6 Results of single tracks in powderexperiments

The results of the single track experiments conducted in powder are represented in tables 5.4 to 5.10. Typical tendencies are obvious, however, some anomalies are also evident. These irregularities can be explained in all probability by the exact position where the cut was made on the specific track. Irregularities in track morphology are most probably to blame. The aforementioned is clearly demonstrated by the measurements for track width produced with 150 W laser power and powder layer thickness of 30 µm at scanning speeds from 1600 mm/s to 2000 mm/s. The track width is logically expected to decrease with the increase of scanning speed but when one investigates the actual track morphology of these specific three tracks,as can be seen in Figure 5.12, it is clear that the position of the cross-sectional cut will directly affect the measurement of the laser sintered track width. This is due to the fact that even though the general track width is narrow, it does have locallised bulges where the “balling” occurred which leads to a much wider track measurement compared to

the rest of the laser sintered track. Measurements of cuts at different positions of each track will result in different values despite the fact that it is the same track. The same argument is applicable to track height and area.

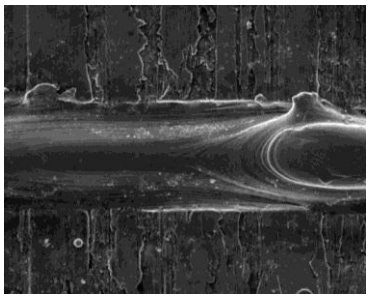	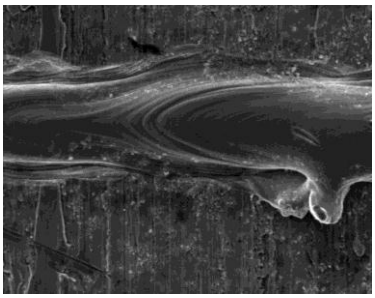	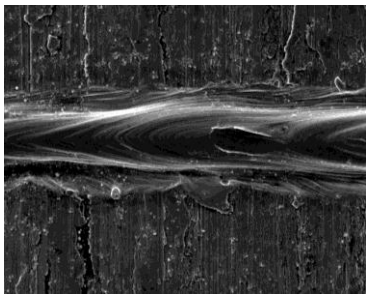
a	b	c

Figure 5.12: Single tracks produced with 150 W laser power, powder layer thickness of 30 µm and scanning speeds of 1600 mm/s (a), 1800 mm/s (b) and 2000 mm/s (c)

Table 5.4: Measured track widths (w1) in µm for powder thickness of 15, 30 and 45 µm.

150 W Laser power				170 W Laser power			
Scanning Speed (mm/s)	w1 Track Width (15 µm powder)	w1 Track Width (30 µm powder)	w1 Track Width (45 µm powder)	Scanning Speed (mm/s)	w1 Track Width (15 µm powder)	w1 Track Width (30 µm powder)	w1 Track Width (45 µm powder)
600	166	178	183	600	163	180	176
800	145	156	156	800	166	162	163
1000	121	130	138	1000	131	138	150
1200	106	111	122	1200	110	108	128
1400	102	94	111	1400	99	99	117
1600	98	97	110	1600	96	95	105
1800	96	99	97	1800	97	98	105
2000	96	100	93	2000	97	99	100

Table 5.5: Measured track heights (h1) in µm for powder thickness of 15, 30 and 45 µm.

150 W Laser power				170 W Laser power			
Scanning Speed (mm/s)	h1 (15 µm powder)	h1 (30 µm powder)	h1 (45 µm powder)	Scanning Speed (mm/s)	h1 (15 µm powder)	h1 (30 µm powder)	h1 (45 µm powder)
600	8	10	25	600	12	11	32
800	6	21	12	800	8	13	25
1000	5	18	19	1000	5	13	29
1200	9	16	19	1200	9	12	30
1400	7	14	33	1400	7	16	35
1600	10	22	18	1600	10	5	15
1800	19	28	30	1800	19	24	9
2000	17	16	43	2000	17	28	9

Table 5.6: Measured track re-melt depth (h2) in µm for powder thickness of 15, 30 and 45 µm.

150 W Laser power				170 W Laser power			
Scanning Speed (mm/s)	h2 (15 µm powder)	h2 (30 µm powder)	h2 (45 µm powder)	Scanning Speed (mm/s)	h2 (15 µm powder)	h2 (30 µm powder)	h2 (45 µm powder)
600	139	156	124	600	178	183	163
800	85	97	68	800	110	108	71
1000	68	47	49	1000	83	76	33
1200	59	66	55	1200	67	70	52
1400	43	49	45	1400	59	57	67
1600	42	50	10	1600	53	49	45
1800	37	29	10	1800	47	42	48
2000	32	27	16	2000	42	44	38

Table 5.7: Total re-melt height (h1+h2) in µm for powder thickness of 15, 30 and 45 µm.

150 W Laser power				170 W Laser power			
Scanning Speed (mm/s)	h1+h2 (15 µm powder)	h1+h2 (30 µm powder)	h1+h2 (45 µm powder)	Scanning Speed (mm/s)	h1+h2 (15 µm powder)	h1+h2 (30 µm powder)	h1+h2 (45 µm powder)
600	147	166	149	600	190	194	195
800	91	118	80	800	118	121	96
1000	73	65	68	1000	88	89	62
1200	68	82	74	1200	76	82	82
1400	50	63	78	1400	66	73	102
1600	52	72	28	1600	63	54	60
1800	56	57	40	1800	66	66	57
2000	49	43	59	2000	59	72	47

Table 5.8: Measurement of track surface area (S1) in μm² for powder thickness of 15, 30 and 45 μm.

150 W Laser power				170 W Laser power			
Scanning Speed (mm/s)	S1 (15 μm powder)	S1 (30 μm powder)	S1 (45 μm powder)	Scanning Speed (mm/s)	S1 (15 μm powder)	S1 (30 μm powder)	S1 (45 μm powder)
600	643	620	3817	600	753	1068	3312
800	450	1142	732	800	389	963	1787
1000	442	1088	1320	1000	289	658	3592
1200	450	858	1325	1200	356	488	1773
1400	318	638	2050	1400	234	763	1630
1600	278	869	1101	1600	336	620	671
1800	444	1453	2434	1800	500	741	227
2000	507	439	3022	2000	430	1066	233

Table 5.9: Substrate re-melt area (S2) in μm² for powder thickness of 15, 30 and 45 μm.

150 W Laser power				170 W Laser power			
Scanning Speed (mm/s)	S2 (15 μm powder)	S2 (30 μm powder)	S2 (45 μm powder)	Scanning Speed (mm/s)	S2 (15 μm powder)	S2 (30 μm powder)	S2 (45 μm powder)
600	13380	15400	12114	600	16233	17337	15546
800	8492	9329	6606	800	10759	10939	6972
1000	5819	4127	4228	1000	7568	6955	2434
1200	4536	4940	4269	1200	5613	5320	4473
1400	3073	3620	3192	1400	4354	4264	5000
1600	2910	3187	335	1600	3365	2584	3083
1800	2174	1620	820	1800	2877	2326	2704
2000	2052	1500	992	2000	4438	2519	1990

Table 5.10: Total re-melt area (S1+S2) in μm² for powder thickness of 15, 30 and 45 μm.

150 W Laser power				170 W Laser power			
Scanning Speed (mm/s)	S1+S2 (15 μm powder)	S1+S2 (30 μm powder)	S1+S2 (45 μm powder)	Scanning Speed (mm/s)	S1+S2 (15 μm powder)	S1+S2 (30 μm powder)	S1+S2 (45 μm powder)
600	14023	16020	15931	600	16986	18405	18858
800	8942	10471	7338	800	11148	11902	8759
1000	6261	5215	5548	1000	7857	7613	6026
1200	4986	5798	5594	1200	5969	5808	6246
1400	3391	4258	5242	1400	4588	5027	6630
1600	3188	4056	1436	1600	3701	3204	3754
1800	2618	3073	3254	1800	3377	3067	2931
2000	2559	1939	4014	2000	4868	3585	2223

5.7 Discussion

The width of stable tracks was strongly dependent on scanning speed for all layer thicknesses (Figure 5.13).The boundary between track stability versus instability, as indicated in figures 5.13a-d, was determined by means of visual inspection and Figure 5.13e-f illustrates the difference between a stable and an unstable single track.

The geometrical characteristics of the sintered tracks strongly depend on the volume of powder material involved in the process. Thus tracks were predominantly wider for the 45 µm powder layer. At high scanning speeds, the track width remained nearly constant approaching the size of the laser beam diameter. The width of tracks produced with 150 W laser power in 30 µm thick powder was higher than that in the 15 µm thick powder bed. In contrast, when 170 W laser power was used, the track widths in 15 µm and 30 µm thick powder beds were similar. The irregularities started at lower scanning speeds in tracks produced by 150 W laser power compared to that of 170 W laser power. For 45 µm powder layers, irregularities began at the lowest scanning speed: this is caused by insufficient energy absorption that in turn prevents the powder entering into a liquid phase melting due to the short interaction time between the laser and the powder at high scanning speeds [19]. For a powder thickness of 30 µm, the track width measurement varied significantly:firstly at low scanning speeds due to the presence of satellites and secondly, at high scanning speeds due to the “balling effect”. At 15 µm layer thickness such obvious differences were not observed most probably due to the low apparent density of the powder layer. For 45 µm powder layers, variability in track width was higher compared to 15 and 30 µm powder layersdue to irregularities in the powder layerdelivered on the substrate.

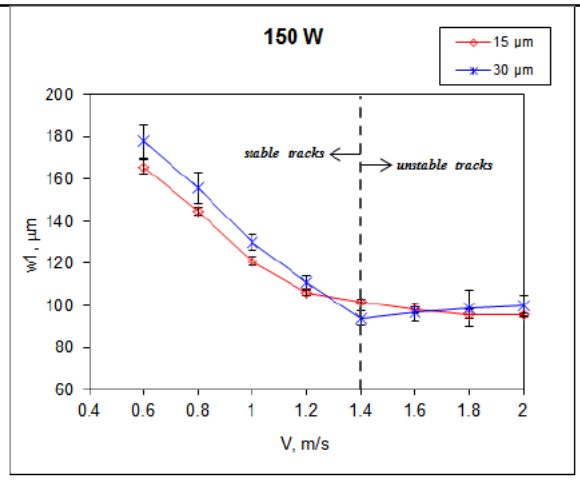

a

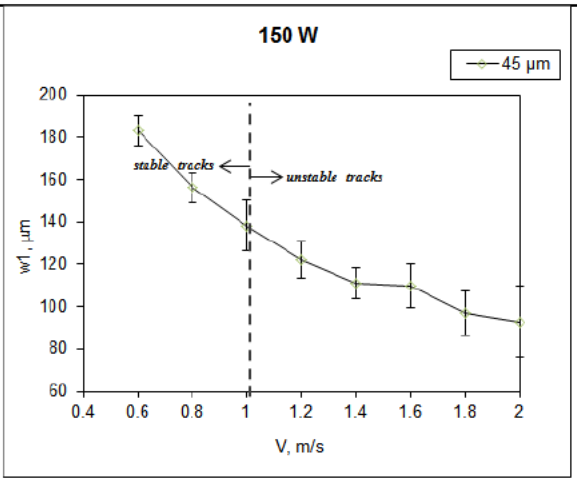

b

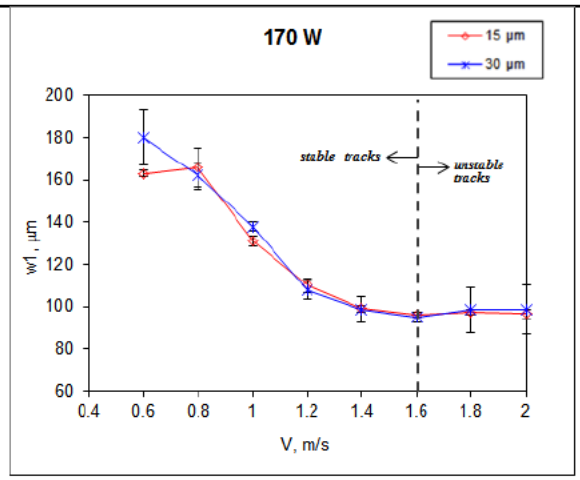

c

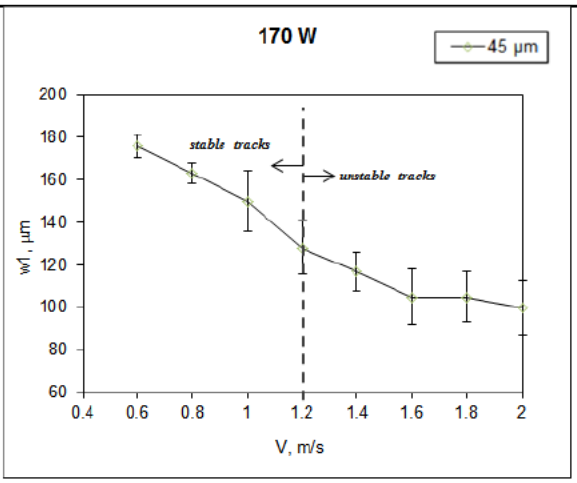

d

Figure 5.13a-d: Measured track widths for powder thickness of 15, 30 and 45 µm

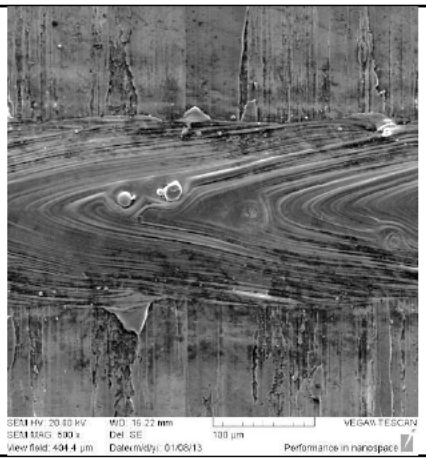

e

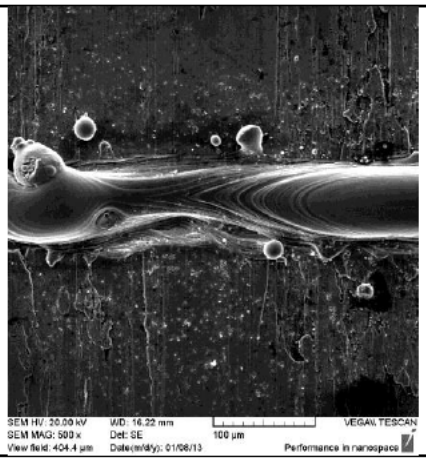

f

Figure 5.13e-f: Illustration of a stable track (e), versus an unstable track (f)

Track height is primarily determined by the thickness of the deposited layer and the apparent density of the powder layer. At 170 W laser power, the height (h1) of the tracks in general were lower than those produced by 150 W laser power, but the width of the tracks produced by 170 W was slightly greater, thus explaining the relatively lower height (Figure 5.14a-d).For stable tracks produced at 150 W at 15 µm layer thickness, the heightsof tracks were about 5-10 µm, for 30 µm thickness it was 10-18 µm and for 45 µm thickness, 12-25 µm.Defects in the deposited layer and melt hydrodynamics caused the height of the tracks to vary significantly.

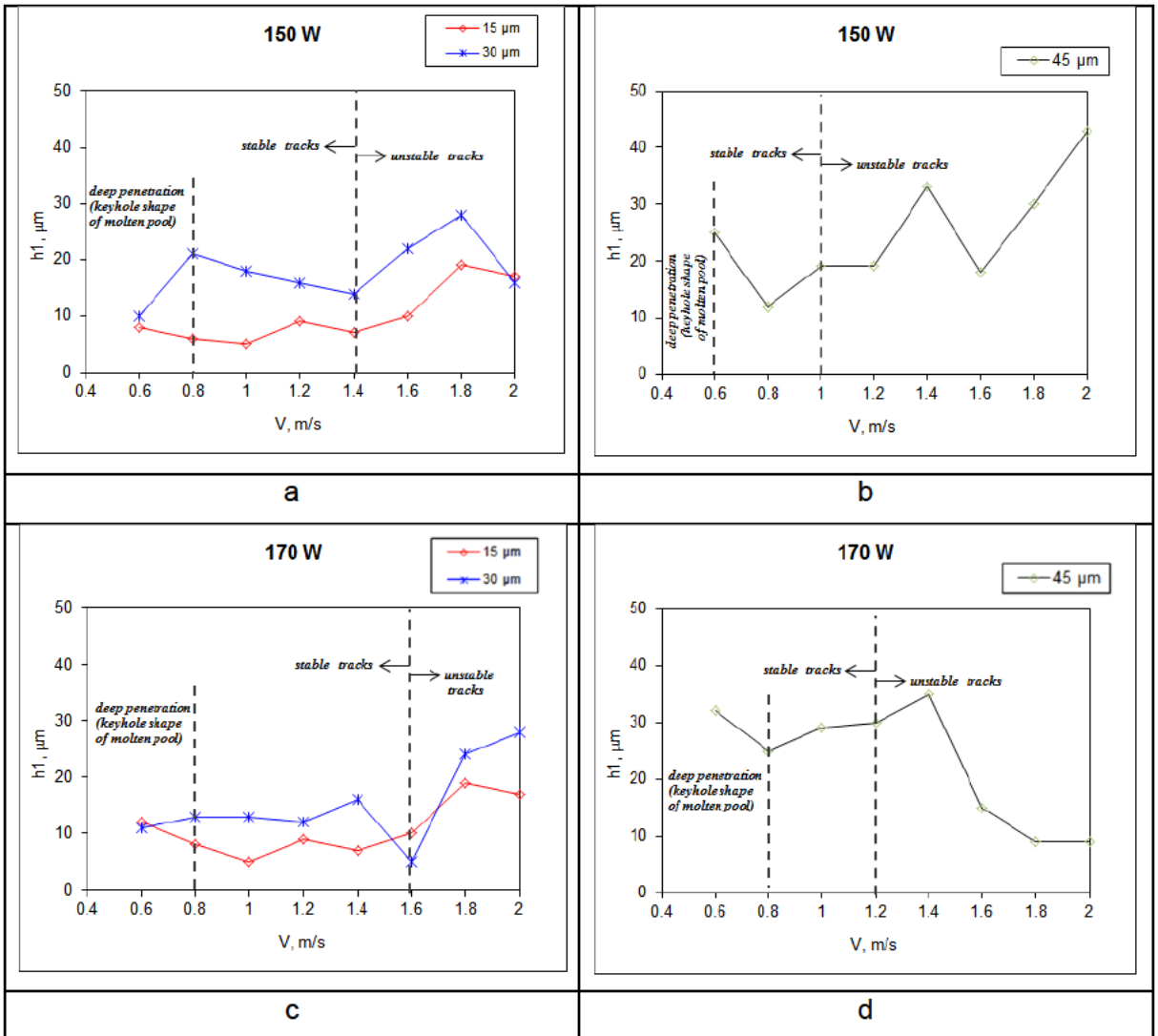

Figure 5.14a-d: Measured track heights for powder thickness of 15, 30 and 45 µm

At low scanning speeds (600-800 mm/s), a “keyhole” shape of melt pool and deep penetration (h2) into the substrate were observed. At 170 W, penetration was deeper for all scanning ranges, and the difference in the penetration depth between the 15 and 30 µm layers was less pronounced. The re-melt depth for 45 µm layers varied significantly with the scanning speed. Deep penetration is one of the determining factors for manufacturing DMLS objects with mechanical properties such as wrought materials, therefore layer thickness may be critical for good layer cohesion. The re-melt depth is over 15 times higher than that of the track height (for example, *P*=170 W, *V*=600 mm/s, figures 5.14c and 5.15c).

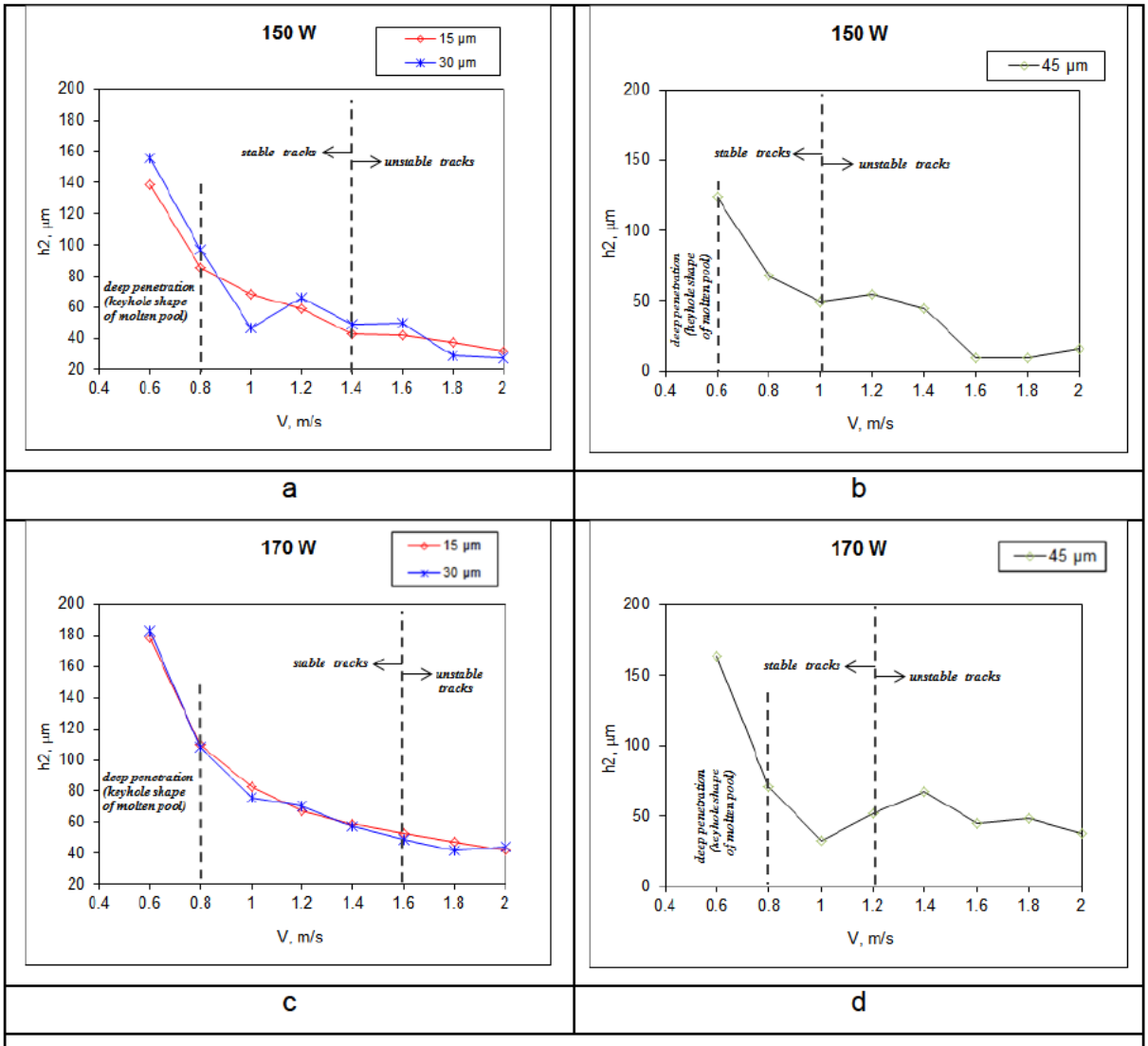

Figure 5.15a-d: Measured re-melt depth for powder thickness of 15, 30 and 45 µm

The total re-melt height (re-melt depth plus the height of the track) is dependent on the scanning speed as well as laser power (Figure 5.16a-d).

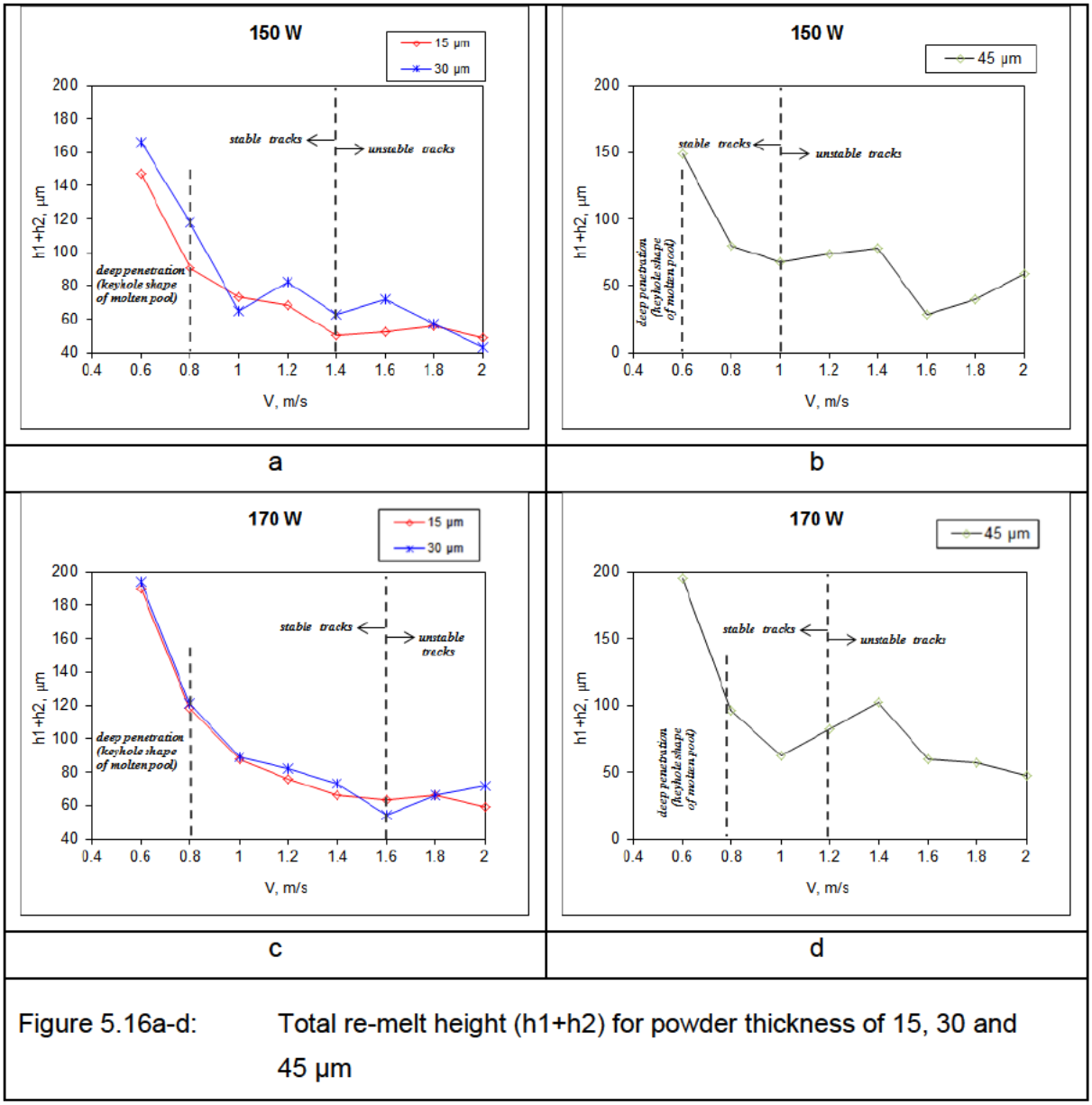

Figure 5.16a-d: Total re-melt height (h1+h2) for powder thickness of 15, 30 and 45 µm

Measurement of the track melt area, (S1) for powder thickness of 15, 30 and 45 µm, showed an increase with the increase of volume of powder material. When tracks were unstable and the balling-effect more pronounced (higher scanning speed at 45 µm layer thickness, Figure 5.17b and Figure 5.17d), the track melt area values fluctuated considerably.

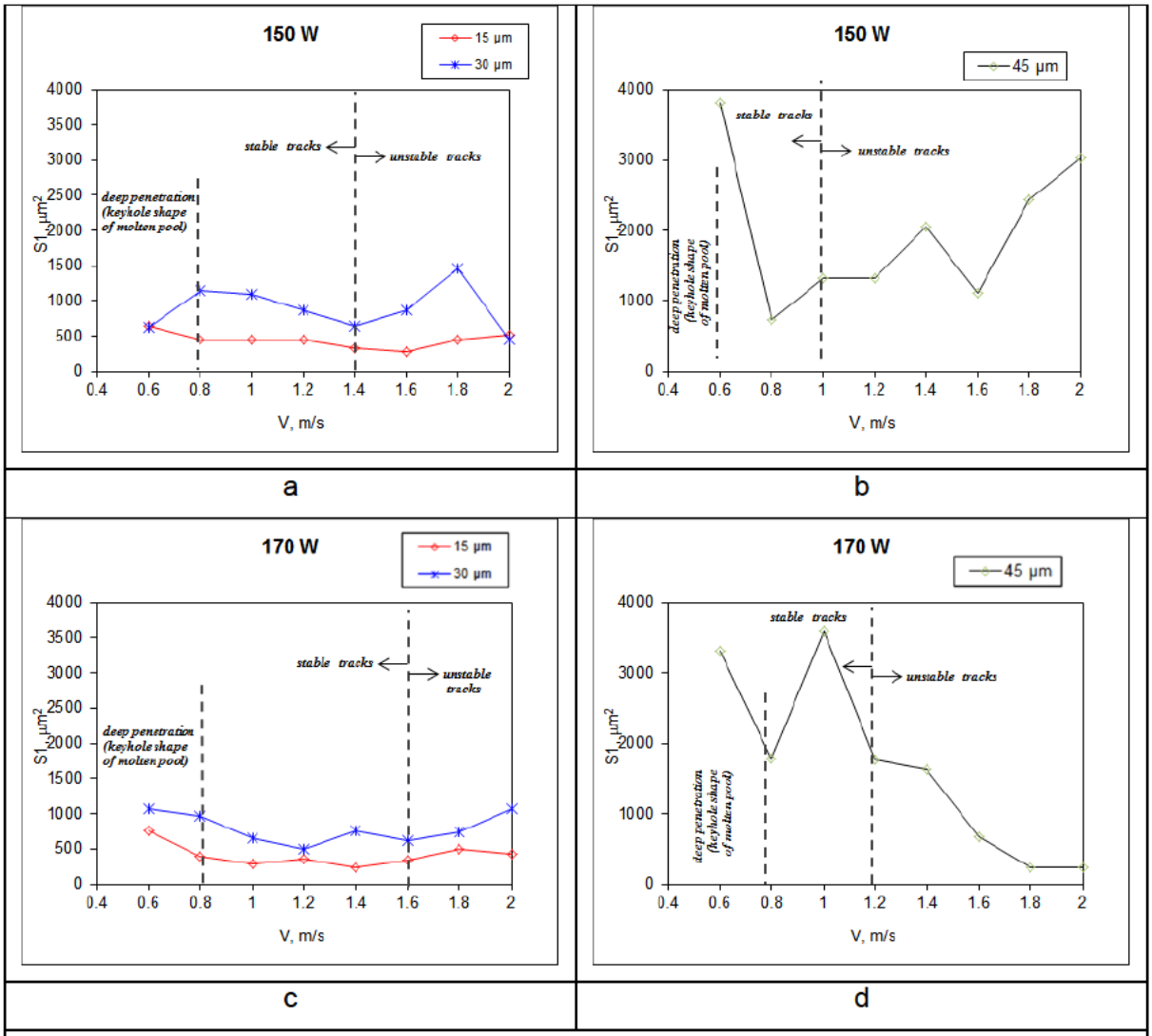

Figure 5.17a-d: Measurement of the track melt area (S1) for powder thickness of 15, 30 and 45 µm

For small layer thicknesses, the laser radiation can interact directly with the substrate and during heating, the powder and substrate material create a joint melt pool simultaneously. For the thicker powder layers, optical penetration of laser radiation starts to play an important role. When laser radiation is exposed to plain metallic surface, its absorption is controlled by intrinsic physical properties and influenced by extrinsic factors. The efficiency of laser-powder interaction is affected also by granulomorphometric characteristics of the powder (Figure 5.18). Particle size and size distribution, particle shape and roughness have an influence on the reflection, absorption and scattering [5].

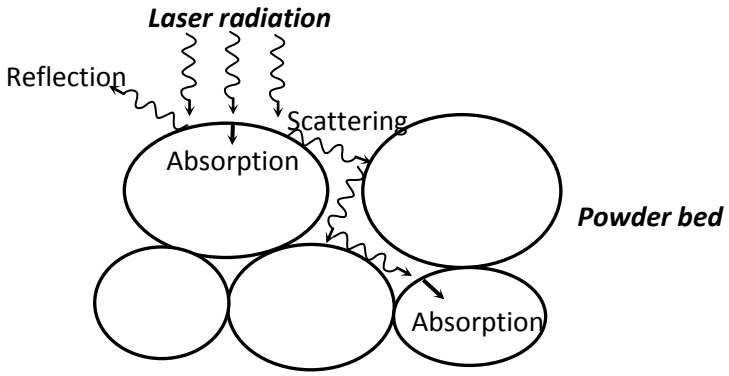

Figure 5.18. The mechanism of interaction of laser radiation with a powder medium [5]

The track re-melt area was almost the same for 15 and 30 µm layer thicknesses due to low apparent density (Figure 5.19a and Figure 5.19c).

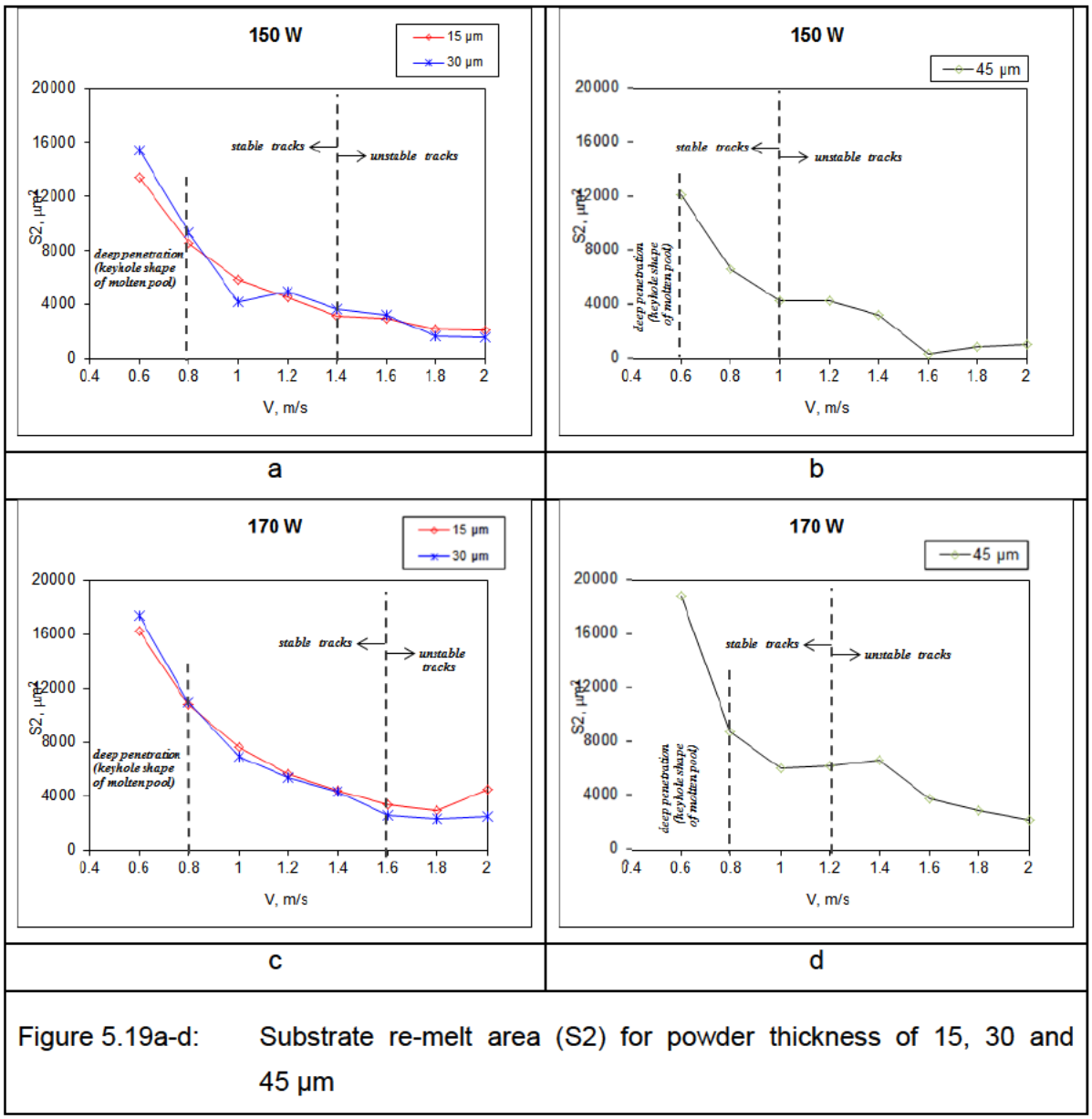

Figure 5.19a-d: Substrate re-melt area (S2) for powder thickness of 15, 30 and 45 µm

Thus, at 45 µm powder layer thickness, the substrate re-melt area was smaller than the 15 µm and 30 µm powder layers.At small layer thicknesses, the total re-melt area depends only on energy input, therefore there was no considerable difference betweenall the layers (Figure 5.20a-d).

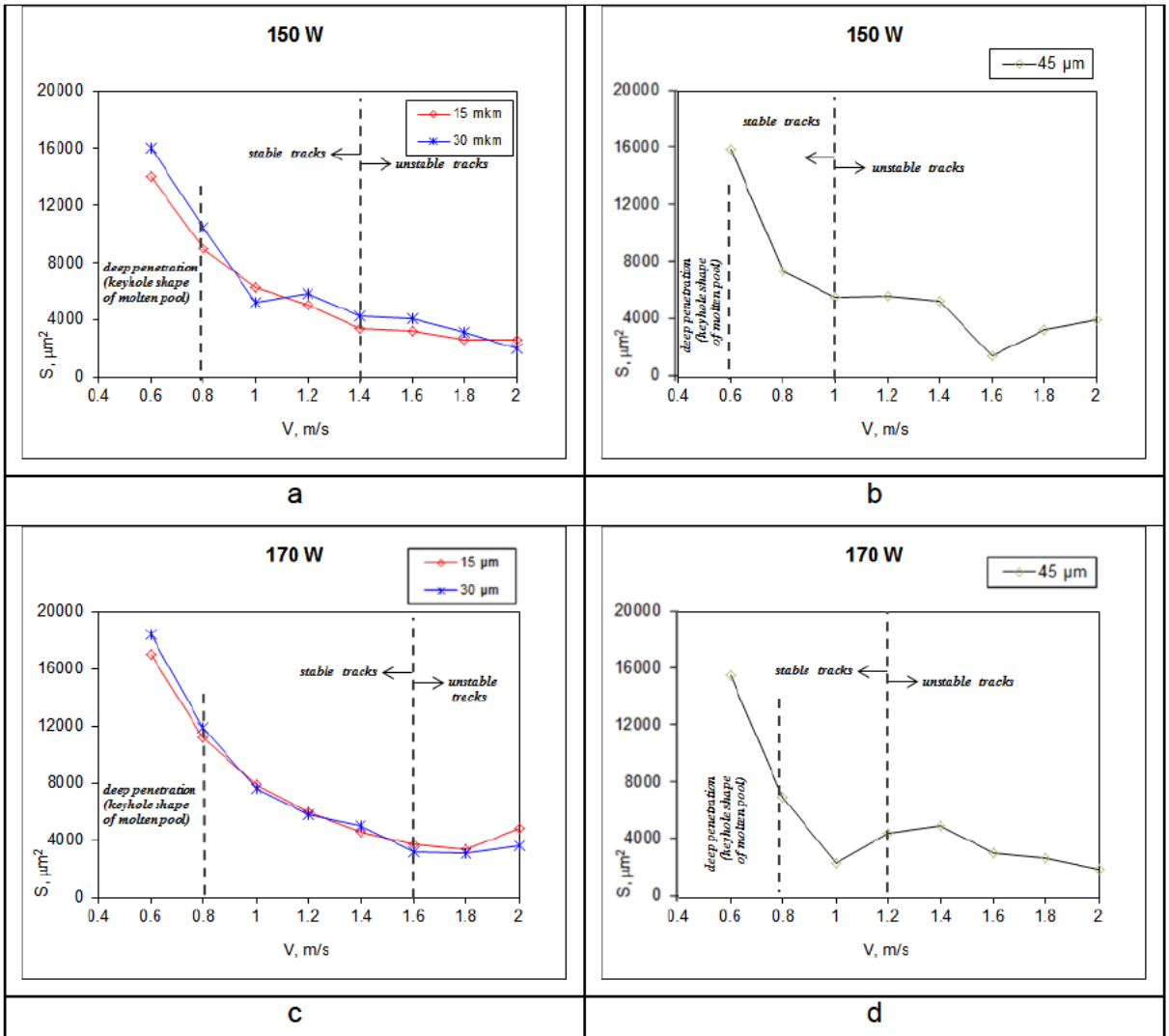

Figure 5.20a-d: Total re-melt area S=S1+S2 for powder thickness of 15, 30 and 45 µm

CHAPTER 6
CONCLUSIONS AND FUTURE DEVELOPMENTS

6.1 Conclusions

6.1.1 State of the technology

AM is a process in which objects are produced directly from 3D CAD data by sequential deposition of material and/or energy and opposite to “classical or conventional” technologies, where substrate material is removed from a blank piece of material to create a functional part. The popularity of AM technology has been growing in leaps and bounds since the 1970’s. However, in order to become more widely adopted by the major role players in the manufacturing industry, AM technologymust be able to produce components that can be employed as final working parts. The latest applicationincludes the production of metal parts via AM processes that can be applied with confidence in the aerospace, automotive and medical industries. Apart from the advantage of less material wastage, another benefit of the AM process isthe creation of objects with the desired shape, internal structure and engineered composition, including special surface properties, within a single fabrication step. DMLS technology is able to produce manufactured parts with the desired microstructure as well as macrostructure.

This work discussed the current state of the metal AM technology with respect to the main variations between the metal powder bed AM systems currently available which use a melting binding process, and included a historical perspective on how this technology evolved up to the state of the technology in 2014. Recent years saw a number of new variations of the same basic technology; mostly following the same technological and application trends.

6.1.2 Titanium and its applications

Titanium has proved to be a material of choice for the increased demands from the manufacturing industry related to suitable materials for extreme environments and operating conditions as well as structural integrity. High corrosion resistance, high strength to weight ratio and bio-compatibility are some of the material properties of titanium that make it such a versatile material and obvious choice when looking for a metal material to manufacture in a MAM process. AM technology provides design freedom which in turn opens areas of possibility previously not even considered. For the purpose of this study, Ti-6Al-4V powder

was used in an experimental study on fabrication of single tracks that will lead to further study in the future of the manufacture of 3D functional medical components. The quality of these components produced with the DMLS process will be directly affected by the quality of each individual laser sintered track of each consecutive layer.

6.1.3 Results and discussion

Continuous tracks with uniform geometrical characteristics were produced in powder layer thicknesses of 15, 30 and 45 µm, under varying laser power and scanning speed. More stable tracks were obtained at 15 and 30 µm layer thickness (Figure 6.3), where powder deposition imperfections, roughness of the substrate and even some variation in laser scanning speed did not result in large differences in geometry of the tracks.

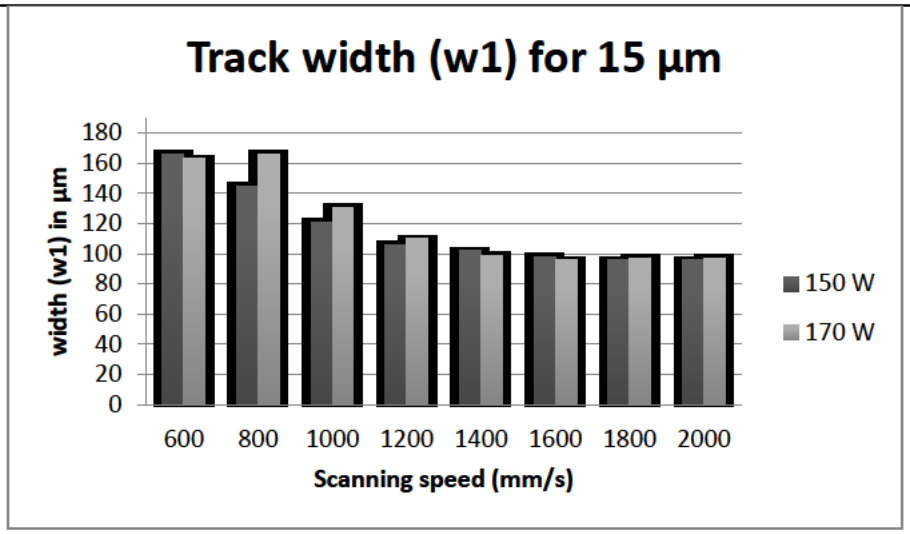

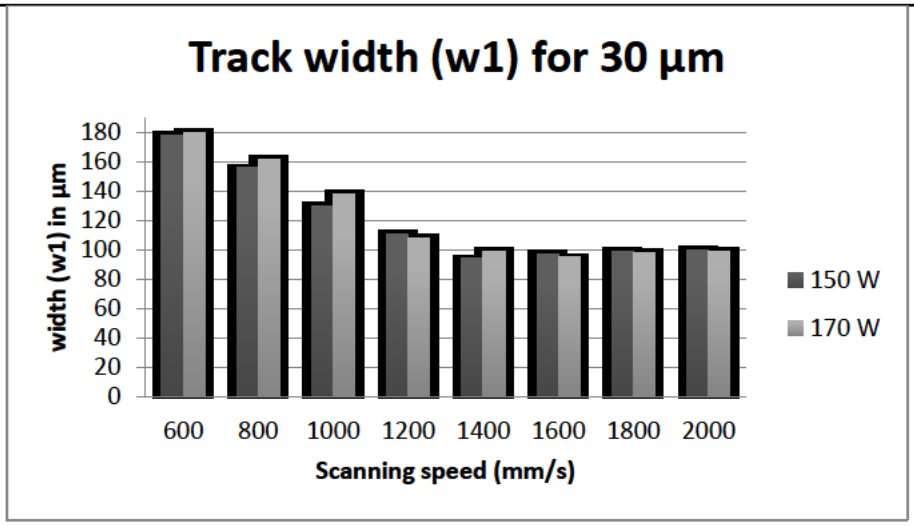

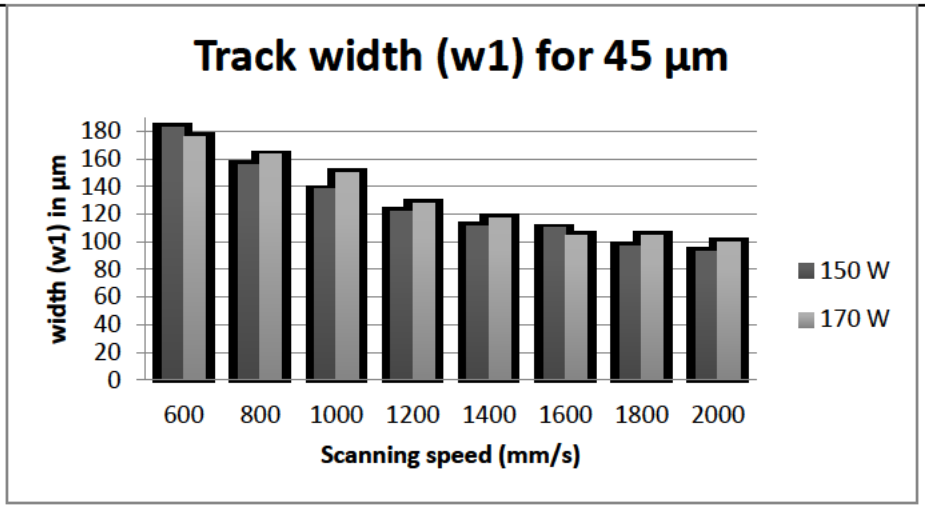

Figure 6.1: Comparison of measured track widths (w) in µm for powder thickness of 15, 30 and 45 µm

Based on visual inspection and measurement, one can conclude that a track width in the order of 110 µm, laser power of 170 W and scanning speed of 1200 mm/s, with a hatch distance of about 70 µm (figures 6.2 and 6.3) could be selected for producing non-porous 3D DMLS parts. Particle size distribution of below 45 µm of the specific powder that was used for this study proved not to be optimal for 45 µm layer thickness: geometrical characteristics and shapes of single tracks varied significantly.

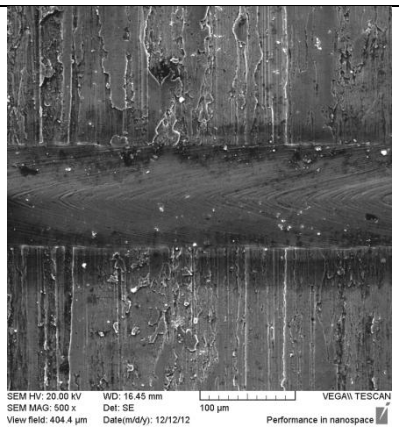

a

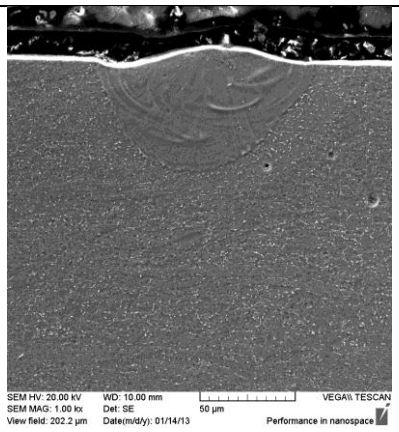

b

Figure 6.2: Top view (a) and cross-section (b) of optimal single track produced at 15 µm layer thickness, 170 W laser power and scanning speed of 1200 mm/s

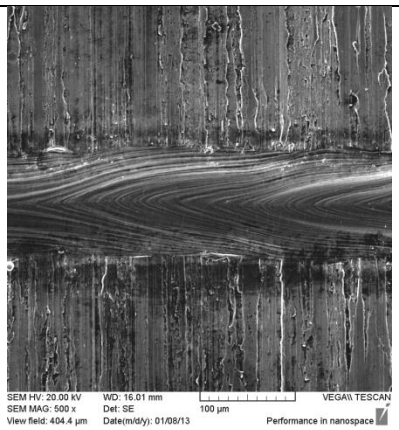

a

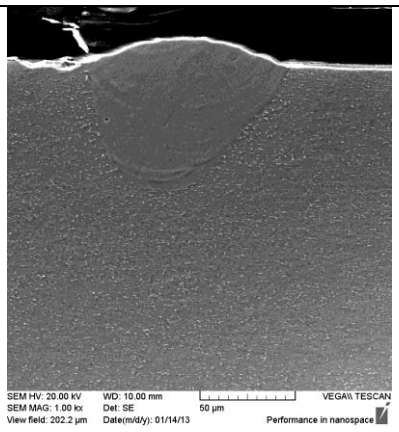

b

Figure 6.3: Top view (a) and cross-section (b) of optimal single track produced at 30 µm layer thickness, 170 W laser power and scanning speed of 1200 mm/s

This study also revealed that by decreasing the scanning speed one could potentially increase the surface quality of parts produced during the DMLS process but will increase the time spent manufacturing the components. An optimal set of parameters for this scenario could be 15 µm powder layer thickness, 1000 mm/s scanning speed and 150 W laser power (Figure 6.4) because this specific set of parameters resulted in a track with uniform geometry and a very low track height (h1) which will minimise the “stair-step” effect associated with AM. This study furthermore identified the possibility of producing 3D structures with possible wall thicknesses of less than 100 µm by increasing the scanning speed which will then produce a very narrow uniform laser track. This increase in scanning speed will save production time but will however negatively affect the surface finish of the 3D part. An optimal set of parameters for producing thin-walled components could be 30 µm powder layer thickness, 1400 mm/s scanning speed and 170 W laser power (Figure 6.5).

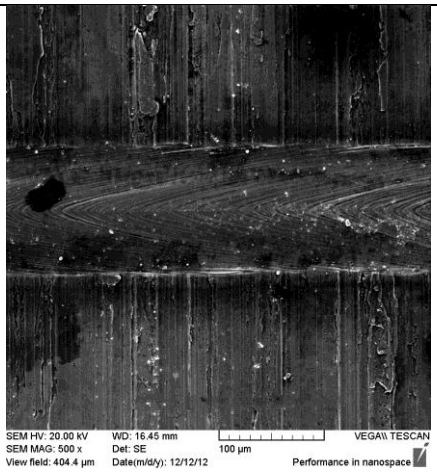

Figure 6.4: Proposed optimal parameter set for high surface quality components:
15 µm powder layer thickness,1000 mm/s scanning speed and 150 W laser power

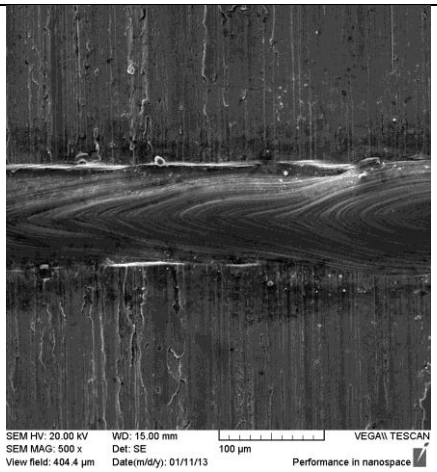

Figure 6.5: Proposed optimal parameter set for thin-walled components:
30 µm powderlayer thickness,1400 mm/s scanning speed and170 W laser power

The theoretical model introduced correlated with experimental data and is useful to estimate geometrical characteristics of single tracks for the conductive mode of laser melting. The differences in experimental and calculated data may be attributed to the fact that the model only considers heat transfer by means of conduction (without convection) and does not account for the temperature dependence of physical characteristics of the laser-irradiated material such as absorption, thermal diffusivity, density and surface tension. With the decrease in scanning speed, the energy increases sufficiently for the boiling point and latent heat to increase up to the point where evaporation occurs and “keyhole mode” is realised.

Nevertheless, this model can be useful for estimating the parameters of the melt pool in the conductive mode of laser melting, and to choose the settings of process parameters for melting of thin powder layers and for re-scanning. Knowledge about temperature distribution may be important for laser heat treatment as well as for the estimation of different phase formations during DMLS. The model predicted lower values of track width at all scanning speeds (Figure 5.11a), and also underestimated the re-melting depth significantly at scanning speeds below ~900 mm/s (Figure 5.11b).

6.2 Future experimental work

Although the past 40 years have seen vast technological advancement in the field of AM, the technology is far from perfect. Limited part size and geometrical distortion, due to residual stress, are a few of the obstacles that hinder the whole-hearted adoption of AM in commercial part production. Another obstacle to overcome is to achieve high-quality components repeatedly, not only on the same job but also on consecutive jobs. More and more machine manufacturers are spending a great deal ofresources addressing this problem, adding process monitoring and -control features to ensure part quality. To solve the residual stress problem, machine manufacturers are considering increased powder bed temperatures. The idea is that higher powder bed temperatures will decrease the temperature gradient associate with these systems. The nature of the melting process with its rapid heating and cooling rates causes very high levels of residual stress (in some cases close to the material's yield strength) to be captured within the manufactured components. A stress-relieving heat treatment is necessary prior to removal of parts from the substrate to minimise geometric distortion. Furthermore,the part will have poor fatigue properties without adequate heat treatment after the part has been completed to improve ductility. This obstacle is the focus of many academic institutions worldwide.

With regard to future work, this single track study should be expanded to finally produce 3D components with optimal parameters. Yadroitsev [5] identified two specific areas of interest, to achieve the aformentioned, namely the overlapping distance (hatch distance) between two laser tracks next to each other (Figure 6.6) and secondly, to what extent the process parameters affects the formation of sintered tracks melted on top of each other (Figure 6.7).

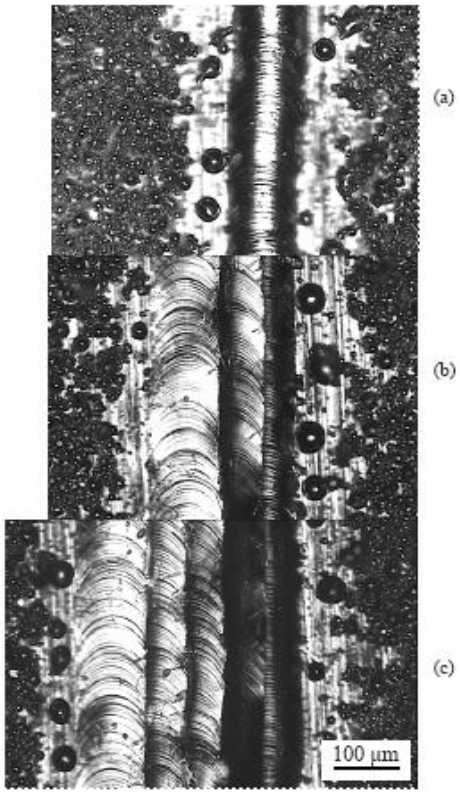

Figure 6.6: Top view of tracks synthesised from 904L stainless steel powder on substrate at different hatch distances: (a), (b), (c) – one, three, and five tracks at 60 µm hatch distance [94]

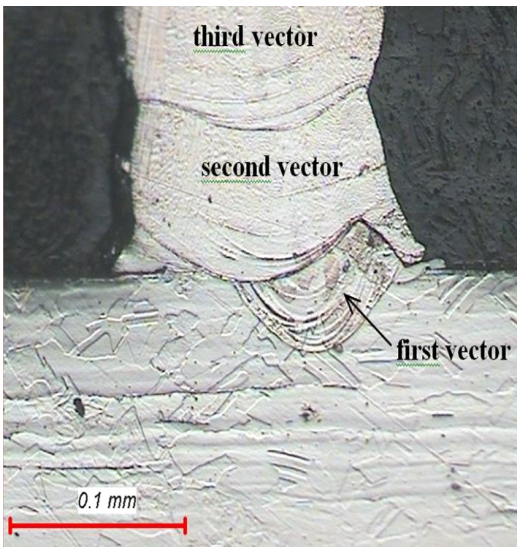

Figure 6.7: Cross-sectional view of tracks produced on top of each other in 904L stainless steel powder with the following parameters: Scanning speed is 100 mm/s; thickness of each powder layer is 50 µm; laser power is 50 W [5]

REFERENCES

1. Wohlers, T. Wohlers Report 2013: **Additive manufacturing and 3D printing state of the industry**. Annual worldwide progress report, Wohlers Associates, Fort Collins
2. **Additive Manufacturing Market, By Application and Technology - Forecast (2012 - 2017)**[online]. Available:<http://www.marketsandmarkets.com/Market-Reports/additive-manufacturing-medical-devices-market-843.html>[Accessed 10 February, 2014]
3. Berger, A.**Additive Manufacturing – A game changer for the manufacturing industry?** [online]. Available: <http://www.rolandberger.com/media/pdf/Roland_Berger_Additive_Manufacturing_20131129.pdf>[Accessed 10 February, 2014]
4. Li, J. P.,Wilson, C.,Wijn, J. R.,VanBlitterswijk, C. A.,De Groot., K. 2007.Fabrication of porous Ti6Al4V with designed structure by rapid prototyping technology. **Key Eng. Mater,** 330-332: 1293
5. Yadroitsev, I. 2009. **Selective laser melting: Direct manufacturing of 3D-objects by selective laser melting of metal powders.** LAP Lambert Academic Publishing GmbH & Co. KG (Saarbrücken, Germany, ISBN-978-3-8383-1794-6)
6. Gunnam, R. 2010.**The future of orthopedic implants analysis and forecasts to 2016** [online]. Available <http://www.freearticlesnow.com/article-the-future-of-orthopedic-implants-analysis-and-forecasts-to-2016-9805.html> [Accessed 8 July, 2010]
7. Gunnam, R. 2010.**The future of orthopedic implants analysis and forecasts to 2016** [online]. Available <http://www.pressreleasepoint.com/future-orthopedic-implants-analysis-and-forecasts-2016> [Accessed 8 July, 2010]
8. Gunnam, R. 2010.**The future of orthopedic implants analysis and forecasts to 2016** [online]. Available <http://www.pr-inside.com/the-future-of-orthopedic-implants-analysis-r1932621.htm> [Accessed 8 July, 2010]
9. Marin, E., Fusi, S., Pressacco, M., Paussa, L., Fedrizzi, L. 2010. Characterization of cellular solids in Ti6Al4V for orthopaedic implant applications: trabecular titanium. **J Mech Biomed Mater,** 3(5):373-81
10. Murr, L.E. et al. 2012. Metal fabrication by additive manufacturing using laser and electron beam melting technologies. **J Mat Sci and Tech** 28(1):1-14

11. **Additive Technologies Focusing on Industrial Applications for Metal and Plastic Parts** [online]. Available <http://www.naefrontiers.org/File.aspx?id=38390> [Accessed 19 Aug, 2014]
12. Wong, K. V., Hernandez, A. 2012. A Review of Additive Manufacturing.**MechEng**2012:1-10
13. Shellabear, M.,Nyrhilä, O. 2004. **DMLS – Development History and State of the Art.**Proceedings of the International Conferences onLaser Assisted Net Shape Engineering. Lane 2004. Erlangen, p393-404
14. **Pierre Ciraud's patent illustration** [online]. Available <http://www.wtec.org/loyola/rp/03_01.htm> [Accessed 2 May, 2013].
15. **Ross Housholder's patent illustration** [online]. Available <http://www.lia.org/blog/2012/04/the-history-of-laser-additive-manufacturing/> [Accessed 2 May, 2013]
16. 3D Systems Completes Acquisition of Phenix[online]. Available <http://www.3dsystems.com/press-releases/3d-systems-completes-acquisition-phenix>[Accessed 19 Aug, 2014]
17. Tian, X., Günster, J., Melcher, J., Li, D., Heinrich, J.G. 2009. Process parameters analysis of direct laser sintering and post treatment of porcelain components using Taguchi's method. **J Euro CerSoc,** 29: 1903-1915
18. Simchi, A., Petzoldt, F., Pohl, H. 2003. On the development of direct metal laser sintering for rapid tooling. **Journal of Materials Processing Technology,** 141: 319-328
19. Gu, D., Shen, Y., Xiao, J. 2008. Influence of processing parameters on particle dispersion in direct laser sintered WC-Co_p/Cu MMCs. **Int J Refr Met & Hard Mat,** 26: 411-422
20. Frank, M.C. 2006. Subtractive Rapid Prototyping: Creating a Completely Automated Process for Rapid Machining. In:Kamrani, A. K. and Nasr, E. A. (eds). **Rapid Prototyping Theory and Practice**. Springer Science+Business Media Inc, New York, p. 166
21. Kolossov, S., Boillat, E., Glardon, R., Fischer, P., Locher, M. 2004. 3D FE simulation for temperature evolution in the selective laser sintering process. **Int J MachTools & Man,** 44: 117-123, Oct
22. Sanner, N.,Huot, N.,Audouard, E. 2005. Programmable focal spot shaping of amplified femtosecond laser pulses. **Optics Letters**. 30 (12): 1479-1482
23. **EOSINT M 270** [online]. Available <http://www.rmsiberia.com/Producto/eosint_m270_en.pdf> [Accessed 2 May, 2013]

24. **EOSINT M 270** [online]. Available <http://www.rmsiberia.com/Producto/eosint_m270_en.pdf> [Accessed 2 May, 2013]
25. **EOSINT M 280** [online]. Available <http://www.detekt.com.tw/download/eos/2%E6%A9%9F%E5%99%A8%E7%A8%AE%E9%A1%9E/%EF%BC%AD%E7%B3%BB%E5%88%97/TD_M280_en_2011-03-29.pdf> [Accessed 2 May, 2013]
26. **EOSINT M 270** [online]. Available<http://www.kraftwurx.com/images/stories/Printers/EOS%20EOSINT%20M270/eosm270-1.jpg> [Accessed 2 May, 2013]
27. **EOSINT M 280** [online]. Available<http://www.eos.info/en/news-events/newsletter/edition-42010.html>[Accessed 2 May, 2013]
28. **Concept Laser** [online]. Available <http://www.concept-laser.de/en/>[Accessed 2 May, 2013]
29. **Concept Laser M1 and M2** [online]. Available <http://www.4cmedikal.com.tr/html_eng/hizli_protorip_sistemler_02.html>[Accessed 2 May, 2013]
30. **Concept LaserM3** [online]. Available <http://concept-laser.hofmann innovation.com/en/industry/mould/machines.html> [Accessed 2 May, 2013]
31. **SLM Solutions** [online]. Available <http://www.additive3d.com/tl_221a.htm> [Accessed 2 May, 2013]
32. **SLM Solution** [online]. Available <http://www.additive3d.com/ind_22.htm> [Accessed 2 May, 2013]
33. **Laser Beam Melting System SLM® 125HL** [online]. Available <http://www.slm-solutions.com/cms/upload/pdf/120923_SLM_125_Flyer.pdf> [Accessed 2 May, 2013]
34. **Laser Beam Melting System SLM® 250HL** [online]. Available <http://www.slm-solutions.com/cms/upload/pdf/120923_SLM_250_Flyer.pdf> [Accessed 2 May, 2013]
35. **Laser Beam Melting System SLM® 280HL** [online]. Available <http://www.slm-solutions.com/cms/upload/pdf/120923_SLM_280_Flyer.pdf> [Accessed 2 May, 2013]
36. **Laser Beam Melting System SLM® 500HL** [online]. Available <http://www.slm-solutions.com/cms/upload/pdf/SLM_500_Flyer.pdf> [Accessed 2 May, 2013]
37. **Laser Beam Melting System SLM® 125HL** [online]. Available <http://www.slm-solutions.com/en/products/slm-equipment/slm-125-hl/> [Accessed 2 May, 2013]
38. **Laser Beam Melting System SLM® 250HL** [online]. Available <http://www.slm-solutions.com/en/products/slm-equipment/slm-250-hl/> [Accessed 2 May, 2013]
39. **Laser Beam Melting System SLM® 280HL** [online]. Available <http://www.slm-solutions.com/en/products/slm-equipment/slm280-hl/> [Accessed 2 May, 2013]

40. **Laser Beam Melting System SLM® 500HL** [online]. Available <http://www.slm-solutions.com/en/products/slm-equipment/slm-500-hl/> [Accessed 2 May, 2013]
41. **Phenix Systems** [online]. Available <http://www.phenix-systems.com/sites/www.phenix-systems.com/files/produit/pdf/brochure_phenix_systems_gb_2012.pdf> [Accessed 2 May, 2013]
42. **Phenix PXS** [online]. Available <http://www.phenix-systems.com/en/pxs> [Accessed 2 May, 2013]
43. **Phenix PXM** [online]. Available <http://www.phenix-systems.com/en/pxm> [Accessed 2 May, 2013]
44. **Phenix PXL** [online]. Available <http://www.phenix-systems.com/en/pxl> [Accessed 2 May, 2013]
45. **ReaLizer SLM 50** [online]. Available <http://www.realizer.com/en/wp-content/themes/realizer/SLM%2050_Schmuck-2011en.pdf> [Accessed 2 May, 2013]
46. **ReaLizer SLM 100** [online]. Available <http://www.realizer.com/en/wp-content/themes/realizer/SLM%20100_2011_EN.pdf> [Accessed 2 May, 2013]
47. **ReaLizer SLM 250** [online]. Available <> [Accessed 2 May, 2013]
48. **ReaLizer SLM** [online]. Available <http://www.realizer.com/startseite/slm-maschinen [Accessed 2 May, 2013]
49. **Renishaw plc** [online]. Available <http://www.renishaw.com/en/laser-melting-systems--15240> [Accessed 2 May, 2013]
50. **Renishaw AM 125** [online]. Available <http://www.renishaw.com/en/am125-laser-melting-machine--15254> [Accessed 2 May, 2013]
51. **Renishaw AM 250** [online]. Available <http://www.renishaw.com/en/am250-laser-melting-machine--15253> [Accessed 2 May, 2013]
52. **3D Systems Corporation** [online]. Available <http://production3dprinters.com/sites/production3dprinters.com/files/downloads/sPro-125-250-SLM-Direct-Metal.pdf> [Accessed 2 May, 2013]
53. **3D Systems sPro™ 125** [online]. Available <http://production3dprinters.com/slm/spro125-direct-metal-slm-production-printer> [Accessed 2 May, 2013]
54. **3D Systems sPro™ 250** [online]. Available <http://production3dprinters.com/slm/spro250-direct-metal-slm-production-printer> [Accessed 2 May, 2013]
55. **ARCAM A1** [online]. Available <http://www.arcam.com/CommonResources/Files/www.arcam.com/Documents/Products/Arcam-A1.pdf> [Accessed 2 May, 2013]

56. **ARCAM A2** [online]. Available <http://www.arcam.com/CommonResources/Files/www.arcam.com/Documents/Products/Arcam-A2.pdf> [Accessed 2 May, 2013]
57. **ARCAM A1** [online]. Available<http://www.arcam.com/products/arcam-a1/index.aspx > [Accessed 2 May, 2013]
58. **ARCAM A2** [online]. Available<http://www.arcam.com/products/arcam-2/index.aspx[Accessed 2 May, 2013]
59. **Matsuura LUMEX Avance-25** [online]. Available<http://www.matsuura.co.uk/matsuura/lumex-avance-25/> [Accessed 2 May, 2013]
60. **Matsuura LUMEX Avance-25** [online]. Available <http://www.matsuura.co.jp/english/contents/products/lumex.html> [Accessed 2 May, 2013]
61. Joshi, V. 2006. **Titanium Alloys: An Atlas of Structures and Fracture Features.** CRC Press. Taylor and Francis Group. (Boca Raton, United States of America) ISBN 0-8493-5010-7
62. Lutjering, G., Williams, J. 2003. **Titanium.** Springer-Verlag.(New York)
63. Donachie, M.J. Jr. 1988. **Titanium: A Technical Guide (2nd Ed.).** ASM International. Metals Park (Ohio) ISBN 0-87170-686-5
64. Freese, H.L., Volas, M.G., Wood, J.R., Textor, M. 2001. **Titanium and its Alloys in Biomedical Engineering.** Encyclopedia of Materials: Science and Technology.Elsevier. (New York)
65. Boyer, R.R. Attributes, characteristics, and applications of Titanium and its alloys. **J of Mat,** 62 (5), 35-43
66. Boyer, R.R. 1996. An overview on the use of titanium in the aerospace industry. **MatSci and Eng,**A217: 103-II4
67. Gorynin, I.V. 1999. Titanium alloys for marine application. **MatSci and Eng,**A263: 112–116
68. Seagle, S.R. 1996. The state of the USA titanium industry in 1995. **MatSci and Eng,**A213: 1-7
69. Yamada, M. 1996. An overview on the development of titanium alloys for non-aerospace application in Japan. **MatSci and Eng,** A213: 8-15
70. **Wilson Titanium Technology** [online]. Available<http://guvvel.znamenie.org/wilson/Tennis/titanium_technology.htm> [Accessed 13 November, 2013]
71. **TaylorMade Titanium driver** [online]. Available: <http://valueguide.pga.com/detail-exec/brand/2784/product_type/204/model/44718/b/TaylorMade/p/Fairway%20Wood/m/Titanium%20Bubble>[Accessed 13 November, 2013]

72. Schutz, R.W., Watkins, H.B. 1998. Recent developments in titanium alloy application in the energy industry. **Mat Sci and Eng,** A243: 305–315
73. Bothe, R.T., Beaton, L.E., Davenport, H.A. 1940. Reaction of bone to multiple metallic implants, **Surg**, **Gyn&Obs,** *7I:* 598-602
74. Leventhal, G.S. 1951. Titanium, a metal for surgery. **J. Bone Joint Surg.**, 33-A(2) 473
75. Wang, K. 1996. The use of titanium for medical applications in the USA. **Mat Sci and Eng,** A213: I34- I37
76. **EOS Titanium Ti64 – for aerospace and engineering applicationsand biomedical implants** [online]. A vailable<http://www.eos.info/en/products/materials/materials-for-metal-systems/eos-titanium-ti64.html> [Accessed 18 July, 2010]
77. **Total knee replacement** [online]. Available <http://www.kneereplacementcosts.com/implant-types.html> [Accessed 13 November, 2013]
78. Baufeld, B., Van der Biest, O., Gault, R. 2010. Additive manufacturing of Ti–6Al–4V components by shaped metal deposition: Microstructure and mechanical properties. **Mat & Des,** 31, S106-S111
79. Klocke, F., Wagner, C., Ader, C. 2003. Development of an integrated model for selective laser sintering. Proceedings of the 36th CIRP International Seminar on Manufacturing Systems, June 03-05, Saarbrucken, Germany, 387-392
80. Simchi, A. 2006. Direct laser sintering of metal powders: Mechanism, kinetics and microstructural features. **Mat Sci and Eng,** 428: 148-158
81. Simchi, A. Pohl, H. 2003. Effects of laser sintering parameters on the microstructure and densification of iron powder. **Mat Sci and Eng,** 359: 119-128
82. Van Elsen, M. 2007. Complexity of selective laser melting: a new optimisation approach. PhD thesis, Katholieke Universiteit Leuven
83. Simchi, A. 2004.The role of particle size on the laser sintering of iron powder. **Metallur and Mat Trans B**, 35 (5): 937-948
84. Yang, S., Evans, J. R. G. 2004. A multi-component powder dispensing system for three dimensional functional gradients. **Mat Sci and Eng,** A379: 351–359
85. Tolochko, N. K., Mozzharov, S. E., Yadroitsev, I. A., Laoui, T., Froyen, L., Titov, V. I., Ignatiev, M. B. 2004. Balling processes during selective laser treatment of powders. **Rapid Proto J,** 10 (2), 78-87
86. Rońda, J.,Siwek,A. 2011. Modelling of laser welding process in the phase of keyhole formation. **Arch of Civ and MechEng,** 3, 739-752

87. P. S. Wei. , 2012, The Physics of Weld Bead Defects. In: **Welding Processes**, ed. R. Kovacevic, InTechDOI: 10.5772/2884, 395-414
88. Fabbro, R. 2011.Melt Pool and Keyhole Behavior Analysis for Deep Penetration Laser Welding. **J Phy D: App Phy**43, 44 (2010) 445501
89. Berger, P. Hügel, H. Hess, A. Weber, R.F. Graf, T. 2011.Understanding of Humping Based on Conservation of Volume Flow. **Physics Procedia**, 12 (A), 232–240
90. Mikli, V., Käerdi, H., Kulu, P., Besterci, M.. 2001.Characterization of powder particle morphology. **Proc. Estonian Acad. Sci. Eng.** 7 (1), 22–34
91. Angeles-Chavez, C., Toledo-Antonio,J. A., Cortes-Jacome, M. A. 2012. Chemical Quantification of Mo-S, W-Si and Ti-V by Energy Dispersive X-Ray Spectroscopy. in: X-Ray Spectroscopy. Edited by Shatendra K. Sharma, Intech, Croatia, p. 133
92. Yadroitsev, I., Bertrand, Ph.,Smurov, I. 2007. Parametric analysis of the selective laser melting process. **App Surf Sci**, 253, 8064–8069
93. Mladenov, G.M.,Koleva, E.G.,Vutova, K.J. 2009. Heat transfer and weld geometry at electron beam welding. **Int Review of MechEng,** 5 (2), 235-243
94. Yadroitsev, I.,Smurov, I. 2011. Surface Morphology in Selective Laser Melting ofMetal Powders. **Physics Procedia,**12, 264-270

APPENDIX 1

	without powder @ 150 W	15 µm @ 150 W	30 µm @ 150 W	45 µm @ 150 W
600 mm/s Top View	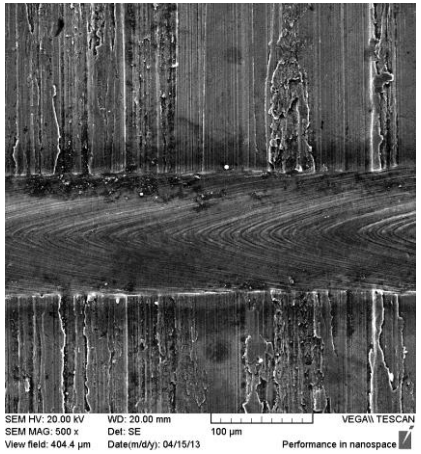	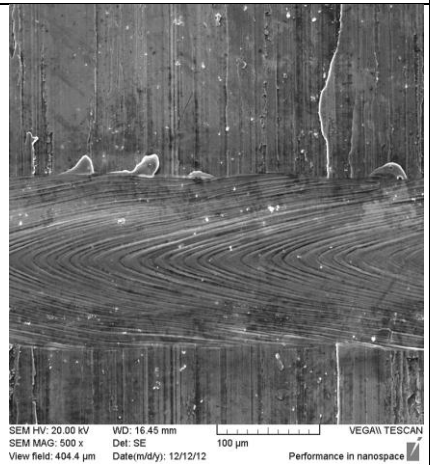		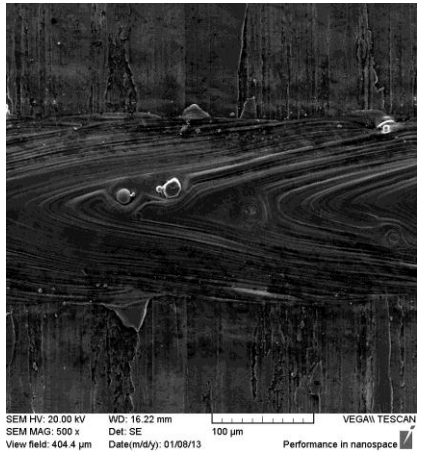
Cross-section	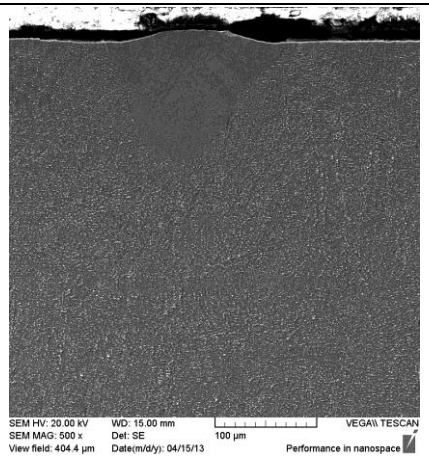	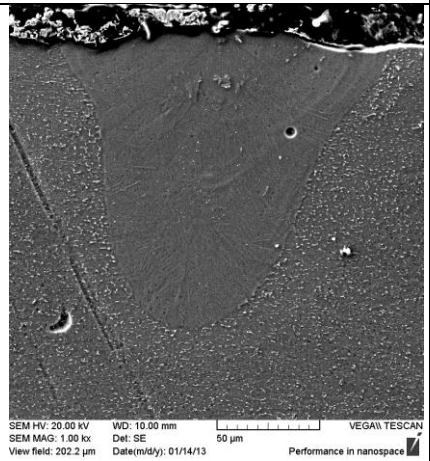	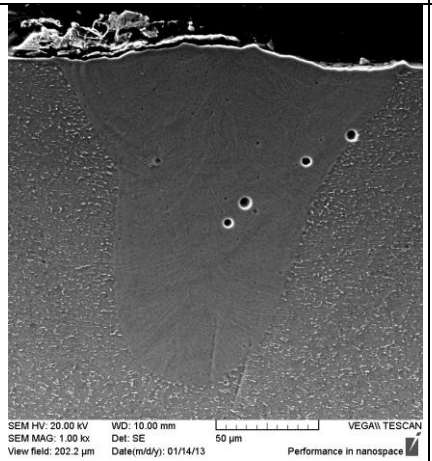	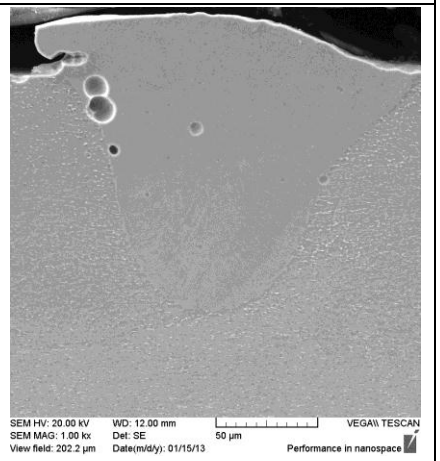

	without powder @ 150 W	15 µm @ 150 W	30 µm @ 150 W	45 µm @ 150 W
800 mm/s Top View	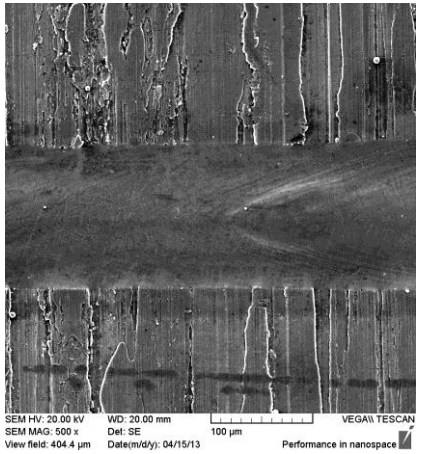	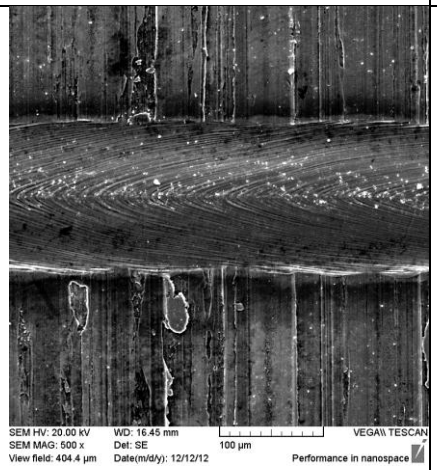		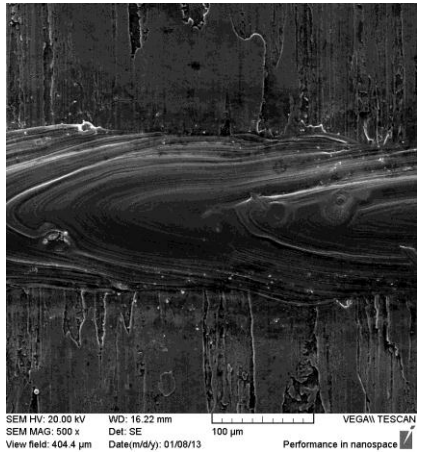
Cross-section	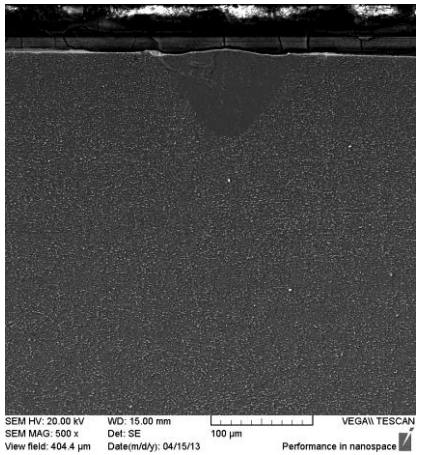	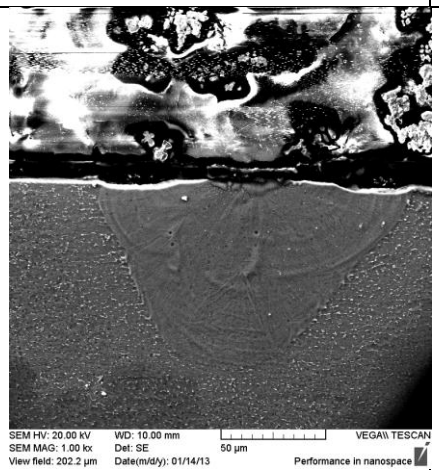	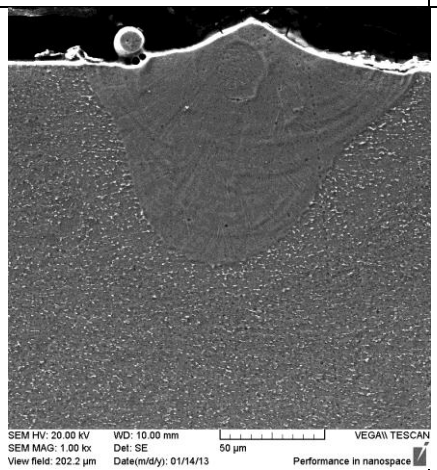	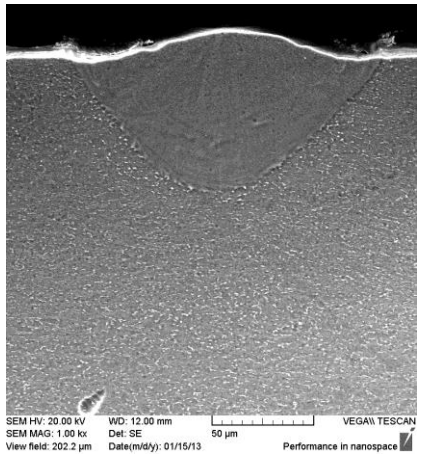

	without powder @ 150 W	15 µm @ 150 W	30 µm @ 150 W	45 µm @ 150 W
1000 mm/s Top View	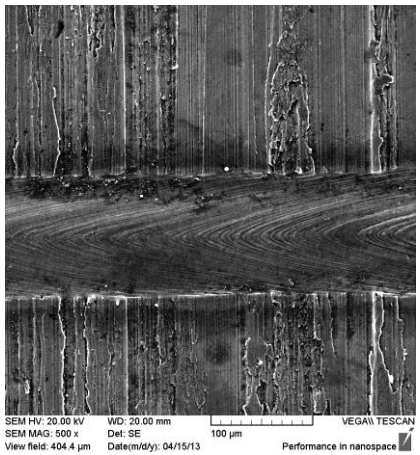	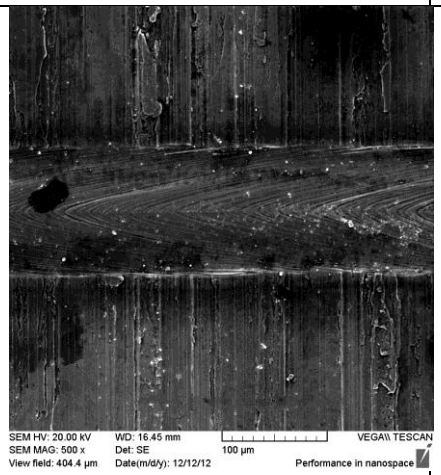	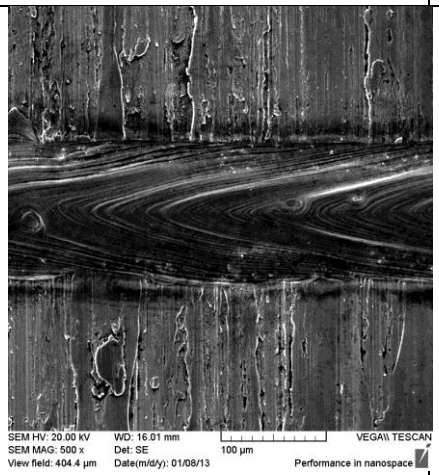	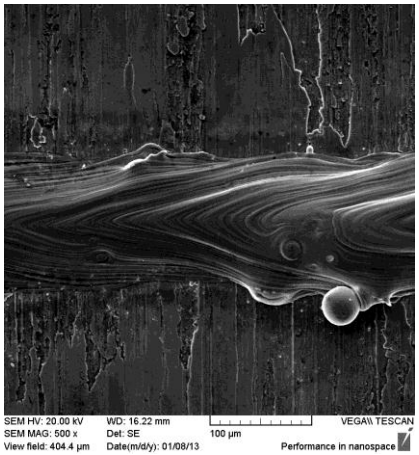
Cross-section	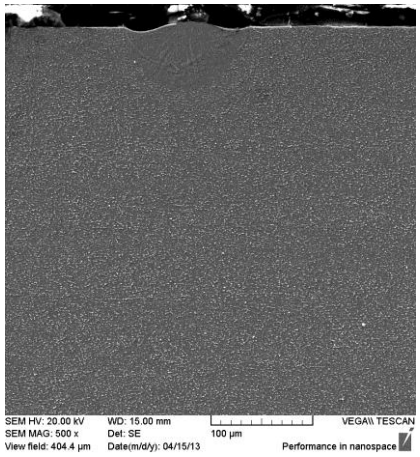	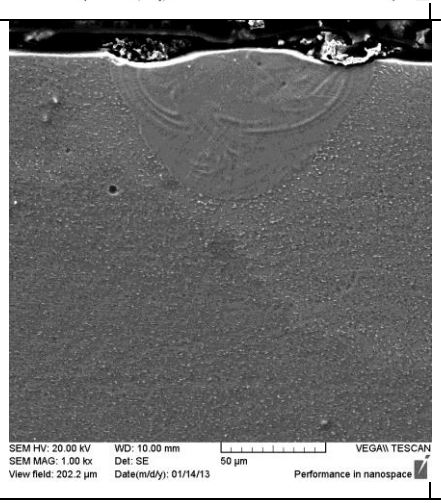	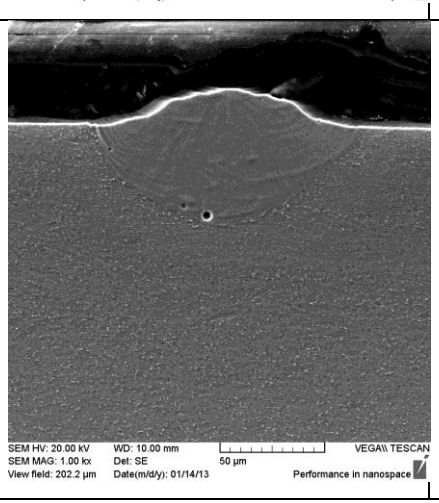	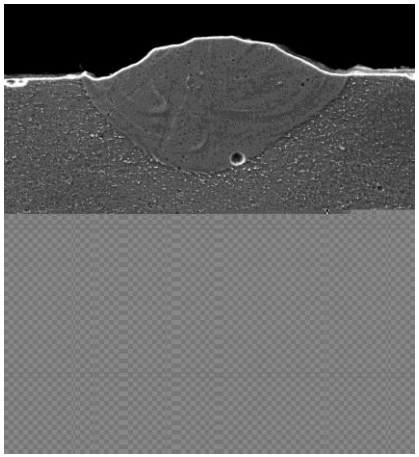

	without powder @ 150 W	15 µm @ 150 W	30 µm @ 150 W	45 µm @ 150 W
1200 mm/s Top View	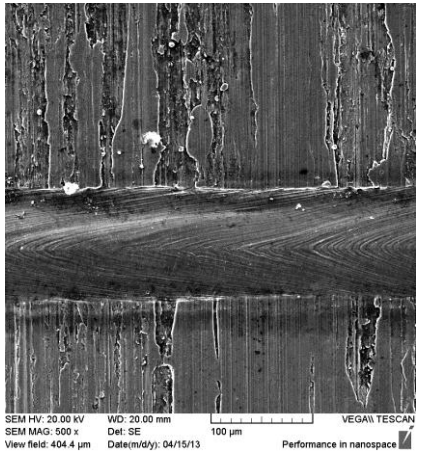	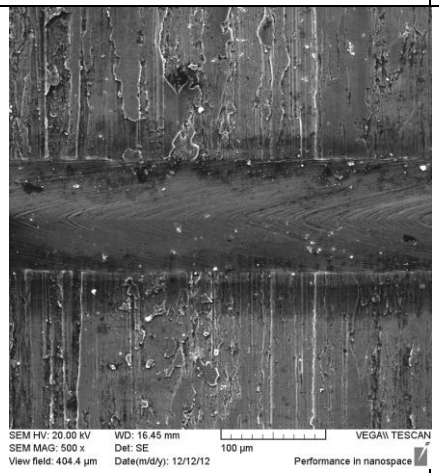	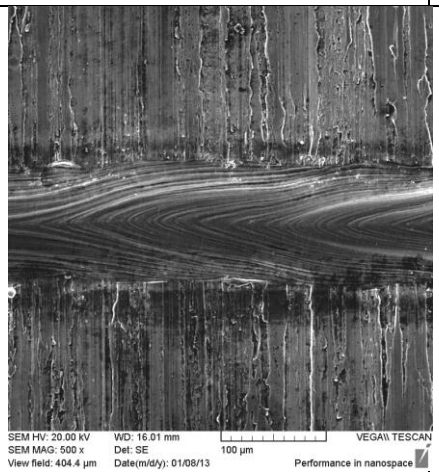	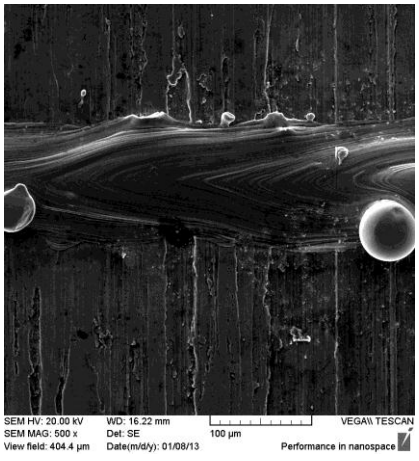
Cross-section	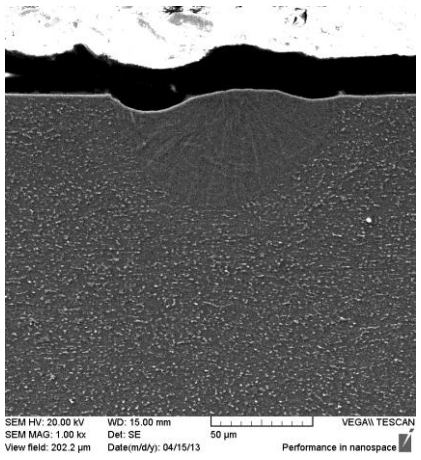	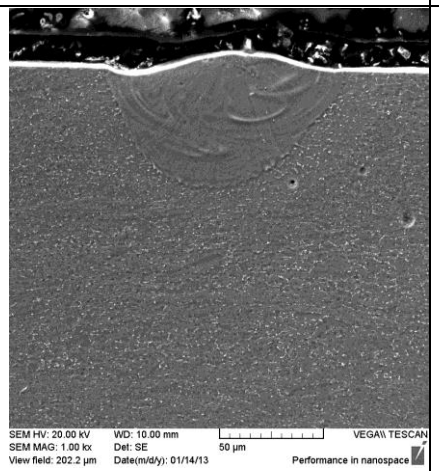	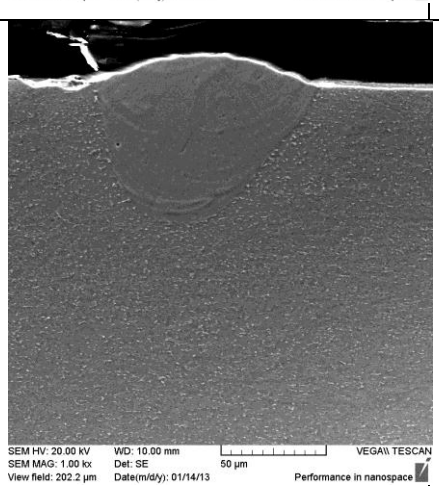	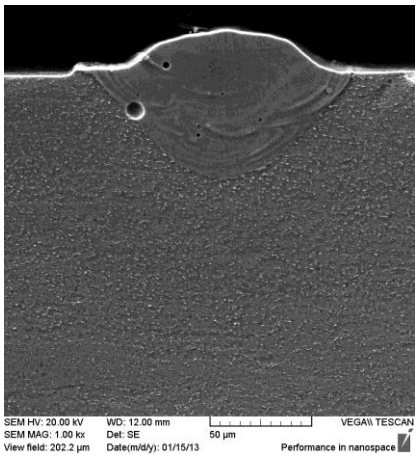

	without powder @ 150 W	15 µm @ 150 W	30 µm @ 150 W	45 µm @ 150 W
1400 mm/s Top View	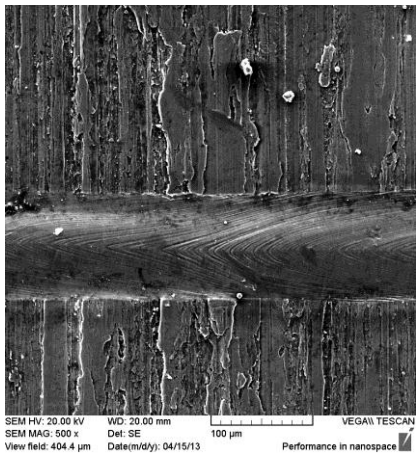	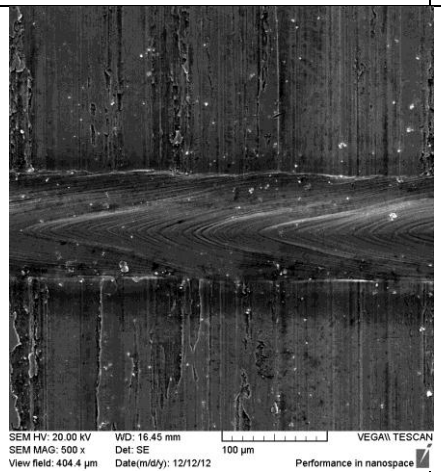	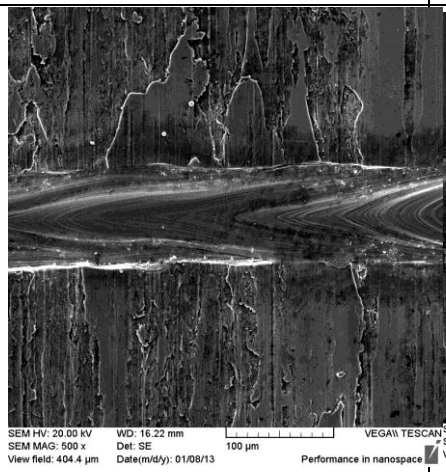	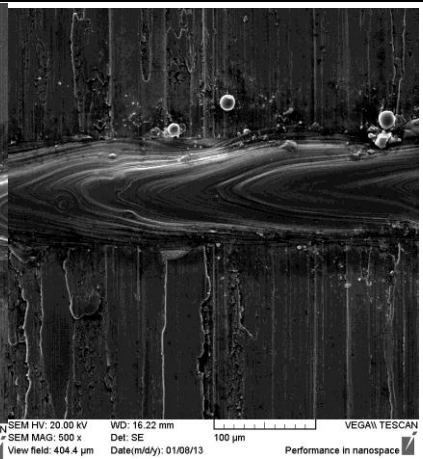
Cross-section	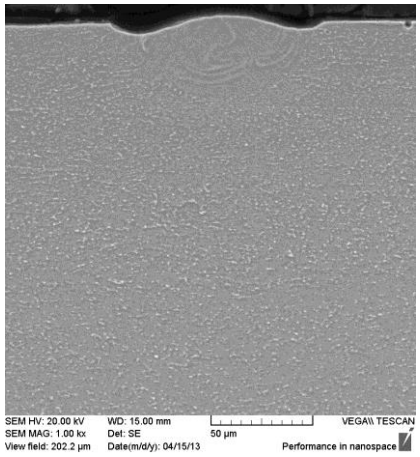	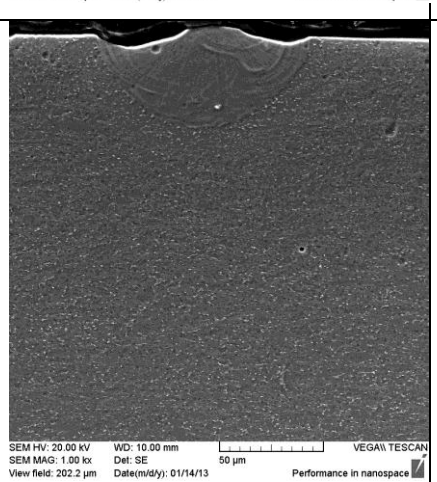	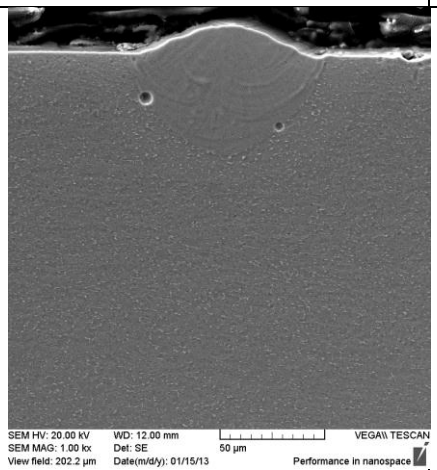	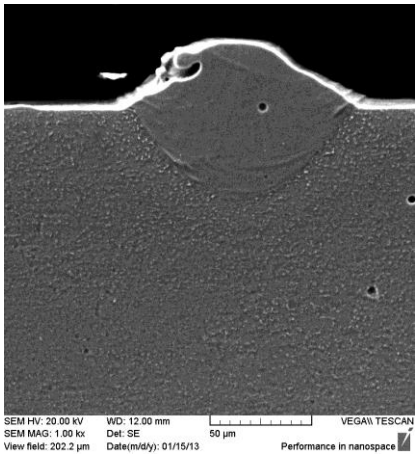

	without powder @ 150 W	15 µm @ 150 W	30 µm @ 150 W	45 µm @ 150 W
1600 mm/s Top View	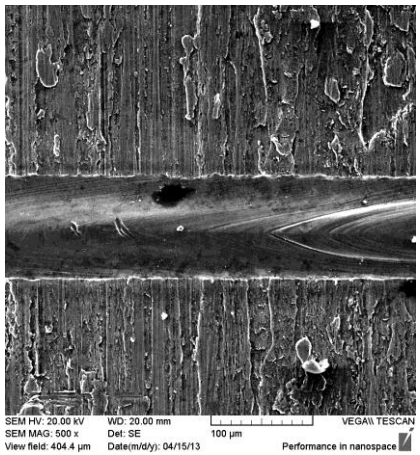	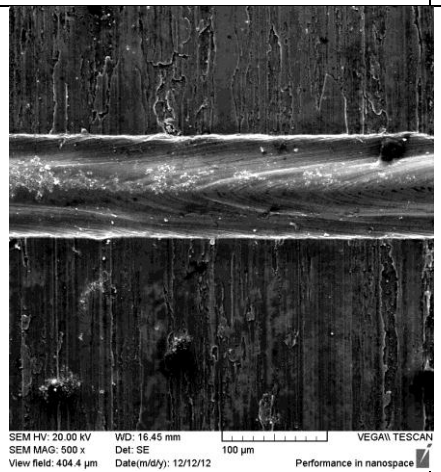	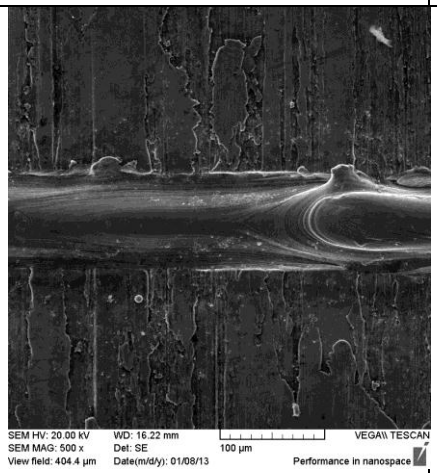	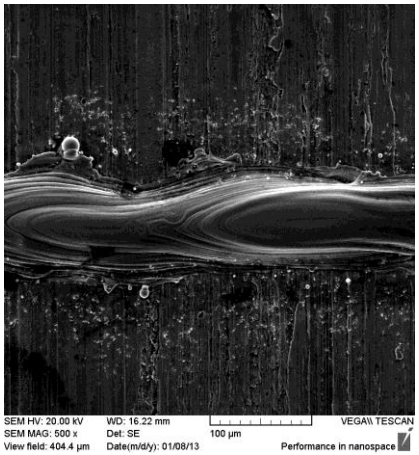
Cross-section	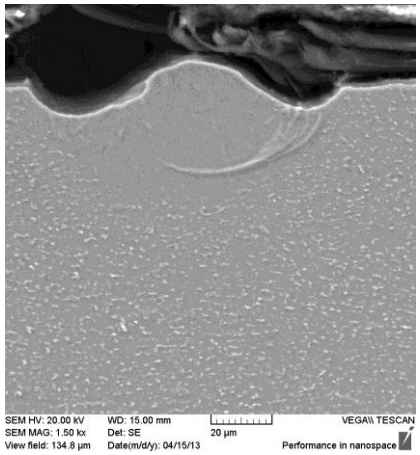	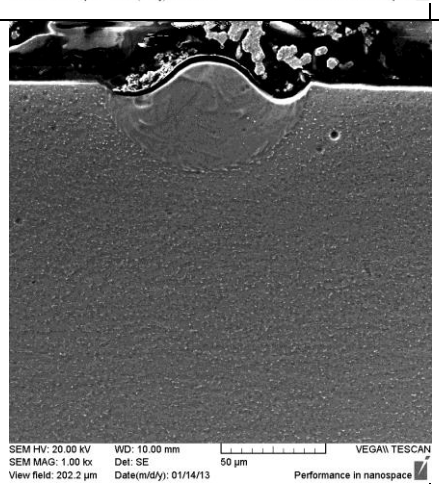	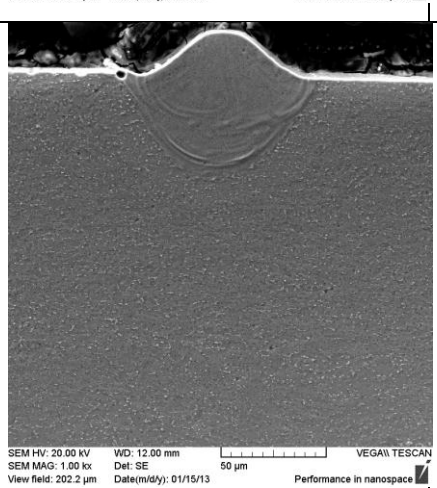	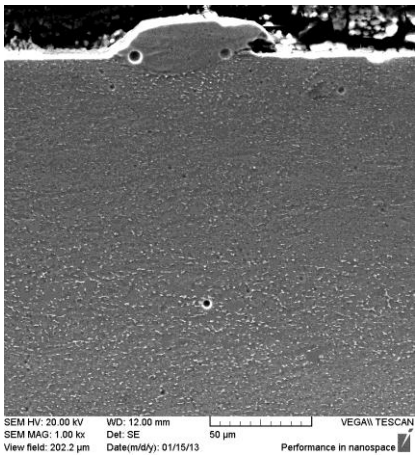

	without powder @ 150 W	15 µm @ 150 W	30 µm @ 150 W	45 µm @ 150 W
1800 mm/s Top View	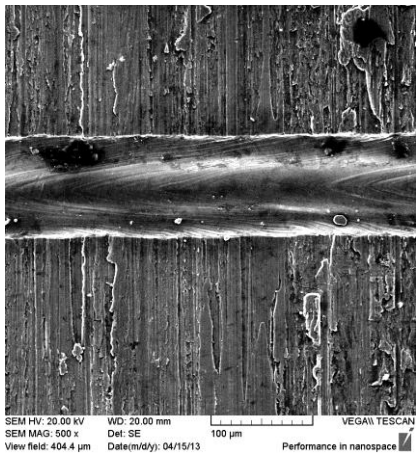	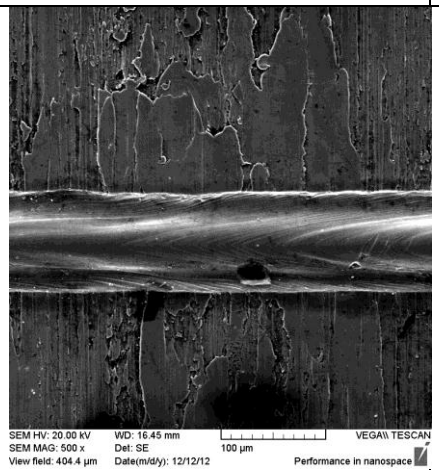	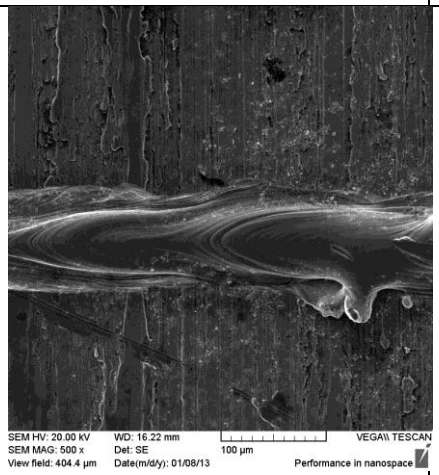	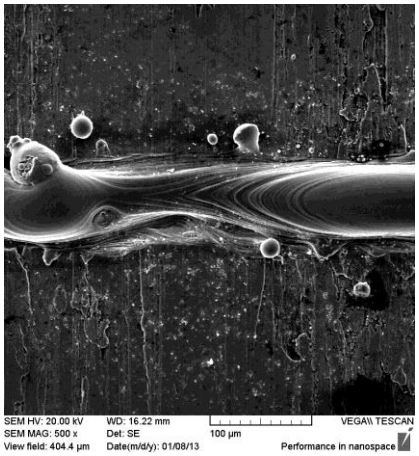
Cross-section	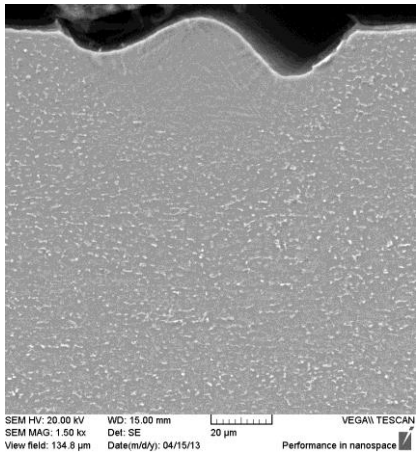	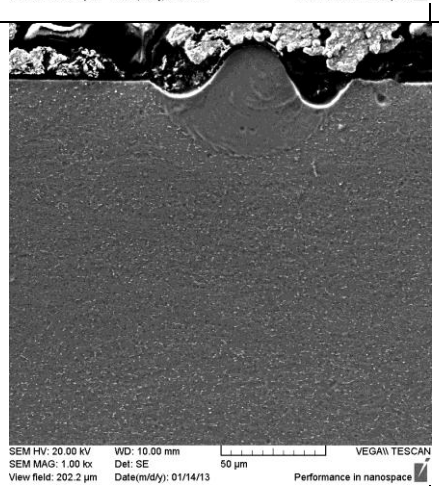	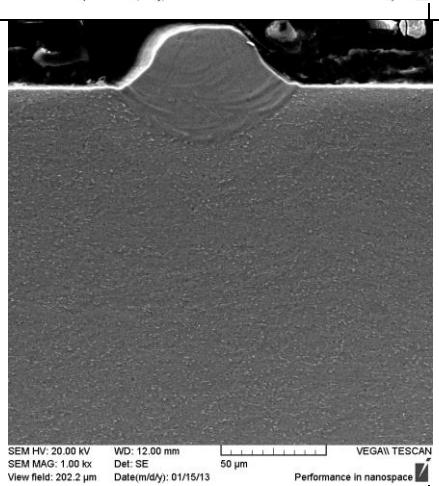	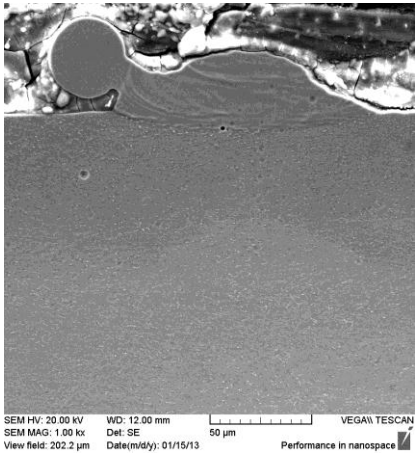

	without powder @ 150 W	15 µm @ 150 W	30 µm @ 150 W	45 µm @ 150 W
2000 mm/s Top View	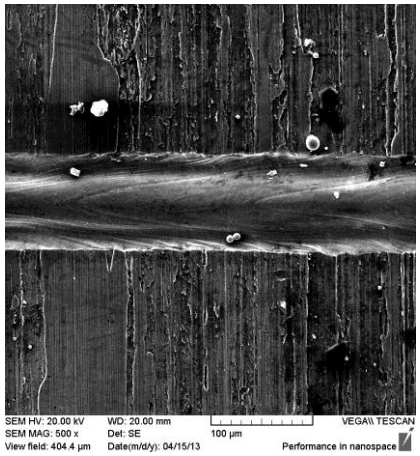	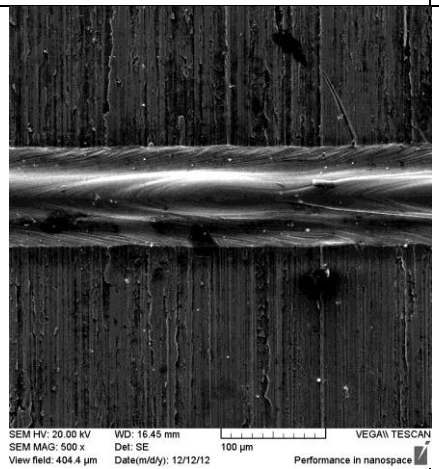	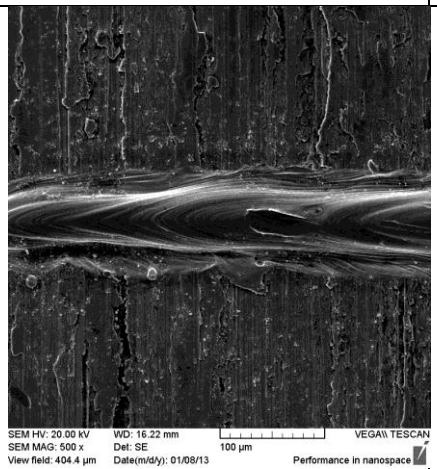	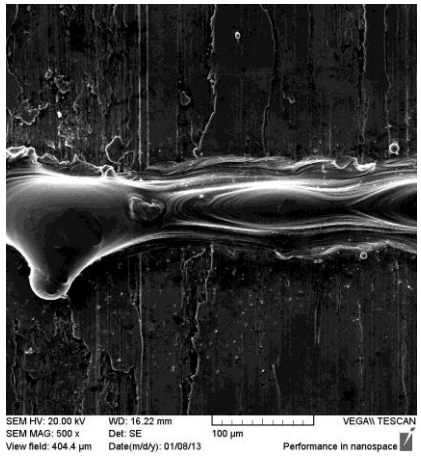
Cross-section	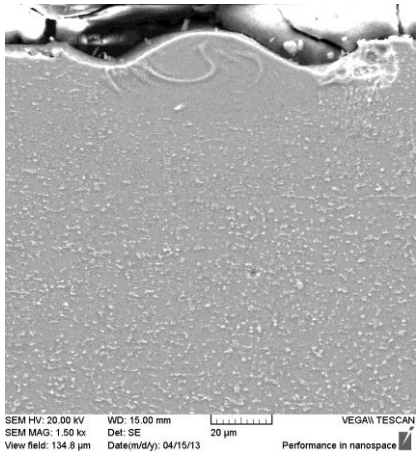	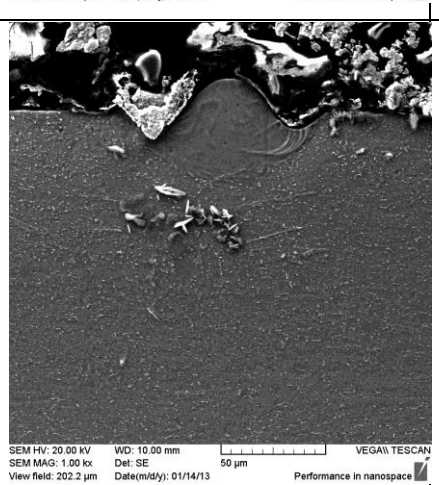	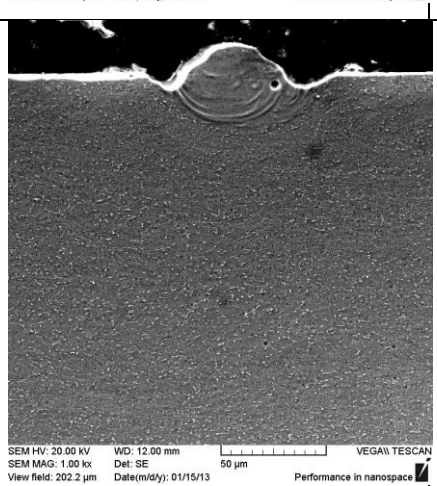	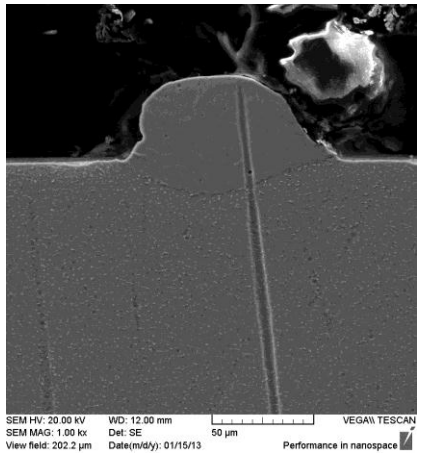

	without powder @ 170 W	15 µm @ 170 W	30 µm @ 170 W	45 µm @ 170 W
600 mm/s Top View		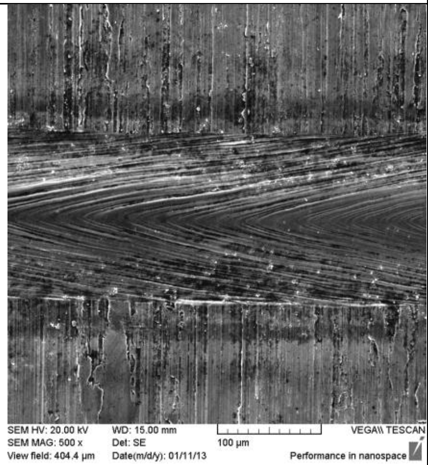	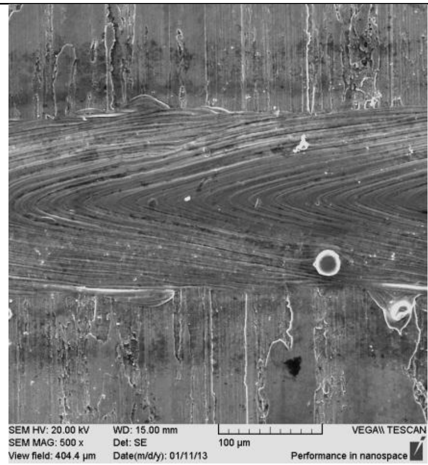	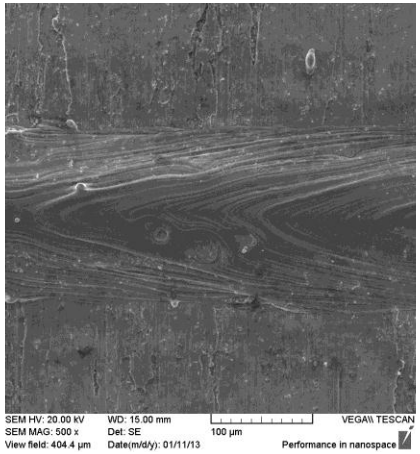
Cross-section	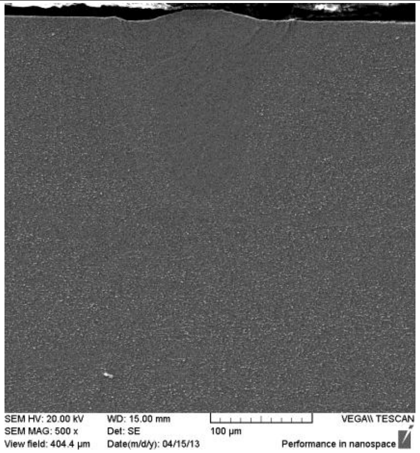	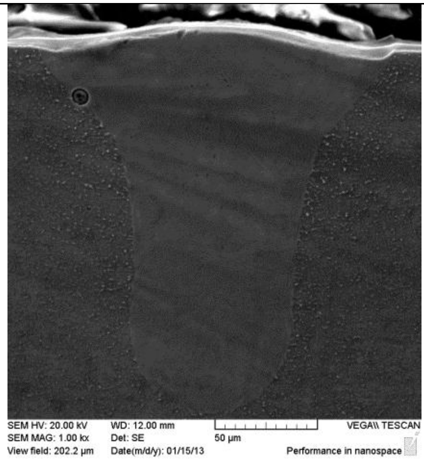	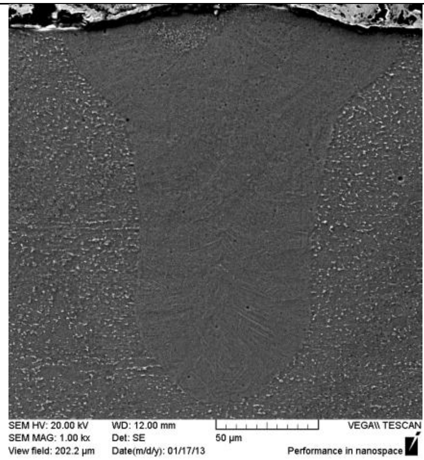	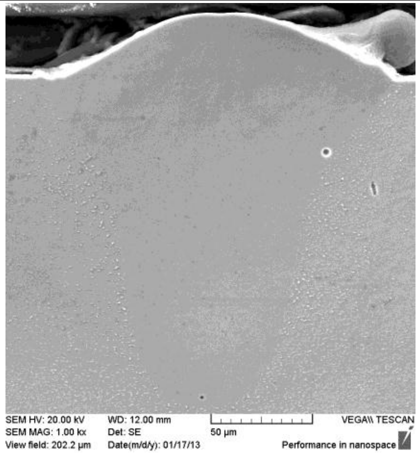

	without powder @ 170 W	15 µm @ 170 W	30 µm @ 170 W	45 µm @ 170 W
800 mm/s Top View	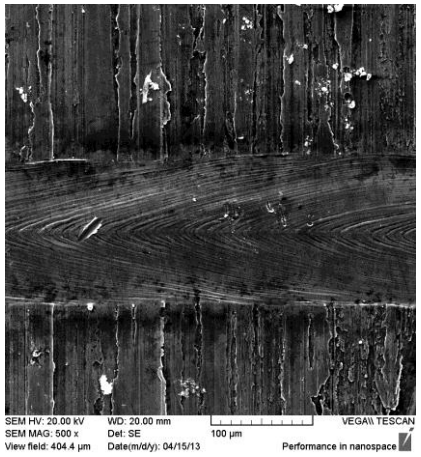	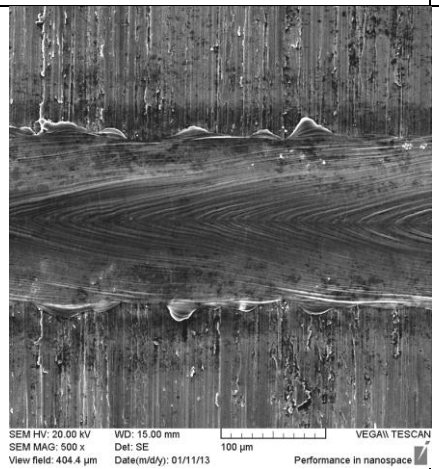	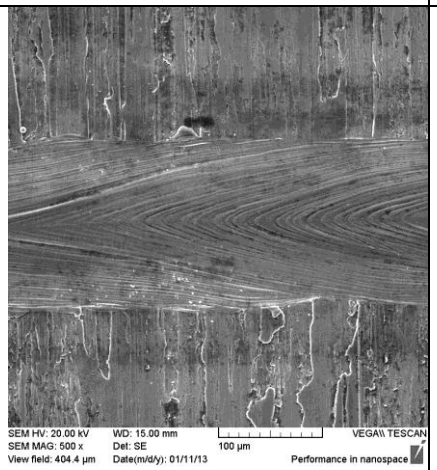	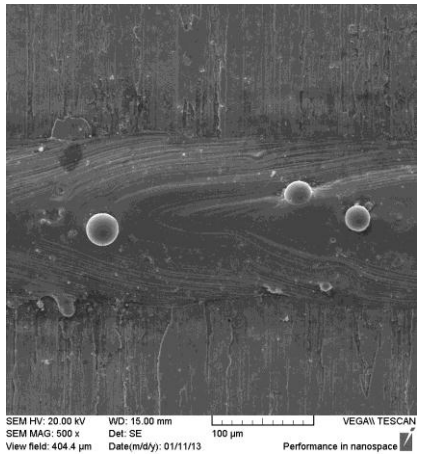
Cross-section	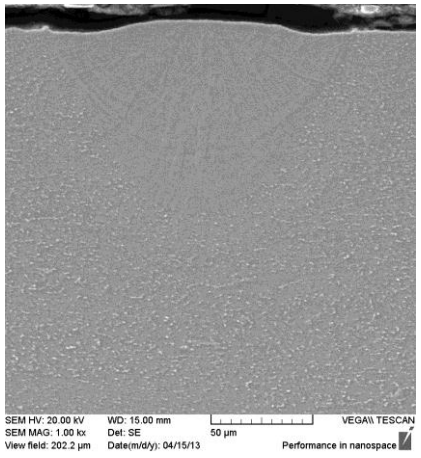	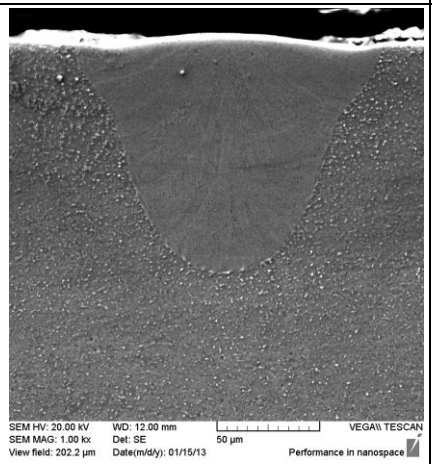	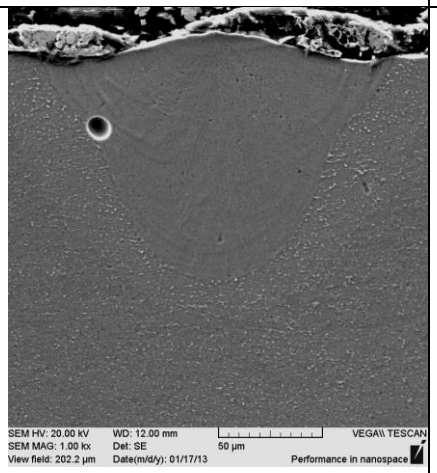	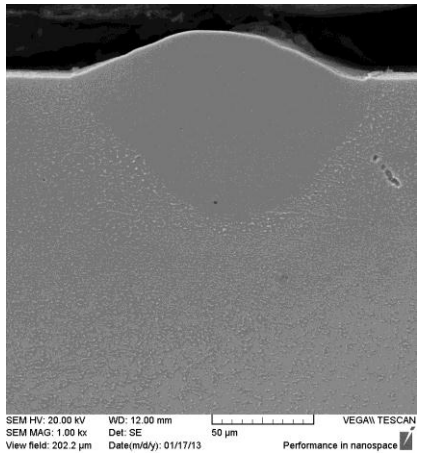

	without powder @ 170 W	15 µm @ 170 W	30 µm @ 170 W	45 µm @ 170 W
1000 mm/s Top View	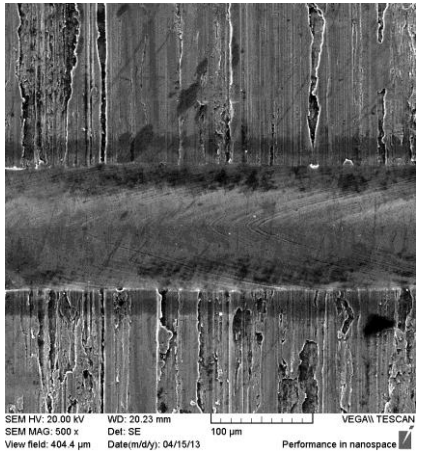	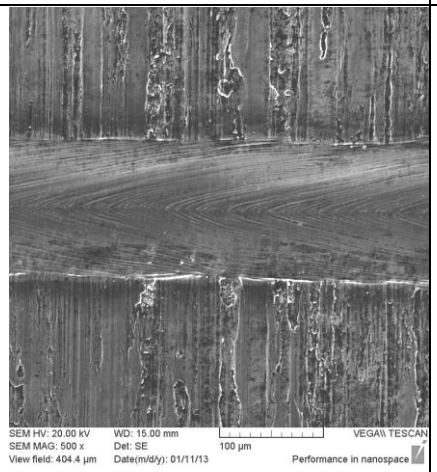	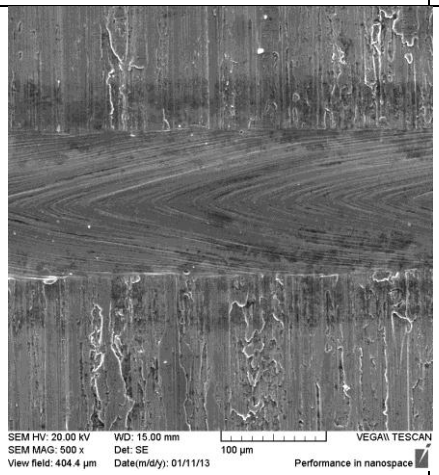	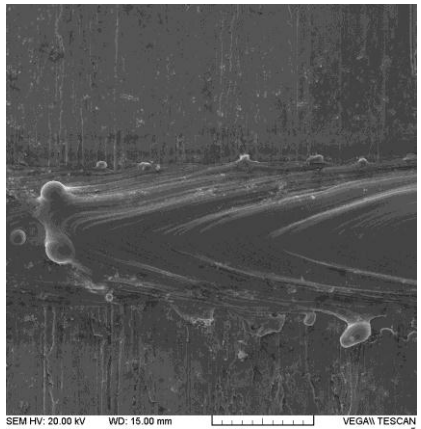
Cross-section	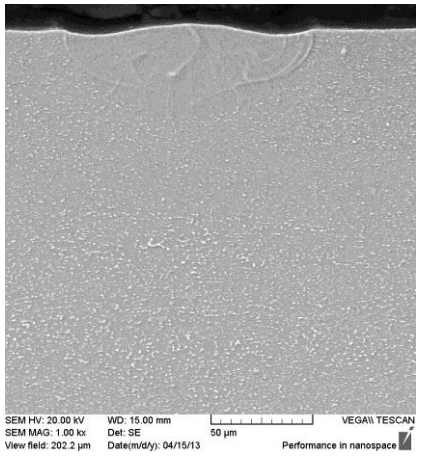	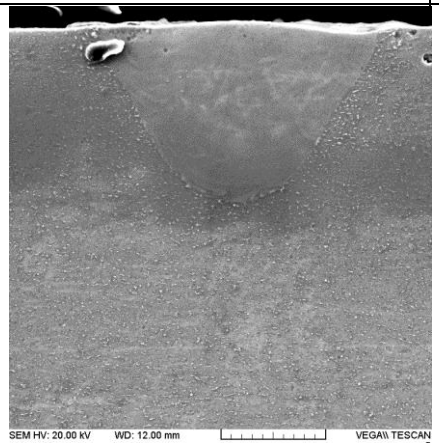		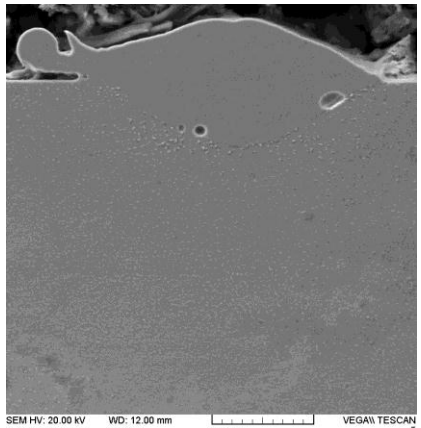

	without powder @ 170 W	15 µm @ 170 W	30 µm @ 170 W	45 µm @ 170 W
1200 mm/s Top View	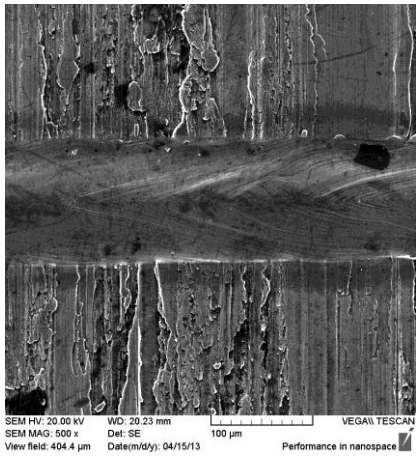	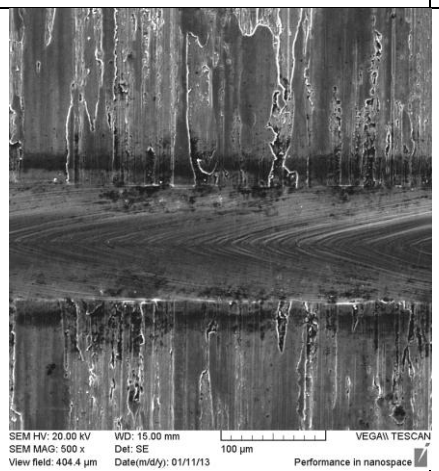	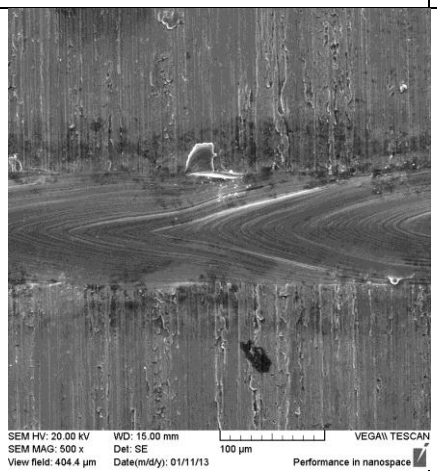	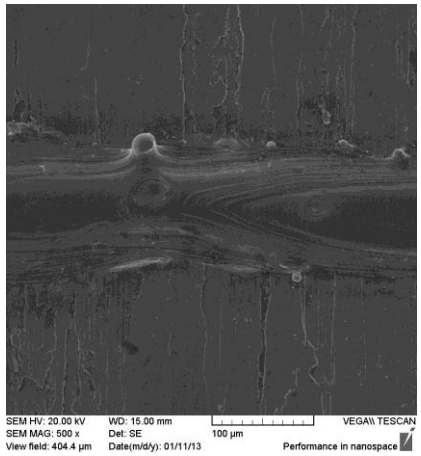
Cross-section	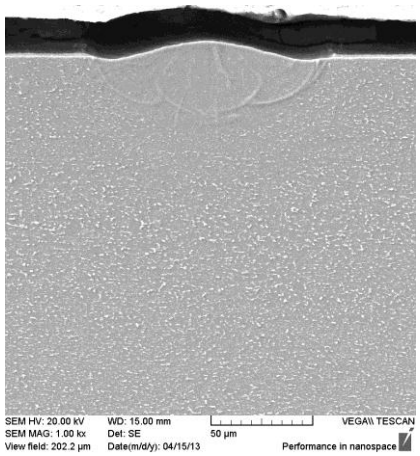	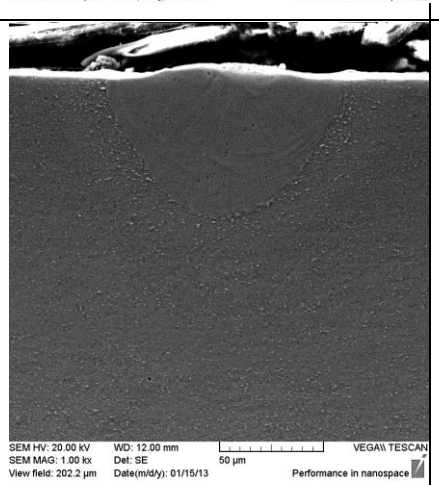	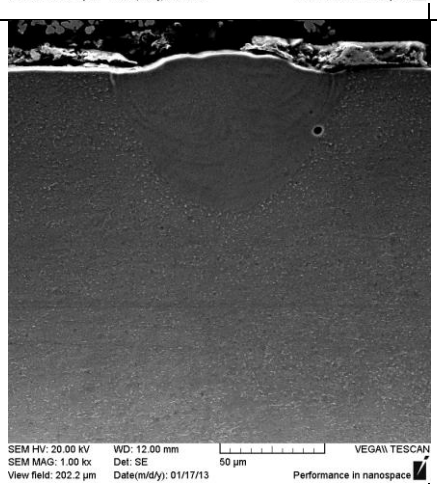	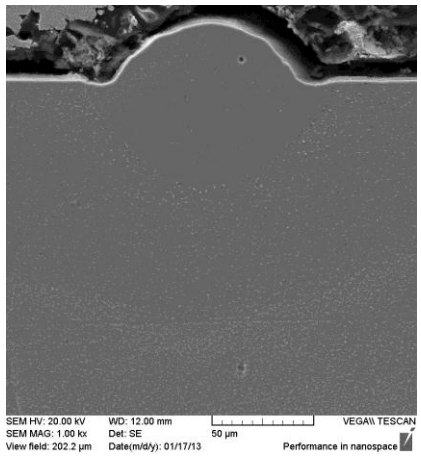

	without powder @ 170 W	15 µm @ 170 W	30 µm @ 170 W	45 µm @ 170 W
1400 mm/s Top View	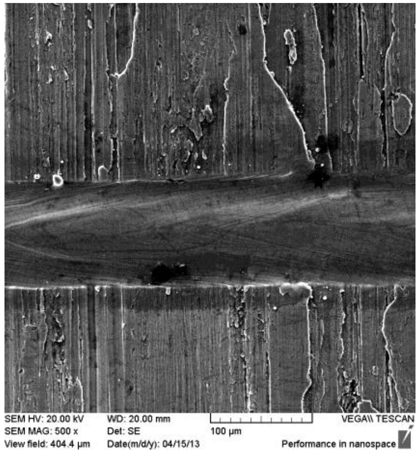	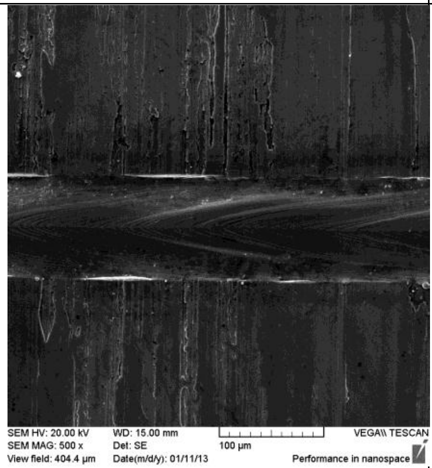	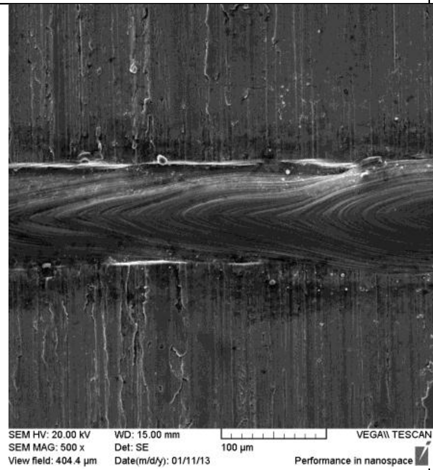	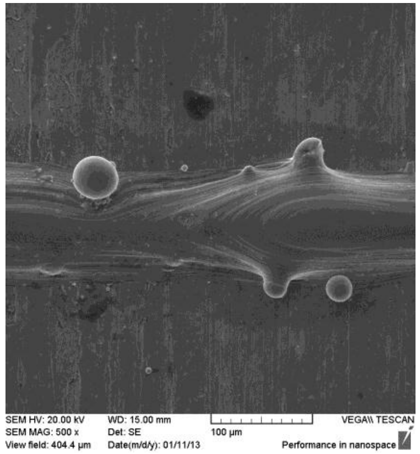
Cross-section	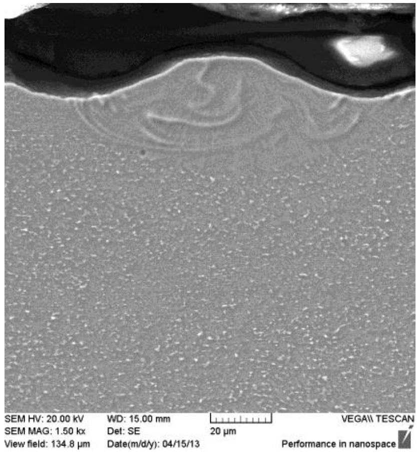	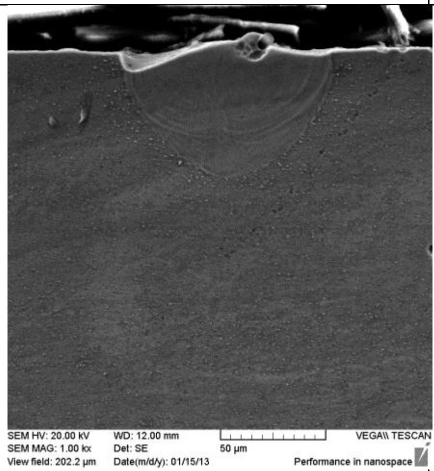	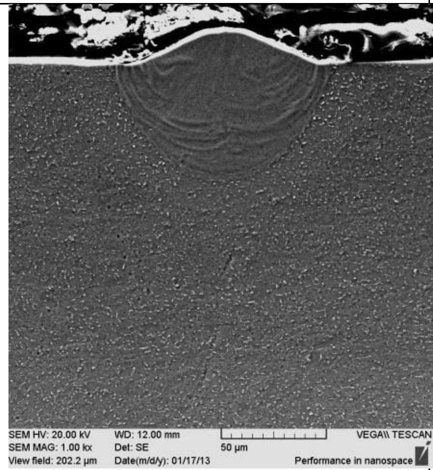	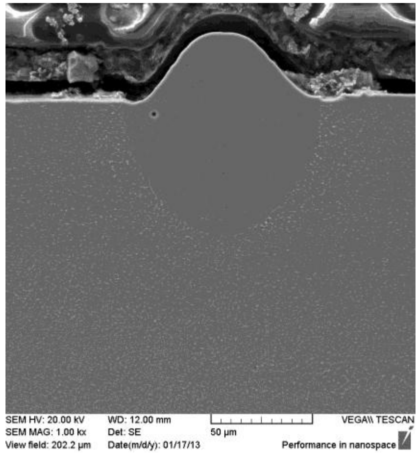

	without powder @ 170 W	15 µm @ 170 W	30 µm @ 170 W	45 µm @ 170 W
1600 mm/s Top View	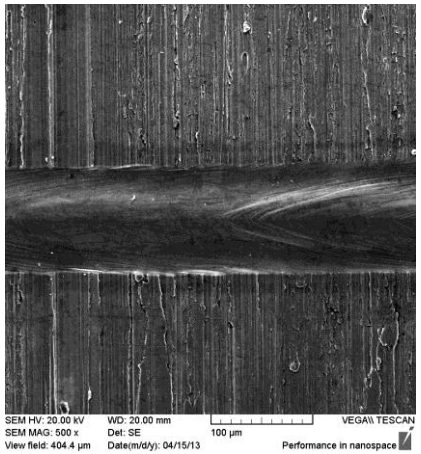	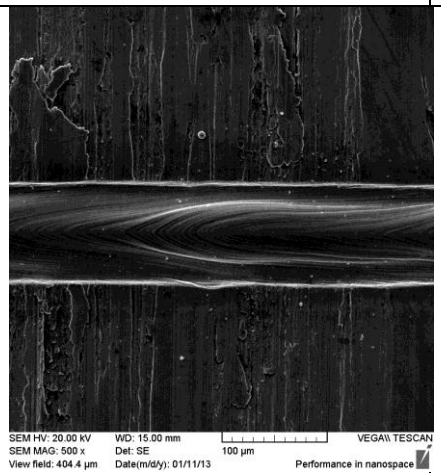	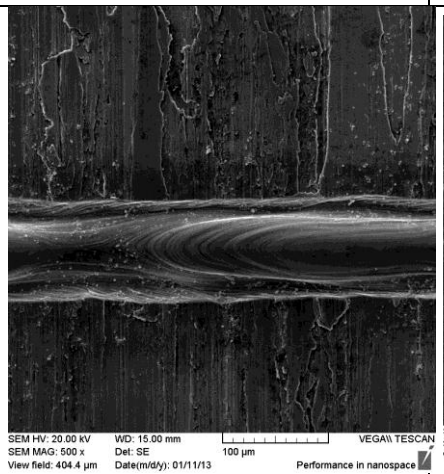	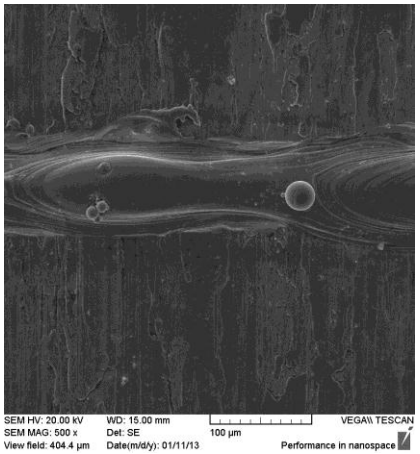
Cross-section	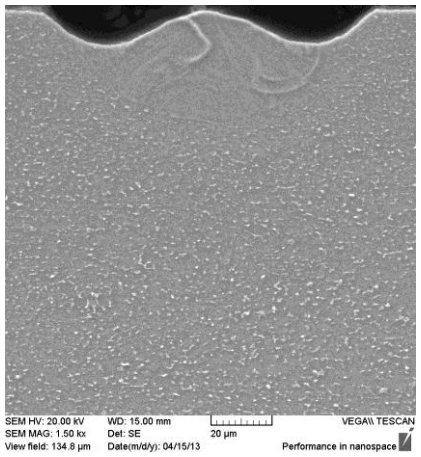	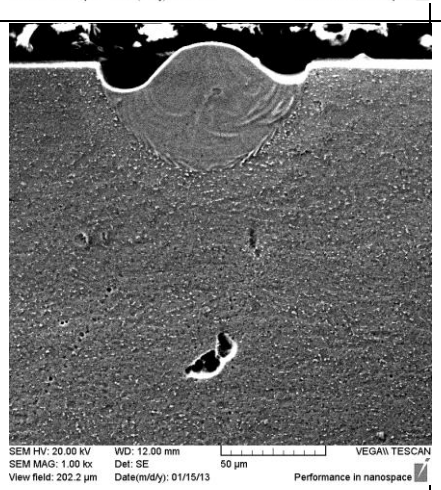	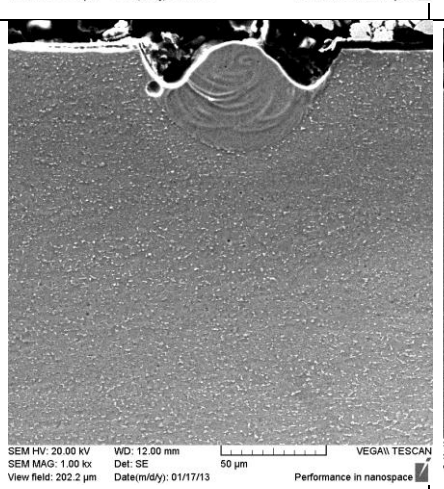	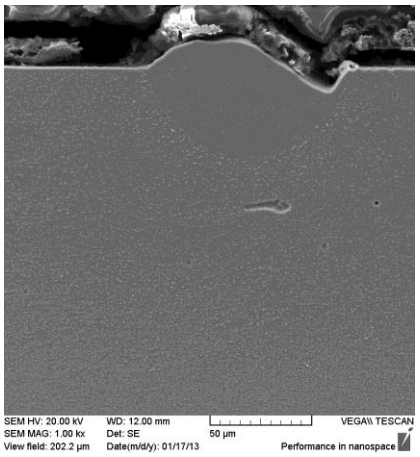

	without powder @ 170 W	15 µm @ 170 W	30 µm @ 170 W	45 µm @ 170 W
1800 mm/s Top View	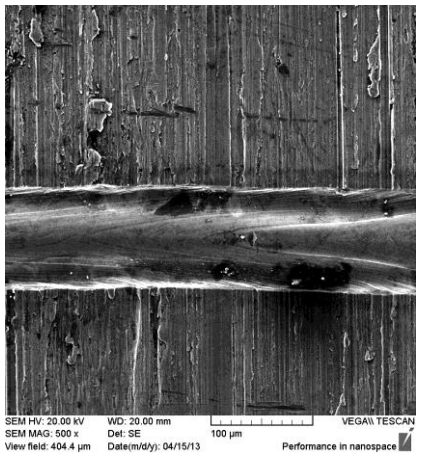	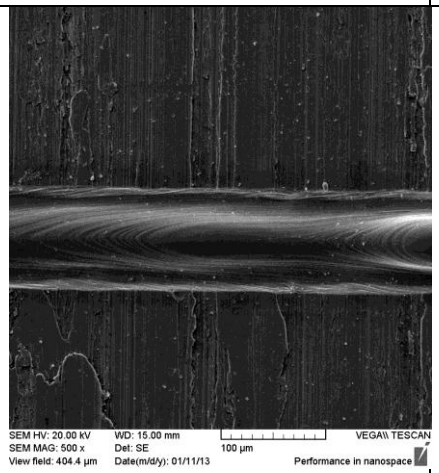	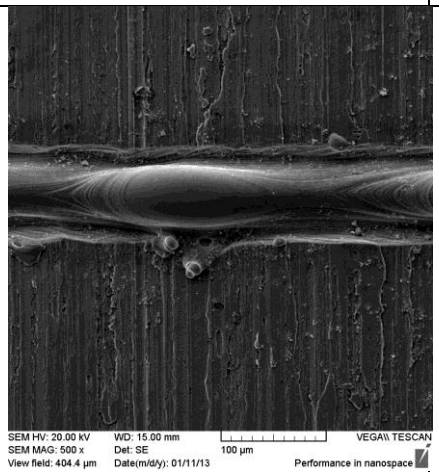	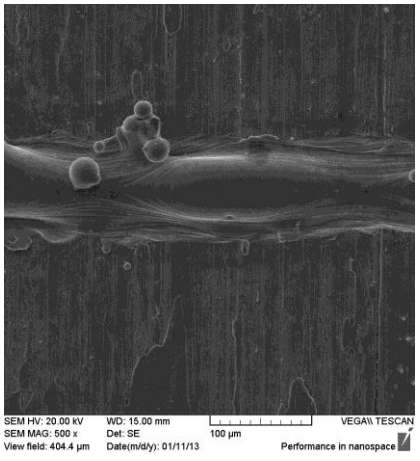
Cross-section	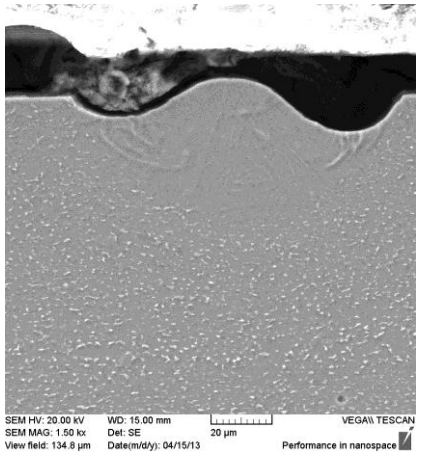	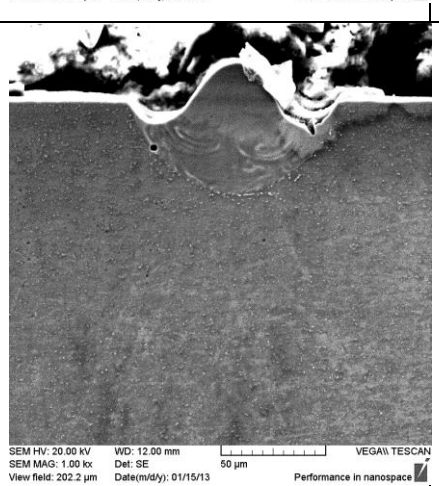	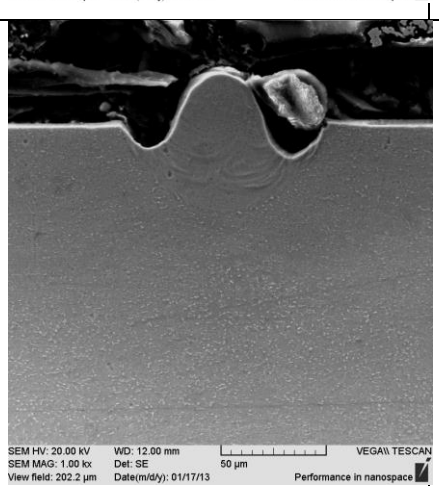	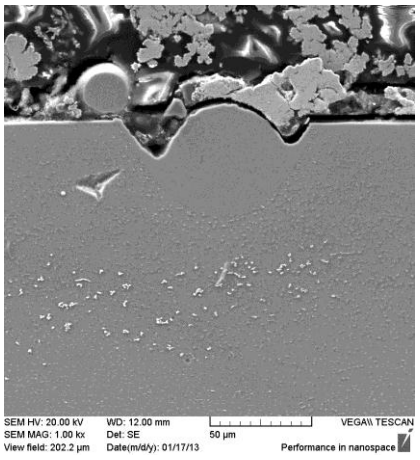

	without powder @ 170 W	15 µm @ 170 W	30 µm @ 170 W	45 µm @ 170 W
2000 mm/s Top View	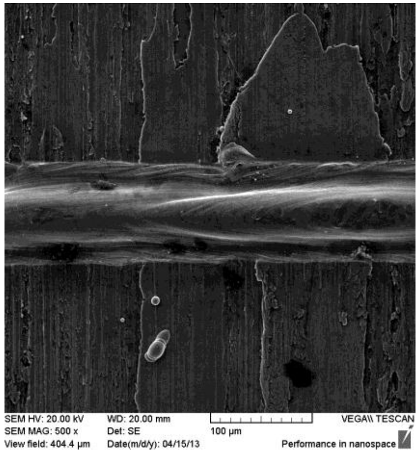	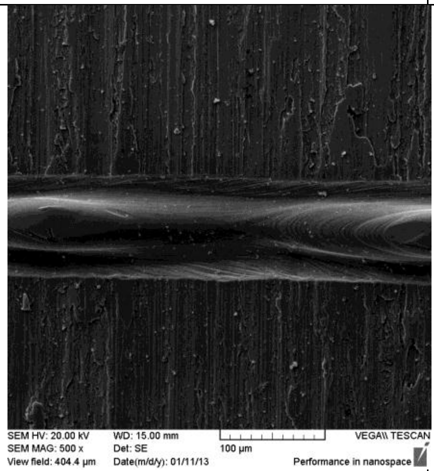	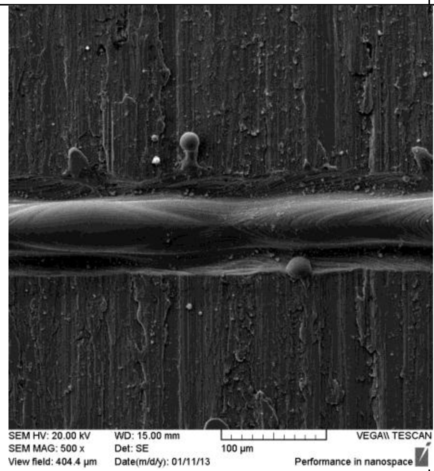	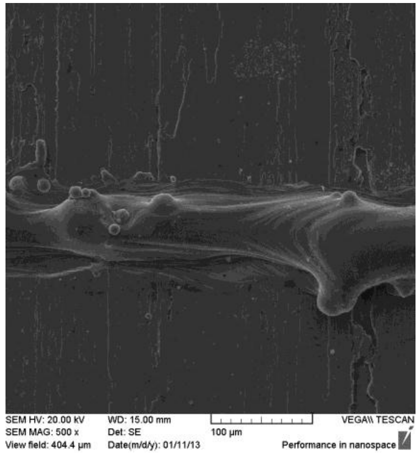
Cross-section